Thesis for the Master's Degree in

Chemistry

Golnaz Isapour

"Schizophrenic Micellization and Sol-Gel Transition of pH- and Temperature Responsive Penta-block Terpolymer $PDEAEMA_x$-*b*-$PNIPAAM_y$-*b*-PEG_z-*b*-$PNIPAAM_y$-*b*-$PDEAEMA_x$ in Aqueous Solutions"

60 study points

Department of Chemistry
Faculty of Mathematics and Natural Sciences
University of Oslo (UiO)
November 2013

Schizophrenic Micellization and Sol-Gel Transition of pH- and Temperature Responsive Penta-block Terpolymer

$PDEAEMA_x$-*b*-$PNIPAAM_y$-*b*-PEG_z-*b*-$PNIPAAM_y$-*b*-$PDEAEMA_x$

in Aqueous Solutions

Golnaz Isapour

Master student

Professor

Bo Nyström
Supervisor

Postdoctoral

Reidar Lund
Co-supervisor

Department of Chemistry
Faculty of Mathematics and Natural Sciences
University of Oslo (UiO)

November 2013

Acknowledgement

Foremost, I would like to express my gratitude to my supervisor, Professor Nyström, who always had faith in me and supported me throughout my thesis with his patience and knowledge. I also thank my co-supervisor, Dr. Lund who I learned a lot from. I am grateful to Professor Knudsen to provide an opportunity to have access to SANS instrument. Many thanks to Dr. Zhu for synthesis the polymers which were studied in this work. I wish to acknowledge the assistance of my friend Dorna, in fluorescence spectroscopy experiments.

In my daily work, I have been blessed with my friends at UiO; Neda, Sara, Leva, Farinaz, Elahe and Atoosa who made the good times better and the hard times easier for me.

I'm deeply grateful to my special friend Kaveh; if it wasn't for him, I never had embarked upon my master's degree in Norway.

Lastly I would like to sincerely thank my parents and sisters for all their love and encouragement.

Golnaz Isapour L.

University of Oslo
November 2013

List of Symbols and Abbreviations

$\hat{a}$	Persistence length
A_f	Amplitude for fast relaxation time in DLS
A_s	Amplitude for slow relaxation time in DLS
ATRP	Atom transfer radical polymerization
A_2	Second virial coefficient
b	Stretch exponential parameter
b_i	Coherent neutron scattering length of atom i
c	Mass concentration
c*	Overlap concentration
CMC	Critical Micelle Concentration
CP	Cloud point
D	Mutual diffusion coefficient
d_f	Fractal dimension
D_f	Apparent diffusion coefficient for faster mode
$D_{polymer}$	Polymer specific density
DLS	Dynamic Light Scattering
dn/dc	Refractive index increment
D_s	Apparent diffusion coefficient for slower mode
Δ	Shell thickness
Δk	Difference of length scattering densities between particle and medium
η	Viscosity
η*	Complex viscosity
η’	Dynamic viscosity of dynamic complex viscosity
η’’	In-phase component of dynamic complex viscosity
$g^1(q,t)$	First order electric field autocorrelation in DLS
$g^2(q,t)$	Intensity autocorrelation function in DLS
G’(ω)	Storage modulus

$G''(\omega)$	Loss modulus
$\dot{\gamma}$	Shear rate
γ	Shear strain
$\Gamma(x)$	Gamma function
$I(q)$	Scattered intensity
$\langle I_b(\theta) \rangle$	Background intensity
I_{rel}	Relative intensity in Fluorescence Spectroscopy
$\langle I_s(\theta) \rangle$	Static time-averaged scattering intensity
k	Coherent scattering length density of the medium
κ	Turbidity
K	Contrast factor in SLS
k_B	Boltzmann constant
K_c	Contrast factor in SANS
k_f	Propagation vectors of the scattered radiation
$\bar{k_i}$	Propagation vector of the incident radiation
k_p	Coherent scattering length density of polymer
L	Length in radius of gyration/ contour length
LCST	Lower critical solution temperature
L_L	Light path
LLS	Laser Light Scattering
L_p	Average distance traveled by a photon in the medium before it is being scattered
λ	Wavelength
m_{B1}	Mass fraction of the blocks B_1
M_w	Weight averaged molecular weight
n	Scaling exponent (or critical relaxation exponent)
n_s	Refractive index of the solution
N_{agg}	Aggregation number
N_A	Avogadro's number
N_p	Number of homogeneous isotropic scatterers

ω	Frequency of oscillation
Ω	Steady angular rotation speed
P(q)	Scattering form factor
P_θ	Particle scattering function
PDEAEMA	Poly(2-(diethylamino) ethyl methacrylate)
PEG	Poly(ethylene glycol)
PNIPAAM	poly(N-isopropyl acrylamide)
Φ	Polymer volume fraction
ξ	Correlation length in SANS
$\vec{q}$	Scattering wavevector
R	Linear fitting correlation coefficient / Radius
R_g	Radius of gyration
$R_{g,\nu}{}^2$	Mean-square radius of gyration for the ν-th component
$R_{g,z}{}^2$	z-mean of the square of the radius of gyration
R_h	Hydrodynamic radius
R_θ	Excess Rayleigh ratio
$R_{ref}(\Theta)$	Rayleigh ratio of the reference solvent
Ʀ	Correlation length in SLS
ρ_m	Mass density of the medium (solvent)
S	Gel strength parameter
S(q)	Structure factor
SLS	Static Light Scattering
SALS	Small angle light scattering
SANS	Small Angle Neutron Scattering
σ	Steady shear stress
τ	Mean relaxation time
τ_f	Relaxation time for the fast process in DLS
τ_{se}	Relaxation time for the slow process in DLS
Θ	Scattering angle
Θ_{tr}	Transition temperature in Densitometry

T	Absolute temperature
$\tan \delta$	Loss tangent in Rheometry
U_E	Electrophoretic mobility
$v_{polymer}$	Specific volume
V_p	Volume of homogeneous isotropic scatterer
ζ	Zeta potential

Abstract

Micellization behavior and sol-gel transition of the new biocompatible, temperature and pH responsive penta-block terpolymers, $PDEAEMA_x$-*b*-$PNIPAAM_y$-*b*-PEG_z-*b*-$PNIPAAM_y$-*b*-$PDEAEMA_x$ synthesized by Atom Transfer Radical Polymerization (ATRP) were investigated in aqueous solutions. The three examined polymers differed in PDEAEMA block length, which was the pH-responsive block and PEG block length as the permanent hydrophilic part of the polymer. The temperature responsive block, i.e., PNIPAAM block length kept constant in the three systems.

Micellization in the dilute regime (0.5% w/w) was investigated by fluorescence spectroscopy, turbidimetry, densitometry, ζ-potential, ^{1}H NMR, Dynamic Light Scattering (DLS), Static Light Scattering (SLS), Small Angle Neutron Scattering (SANS) and steady shear viscosity measurements. A core-shell spherical model was proposed for the micelles. Critical Micelle Concentration (CMC) at a higher pH, detected to have a lower value. Cloud point (CP) and transition point in Density measurements were consistent in the three polymers and at a higher pH, the transitions were observed at lower temperatures. ζ-potential measurements propounded the PDEAEMA block to be situated toward the surface of the micelles at pH below the pK_a of the penta-block terpolymers ($6<pK_a<7.4$) . Steady shear measurements showed an increasing trend of the viscosity by heating up the solutions. At pHs above the pK_a of the penta-block terpolymers and temperatures above the Lower Critical Solution Temperature (LCST), the solutions displayed a shear-thinning behavior. The longer PDEAEMA block along with a longer PEG block offered well-shaped and monodispersed micelles in the aqueous solutions. The shorter PEG block resulted in a higher level of hydrophobicity in the polymer, while the shorter PDEAEMA block along with a longer PEG block made the penta block terpolymer more hydrophilic. The micellar characteristics were different in heavy water (D_2O) than in phosphate buffer solution (PBS). In DLS, bimodal correlation functions were recognized in PBS solutions, while polymers in D_2O solutions mostly showed single mode correlation functions.

At a higher concentration (20% w/w) a sol-gel transition was observed for the three penta-block terpolymers. At a higher pH for the solutions of higher level of hydrophobicity, the gel point was observed at a lower temperature.

The dual-responsive properties of the described system, along with the possibility to tailor the blocks' length suggest potential application values in drug-controlled delivery, both in the micellar form in dilute regime, and in the gel form for localized and sustained delivery.

Keywords:

Micellization
Penta-block Terpolymer
Dynamic Light Scattering (DLS)
Static Light Scattering (SLS)
Small Angle Neutron Scattering (SANS)
Sol-gel Transition

Contents

1 Preamble

One of the features of amphiphilic block copolymers is self-assembly of the polymers when dissolved in a selective solvent, i.e., a solvent thermodynamically good for one block and poor for the other. Depending on the equilibrium between the driving forces governing the micellization process, block copolymers form micelles with different size, morphology and structure. Spheres, spheroids, cylinders, vesicles, disks and worm-like objects are the main structures that have been reported. Different methods of micelle preparation and also experimental factors (solvent, concentration, temperature, pH, etc.) influence the packing of the unimers into the micelles. In case of stimuli-responsive polymers, self-assembly of macromolecules changes under different physical (temperature, light, ionic strength of solvent, etc.) and/or chemical (pH, reactants, etc.) conditions of the medium of the experiment [1]. By increasing the concentration of amphiphilic copolymers, at a right concentration, depending on the block building groups and their interactions with other groups and the selective solvent, three-dimensional network might be formed.

In this study, the "direct dissolution" method was chosen to prepare micelles. The samples were prepared with the linear ABCBA penta-block terpolymers $PDEAEMA_x$-*b*-$PNIPAAM_y$-*b*-PEG_z-*b*-$PNIPAAM_y$-*b*-$PDEAEMA_x$[1] in two concentration regimes: dilute (0.5% w/w) and semi-dilute (20.0% w/w). In dilute regime, two different solvents, heavy water (D_2O) and phosphate buffer solution (PBS) at different pH values were used. For the former, pH was adjusted to 3.0, 7.4 and 9.0 using very small drops of 1M HCl or 1M KOH and in the latter, buffer solutions were formulated for pH 3.0, 5.0, 6.0, 7.4 and 9.0. Here the main aims were investigating the effect of the following parameters on the self-assembly:

[1] **PDEAEMA**: poly(2-(diethylamino) ethyl methacrylate)

PNIPAAM: poly(N-isopropyl acrylamide)

PEG: poly(ethylene glycol)

- pH (3.0, 7.4, 9.0)
- temperature (in the range of 25-50 °C)
- block length (x, y, z)
- ionic strength (comparison between PBS and D_2O)

In semi-dilute regime, PBS with pH 3.0 and 7.4 were used to prepare the solutions; upon heating the samples, hydrogel structures were formed, and rheological behavior and physical structures of the hydrogels at different pH values and over a temperature range from 10 to 50 °C were investigated.

Three ABCBA penta-block terpolymers were studied, in which the blocks' length (x,y,z) were changed (Figure 1). The nomenclatures were chosen in terms of ratio of blocks' length to their corresponding blocks in PDEAEMA$_{34}$-*b*-PNIPAAM$_{58}$-*b*-PEG$_{34}$-*b*-PNIPAAM$_{58}$-*b*-PDEAEMA$_{34}$. The number average molecular weight (M_n) and polydispersity index (PDI= M_w/M_n) were determined from ^{1}H NMR spectra and GPC[2] measurements, respectively (Table 1)

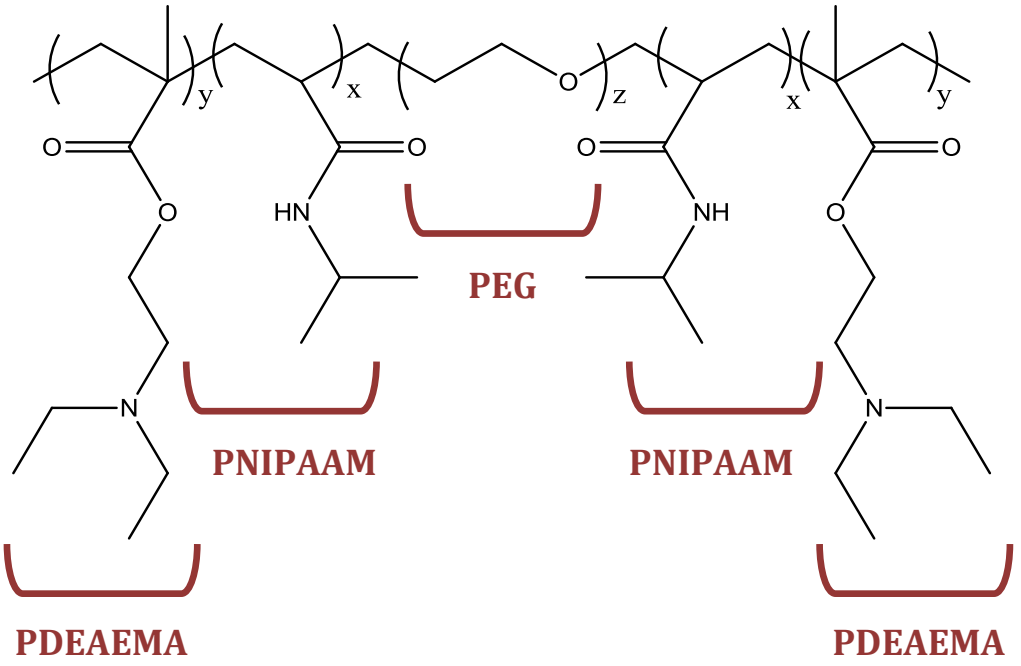

Figure 1 - Structure of PDEAEMA$_x$-*b*-PNIPAAM$_y$-*b*-PEG$_z$-*b*-PNIPAAM$_y$-*b*-PDEAEMA$_x$

[2] Gel Permeation Chromatography (GPC)

ABCBA	A/B/C/B/A length	M_n (g/mol)	PDI
$De_1Ni_1PEG_1$	34/58/34/58/34	27000	1.17
$De_{0.8}Ni_{1.2}PEG_{2.3}$	27/68/77/68/27	29000	1.11
$De_{0.1}Ni_1PEG_2$	2/57/68/57/2	17000	1.17

Table 1- $PDEAEMA_x$-*b*-$PNIPAAM_y$-*b*-PEG_z-*b*-$PNIPAAM_y$-*b*-$PDEAEMA_x$ synthesis data

In this study, self-assembly of $PDEAEMA_x$-*b*-$PNIPAAM_y$-*b*-PEG_z-*b*-$PNIPAAM_y$-*b*-$PDEAEMA_x$ in aqueous solution was investigated by various methods and experiments, with a main focus on scattering methods and rheological experiments.

1.1 Introduction to Self-assembly of Block Copolymers

Amphiphilic block copolymers contain hydrophilic and hydrophobic blocks and depending on thermodynamic conditions and all inter- or intra-molecular interactions among different components in the system, they can be self-assembled into micelles. In aqueous solutions the hydrophilic block occupies the outer surface of the micelle ("shell") and hydrophobic block keeps the least contact with the solution (Figure 2) forming a "core". Based on this behavior, amphiphilic block copolymers have extensively been used in drug delivery applications [2-4], especially for hydrophobic drugs which are solubilized by the hydrophobic block in the core of the micelles [5]. Moreover, minimizing premature drug release, maximizing drug circulation time, decreasing systemic toxicity, and increasing drug availability to the targeted organs have made the polymeric self-assembling system the focal point of many studies [6].

Critical Micelle Concentration (CMC) is one of the key characteristics in polymeric micelles as drug delivery carriers. There are many factors influencing the micelle's formation, such as block copolymer composition and proportion, solvent type, additive and temperature, pH etc. In comparison with small molecule surfactants, polymer micelles have lower CMC; therefore have a strong resistance to dilution and stability in blood. A low CMC value is desired to avoid the

dissociation of micelles during the dilution of drug delivery systems by body fluid [7-8].

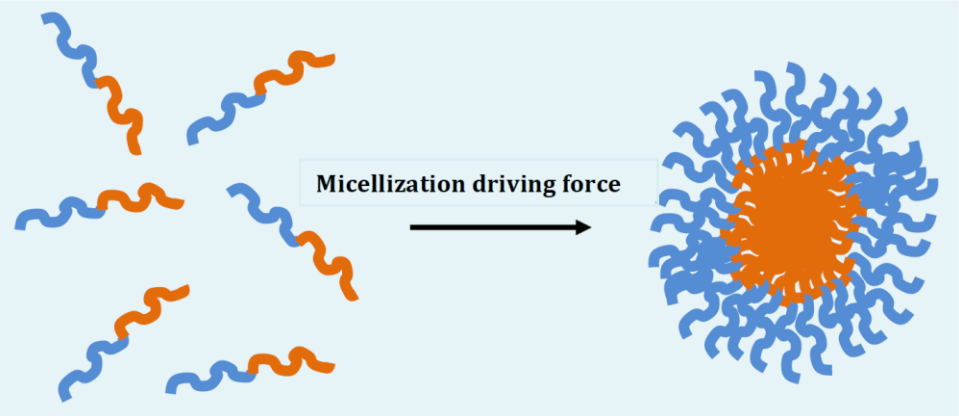

Figure 2 – Micellization of a block copolymer in aqueous solution, orange block and blue block represent the hydrophobic and hydrophilic block, respectively

1.1.1 "Schizophrenic" micellization

"Schizophrenic" micellization behavior describes self-assembly of block copolymers that can switch between two different states of micelles by changing the environmental conditions. This behavior was first reported by Armes [9] for an AB diblock copolymer in aqueous solution which block A and block B were pH responsive and ionic strength responsive, respectively. The structure was changed from micelle (B forming the core) to inverse micelle (A forming the core) by changing the stimuli [10]. Although, the majority of schizophrenic block copolymers combine two different response parameters; there are examples that this behavior was observed only by changing one parameter, for instance pH [11] or temperature [12]. In drug delivery applications, the schizophrenic micellization can be exploited to target a payload, e.g., a drug to specific tissues which have different physiological conditions such as pH or temperature than other issues [4, 13-14]. The block copolymers can also release the payload in response to external stimuli, e.g., local heating or cooling [2, 8].

1.1.2 General properties of $PDEAEMA_x$-b-$PNIPAAM_y$-b-PEG_z-b-$PNIPAAM_y$-b-$PDEAEMA_x$

Poly(N-isopropyl acrylamide) (PNIPAAM) in aqueous solutions typically exhibits a thermal transition from hydrophilic to hydrophobic upon heating. The lower critical solution temperature (LCST) is reported to be about 32 °C [15], however it has been indicated that LCST depends on the length of chain [16], concentration and polymer architecture (linear or branched) [17]. Below LCST, the hydrogen bond interactions between the amide group of PNIPAAM and the surrounding water make the polymer soluble and PNIPAAM chains adopt a randomly coiled structure; above LCST, intra-molecular hydrogen bonds between amide groups and increasing hydrophobic interactions among isopropyl groups result in a compact conformation and the consequent collapse [18-21]. PNIPAAM can also form crosslinks and turn to a hydrogel in which the thermoresponsive behavior is represented as swelling of the polymeric network below LCST and the release of water above it [19, 22].

Poly (2-(diethylamino) ethyl methacrylate) (PDEAEMA) in aqueous solutions with pH below ~ 7.3, is a cationic hydrophilic polymer, simply owing to its amine groups on the side chain which are protonated and therefore the polymer can be dissolved in the aqueous solutions as unimers. Upon increase of pH above ~ 7.3, deprotonation of the side chains causes the PDEAEMA dehydration and collapse of the polymer chains due to the steric effect of the two ethyl groups on the polymer chain [21, 23]; it therefore turns to a hydrophobic weak polybase (pK_a of 7.3) . Although PDEAEMA is frequently referred to as being only pH-sensitive, it has been investigated that PDEAEMA could be both pH- and temperature-responsive [24].

Poly (ethylene glycol)(PEG) is a hydrophilic polymer which with the arrangement in this study, can act as a steric stabilizer for the penta-block terpolymer, allowing the formation of stable micellar aggregates at intermediate pH and temperatures [7].

PNIPAAM and PDEAEMA contribute to temperature and pH responsiveness, respectively in $PDEAEMA_x$-*b*-$PNIPAAM_y$-*b*-PEG_z-*b*-$PNIPAAM_y$-*b*-$PDEAEMA_x$. So far, Self assembly of similar block copolymers, mostly triblock copolymers including PNIPAAM and/or PDEAEMA with PEG has been studied. In many cases schizophrenic micellization has been realized [21]. In general, at acidic pH (pH less than pK_a of PDEAEMA) and elevated temperatures (temperature above LCST of PNIPAAM), PNIPAAM-core micelles are self-assembled and at alkaline pH and lower temperature inverted structures with PDEAEMA in micelles' core are formed. The critical pH and temperature to distinguish between the two structures, depending on polymer block type and blocks' arrangement, are different in each case. Recently self-assembly behavior of a $PDEAEMA_x$-*b*-$PNIPAAM_y$-*b*-PEG_z-*b*-$PNIPAAM_y$-*b*-$PDEAEMA_x$ has been studied and a core-shell-corona micelles has been offered [7]. In this work, the penta-block terpolymers with different lengths of blocks were characterized and the self-assembly in low and high concentrations were investigated.

Determination of CMC, LCST and critical pH of the responsive polymers provides key information in drug delivery. In this study CMC was determined by fluorescent spectroscopy and critical temperature and pH were characterized by density and turbidity measurements. ^1H NMR spectroscopy, Zeta-potential measurements, scattering techniques and rheology experiments provided detailed information on the system.

1.2 Introduction to Scattering

Scattering (light, x-ray and neutron) is a strong method to characterize a wide variety of material properties, e.g. thermodynamic, dynamic and structural features. This study focuses on those properties of the linear ABCBA penta-block terpolymers in aqueous solutions (concentration of 0.5% w/w and 20.0% w/w), which are obtained via measurements of the total intensity of scattering of light and neutron as a function of the scattering angle θ, at different temperatures and pH values.

In all scattering experiments, the intensity is proportional to the square of the sum of the amplitude of the scattered waves from each of the scattering centers, and information about the structure of the system comes from the fact that the scattering center positions are important in determining the angular dependence of intensity. The scattered wave amplitude itself depends on the type of radiation scattered and the nature of the scattering object. For instance, if the scattering center is a particle comparable in size to the wavelength of the radiation used, the amplitudes will also depend on q [3] and the distribution of scattering material within the particle.

Figure 3 shows a schematic scattering process. The scattering centers are represented by circles. Two scattering centers are scattering the beam into a given direction, along which a detector is placed. The $\overline{k_\iota}$ and $\overline{k_f}$ vectors are the propagation vectors of the incident and scattered radiation, respectively that have lengths given by $2\pi/\lambda$ (elastic scattering). The radiation is observed at a scattering angle θ. Scattering vector, $\vec{q}$, the important quantity in all scattering experiments is defined as $\vec{q} = \overline{k_\iota} - \overline{k_f}$.

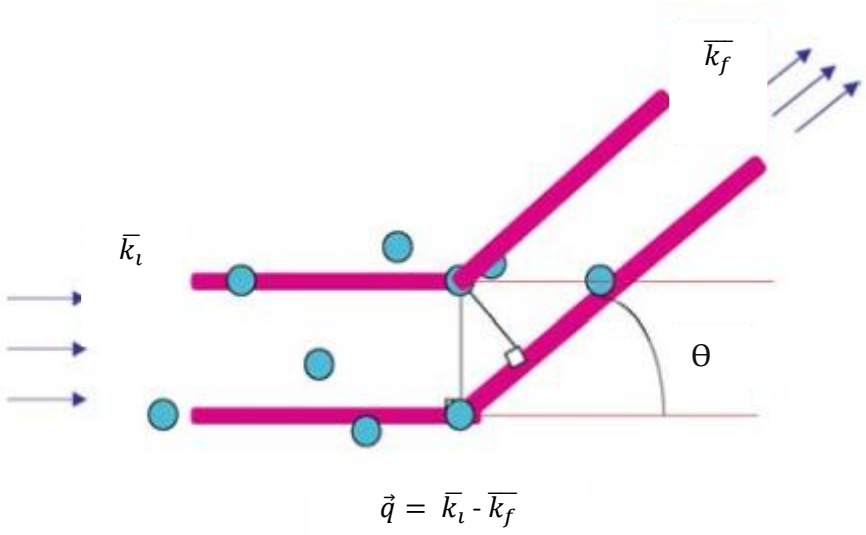

Figure 3- Schematic scattering process

[3] q : scattering wavevector- will be defined in the next paragraph

Given the phase difference between the scattered waves from the two scattering centers and assuming that the radiation wavelength is not changed by the scattering, $\vec{q}$ is related to the scattering angle θ as equation 1 ,

$$q=\frac{4\pi}{\lambda}\sin\left(\frac{\theta}{2}\right) \qquad \text{Eq.1}$$

With different wavelengths used in scattering experiments, structure of the scattering system is determined. The wavelengths, propagation vector lengths and energies used for the three types of radiation in a typical scattering experiment are shown in table 2 [25].

Radiation	Wavelength λ (nm)	Approximate Propagation Vector Length= 2π/λ (nm-1)	Approximate Energy
X-rays	0.05-0.2	~ 0.1	~ 10 keV
Neutrons	0.1-1	~ 0.2	100-1 meV
Light	400-800	~ 0.01	10-20 eV

Table 2- Wavelengths and energies frequently used in scattering experiments

The magnitude of the scattering vector q, not the scattering angle θ, nor the wavelength λ of the probing radiation in the scattering medium, but the ratio of $\sin(\theta/2)/\lambda$, is the appropriate variable in all scattering experiments, irrespective of the wavelength or even the nature of the probing radiation, such as visible light, X-rays, or neutrons. For instance, in case of visible light with wavelengths in the range ~ 350-680 nm, q takes relatively small values even at high scattering angles and therefore the smallest size measured by this range of q is about 10 nanometers (R_h[4]) [26].

In scattering of light or any other wave from micelles or particles, depending on the magnitude of qR_g[5], three regimes are considered; the regimes are the Rayleigh regime where $qR_g << 1$, in which the scattered intensity is constant,

[4] R_h- Hydrodynamic radius

[5] R_g- Radius of gyration

independent of the scattered angle, the Guinier regime where $qR_g < 1$, in which a small angle dependence is seen due to the overall size of the micelle or particle, and a power law for $qR_g > 1$, in which the intensity angular dependence contains information regarding the particle's or cluster's structure [27]. Based on the system properties, data analysis is performed in the appropriate regime.

A brief introduction of each scattering method is discussed in the next sections.

1.2.1 Static Light Scattering (SLS)

The static, time-averaged scattering intensity $<I_s(q)>$ measured as function of scattering wavevector (q) is related directly to the Fourier transform of the density-density correlation function and therefore contains all of the structural information. It is assumed that the intra-particle scattering form factor P(q) and the solution structure factor S(q) combine in $<I_s(q)>$ as

$$<I_s(q)> = KcP(q)S(q) \qquad \text{Eq.2}$$

where K is a contrast factor and c is the mass concentration.

Static light scattering data for polymeric systems are usually analyzed in terms of the classical Zimm equation (Eq. 3), to determine the weight averaged molecular weight (M_w), the z-mean of the square of the radius of gyration ($R_{g,z}^2$), and the second virial coefficient (A_2) :

$$\frac{Kc}{R_\theta} = \frac{1}{M_w}\left(1+\frac{q^2}{3}R_{g,z}^2\right) + 2A_2c \quad (c \to 0\ ,\ \theta \to 0) \qquad \text{Eq.3}$$

where $K= 4\pi^2 n_s^2 (dn/dc)^2/(N_A\lambda_0^4)$, c is the concentration of solution, n_s is refractive index of the solution, dn/dc is the refractive index increment, and N_A the Avogadro's number. R_θ is defined with equation 4:

$$R_\theta = \frac{\Delta<I_s(q)>}{<I_{ref}(q)>} R_{ref}(\theta) \left(\frac{n_s}{n_{ref}}\right)^2 \qquad \text{Eq.4}$$

where $<I_s(q)>$ is the average scattering intensity. The contribution $<I_b(q)>$ from background stray light and solvent was measured using the same cell containing

the filtered solvent only. The background was subtracted from $<I_s(q)>$ yielding $\Delta<I_s(q)>$. The data were then converted into absolute scattering intensities, i.e., "excess Rayleigh ratios" using equation 4, where $R_{ref}(\Theta)= 39.6 \times 10^{-4}$ m^{-1} is the Rayleigh ratio of the reference solvent toluene[28] and n_s and $n_{rel}= 1.499$ are the refractive indices of the solution and the reference solvent, respectively [29].

The angular dependence of the reduced-scattering intensity often contains further information on the micelle or particle shape. In general, Kc/R_θ can be given in the following form for dilute systems:

$$\frac{Kc}{R_\theta} = \frac{1}{M_w}\frac{1}{P_\theta} + 2A_2c \quad (c \to 0) \qquad \text{Eq.5}$$

where P_θ depends on micelle or particle shape [30]. P_θ for a few systems are represented in table 4.

Static light scattering of the systems in the mentioned concentration range (0.5% w/w) will principally focus on optically isotropic polymers (or micelles) which will emphasize polarized scattering. It is assumed that the electric field acting on all parts of the penta-block terpolymers is the same as that acting on the surrounding medium (RGD[6] scattering). In the RGD regime, the scattering from a single polymer chain is taken from the sum of independent Rayleigh scattering from the elements comprising the polymer chain. In this technique, time-averaged properties such as molecular weight, radius of gyration and polymer-solvent interactions are determined.

In scattering at small q values, the mean-square radius of gyration $R_{g,\nu}{}^2$ for the ν-th component is expressed as follows in equation 6,

$$R_{g,\nu}{}^2 = \left(\frac{R_g^2}{M^\varepsilon}\right) M^\varepsilon{}_\nu \qquad \text{Eq.6}$$

where $\frac{R_g^2}{M^\varepsilon}$ and ε are constants for a monodisperse polymer which are determined by theoretical considerations. Here components may differ in molecular weight and/or structure. Table 3 represents $R_g{}^2$ for a few common models.

[6] Rayleigh-Gans-Debye

Model	Length scales	R_g^2
Disk	R= radius	$R^2/2$
Cylinder	L= length	$L^2/12+R^2/2$
Sphere	R= radius	$3R^2/5$
Sphere shell	R= radius (outer) Δ= shell thickness	$\frac{3R^2}{5}\left(\left[\frac{1-\left(\frac{\Delta}{R}\right)^5}{1-\left(\frac{\Delta}{R}\right)^3}\right]\right)$
Sphere shell (extremely thin)	R= radius (outer)	R
Random-flight linear coil	$\hat{a}$=persistence length L= contour length	$\hat{a}L/3$

Table 3- Mean-square radius of gyration for some specific models at small q values

In scattering at an arbitrary q, form factor P(q,0) is taken into consideration. In case of having identical scattering components, P(q,0) for a few commonly used models are represented in table 4 [30-31].

Model	R^2_g	P(q,0)
Disk [7] (extremely thin)	$R^2/2$ y= Rq	$(2y^2)[1-J_1(2y)/y]$
Sphere	$3R^2/5$ y= Rq	$(9/y^6)[\sin(y)-y\cos(y)]^2$
Shell (extremely thin)	R y=Rq	$[\sin(y)/y]^2$
Random-flight linear coil	$\hat{a}\,L/3$ y=$\hat{a}\,Lq^2/3$	$2/y^4[\exp(-y^2)-(1-y^2)]$

Table 4- Scattering functions at an arbitrary q for some specific models

It is necessary to keep the concentration in dilute regime; with increasing the concentration, the effect of interference among the scattered rays from different scattering centers will result in a decrease in the scattering and changing the form factor P(q,c).

[7] $J_1(\ldots)$ is the Bessel function of the first order

Static light scattering also provides a powerful asset to investigate intermolecular (or interparticle) association. In general, two forms might be experienced: 1) association involving two or more components at equilibrium at any given concentration, and 2) metastable association, in which the components present (i.e., including aggregated structures) depend on processing history, but do not change sensibly with concentration in the range of interest for light scattering. Of course, intermediate situations may also occur. Figure 4 depicts different forms of association observed in solution in terms of q^2-dependency of KcM/R(q,c).

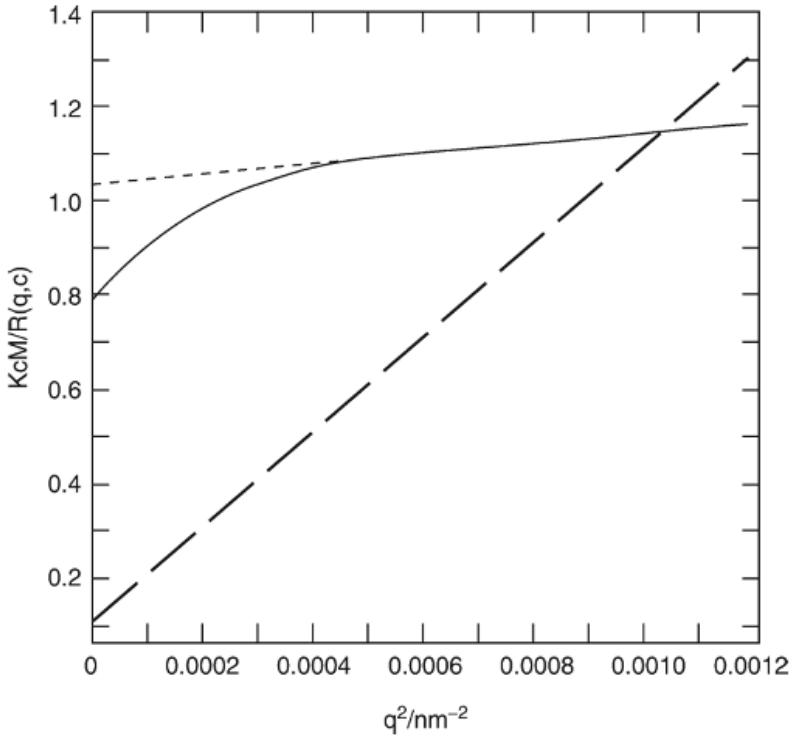

Figure 4- Illustrations of KcM/R(q, c) for two extreme forms of association [31]

In type I association (— —), the aggregates form a loose super-molecular structure which might lead to gelation at a higher component concentration. The molecular weight obtained with this system is much larger than the true value of M_w for the components. In type II association (—), the aggregates are more compact, giving much enhanced scattering in particular at small scattering angle. This is usually taken as an evidence for the presence of an aggregated species mixed with the components that are either fully dissociated, or much less aggregated. The scattering from the fully dissociated polymer is also shown (- - -) [31].

Zimm equation is not the only approximation for analyzing scattering data; Guinier plot for $qR_g < 1$ is used as equation 7, describing the linear relationship between the observed scattering intensities, I(q) and scattering angle (q).

$$\text{Ln } I(q) = \text{Ln } I(0) - (R^2_g/3)\, q^2 \qquad \text{Eq.7}$$

where I(q) is the scattered intensity. This equation is valid regardless of refractive index or morphology, therefore is very useful to determine cluster or particle size through R_g. In order to get a linear plot, usually Ln (I (q)) is plotted versus q^2, and then the slope would be $R^2_g/3$[27, 32].

To qualitatively analyze random coils or to detect branching and compactness especially for protein and biopolymer structures, Kratky plot is usually a useful approach to get a rough impression from the data. Here $q^2.I(q)$ is plotted versus q and changes in the behavior of the curve reveal the system structure [32].

1.2.2 Dynamic Light Scattering (DLS)

In DLS, time-dependent properties based on local intensity fluctuations of the scattered light are determined.

In the solutions of block copolymers or particles, the experimentally recorded intensity autocorrelation function $g^2(q,t)$ is directly related to the first order electric field autocorrelation $g^1(q,t)$ through the Siegert [33] equation (Eq.8):

$$g^2(q,t) = 1 + B|g^1(q,t)|^2 \qquad \text{(Eq.8)}$$

where B (≤1) is an instrumental parameter. Based on the size-related properties in the solution system, some of the correlation functions are fitted by a single stretched exponential equation as follows (Eq.9):

$$g^1(t) = A \exp\left[- (t/\tau_{se})^b \right] \qquad \text{Eq.9}$$

where A is the amplitude for relaxation time, and in some cases, the sum of a single exponential and a stretched exponential is used (Eq.10):

$$g^1(t) = A_f \exp\left[- (t/\tau_f)\right] + A_s \exp\left[-(t/\tau_{se})^b\right] \qquad \text{Eq.10}$$

with $A_f + A_s = 1$. The parameters A_f and A_s are the amplitudes for the fast and the slow relaxation time, respectively. The variables τ_f and τ_{se} are the relaxation times characterizing the fast and the slow process, respectively. The parameter b ($0< b \leq 1$) is related to the width of the distributions of relaxation times. The mean relaxation time for the slow mode is given by equation 11:

$$\tau_s = \frac{\tau_{se}}{b}\,\Gamma\left(\frac{1}{b}\right) \qquad \text{Eq.11}$$

where $\Gamma(x)$ is the gamma function.

When the fast and slow relaxation modes are diffusive (q^2- dependent), i.e., $D_f = (1/\tau_f)/q^2$ and $D_s = (1/\tau_s)/q^2$ [8], the apparent hydrodynamic radii R_h of the species (assuming a spherical shape in the dilute solution) can be calculated by using the Stokes–Einstein equation (Eq.12-a , 12-b) :

$$R_{hf} = \frac{k_B T}{6\pi\eta D_f} \qquad \text{Eq.12-a}$$

$$R_{hs} = \frac{k_B T}{6\pi\eta D_s} \qquad \text{Eq.12-b}$$

where k_B is the Boltzmann constant, T is the absolute temperature, η is the viscosity of the solvent, and D is the mutual diffusion coefficient [34].

The ratio of the average distance traveled by a photon in the medium before it is being scattered, L_p, and the light path, L_L, in the sample provides a guide on how much scattering is to occur in the sample. For $L_p/L_L >> 1$, most of the photons pass through the sample un-scattered, i.e., most of the light is being transmitted. The sample is transparent and single scattering dominates. If $L_p/L_L \sim 1$, both single scattering and multiple scattering exist. Then, the sample is turbid, but light is still being partially transmitted. This is the condition in which cross-correlation techniques have been developed. Finally, for $L_p/L_L << 1$ the sample is opaque, implying that a photon is scattered many times before it can pass through the

[8] D_f and D_s are apparent diffusion coefficients for faster and slower modes, respectively.

sample. This is called multiple scattering conditions and cross-correlation technique is not applied simply like it does for single scattering. In this study, it was verified that the scattering measurements were performed under the single scattering condition [26].

1.2.3 Small Angle Neutron Scattering (SANS)

SANS is a powerful technique to analyze the size, shape, intra- and inter-structures of complex systems with typical size ranging from a few nanometers to tenths of a hundred nanometers. The difference of scattering length densities between isotopes and in particular between hydrogen and deuterium atoms is the basis of SANS experiments. One of the main sources of neutrons is steady-state reactors which produce neutrons by fission processes. Different institutes have developed data treatment programs for SANS instruments, all of them obtain the absolute intensity as a function of q. The intensity per unit volume V of N_p homogeneous isotropic scatterers of volume V_p and coherent length scattering density k_p dispersed in a medium of length scattering density k is the product of the form factor and the structure factor weighted by a contrast factor K_c follows:

$$I(q) = \Phi V_p \Delta k^2 P(q) S(q) = K_c P(q) S(q) \qquad \text{Eq.13}$$

Φ is the polymer volume fraction. Δk is the difference of length scattering densities between particle and medium. P(q) (as it was mentioned in 1.2.1 SLS) is called the particle form factor and describes the geometry of the scattering object. P(q) tends to 1 for q=0 or at small qR_g. S(q), the structure factor describes the correlation between particle mass centers and goes to 1 at high q for systems without long-range intermolecular order [35].

k, P(q) and S(q) are determined considering the system properties. For example, the form factor of homogeneous sphere of radius R is:

$$P_s(q,R) = [F_s(q,R)]^2 \qquad \text{Eq.14}$$

and

$$F_s(q,R) = [\, 3 \frac{\sin(qR) - (qR)\cos(qR)}{(qR)^3}]$$

S(q) is related to the pair correlation function (or radial distribution function) g(r), in case of isotropic interactions it becomes as follows:

$$S(q) = 1 + 4\pi \frac{N}{V} \int_V (g(r) - 1)\, r^2 \frac{\sin qr}{qr}\, dr \qquad \text{Eq. 15}$$

where N is related to elastically scattered incident flux.

Typically, the structure factor is a dimensionless oscillatory function that tends to unity at high q and equals 1 for dilute solutions where intermolecular interactions can be neglected. The experimental structure factors can be obtained by measuring the absolute intensity at two particle concentrations and by dividing the scattering at the highest concentration by the one at lowest concentration in dilute condition.

* * *

SLS, DLS and SANS provide complementary information on the system structure. The combination of scattering methods with electron microscopy which is an excellent technique to study the morphology of the system, offers a more reliable image of the sample.

1.3 Introduction to sol-gel transition

Hydrogels as a special class of polymer networks have received great attention in drug delivery and tissue engineering owing to the hydrophilic network, prolonged delivery period, low dosage of drug and alleviation of the side effects by protection of drugs from hostile environment in the body [36]. Stimuli-responsive polymers with sol-gel transition have eased the gel application into the body, since there would be no surgical procedures to insert the gel; therefore drugs can be mixed homogeneously with the polymer solutions and simply injected at target sites. Physical conditions in the target sites (temperature, pH and etc.), trigger a gel formation from the injected solution, and ultimately by degradation of the hydrogel release the drug [36-38].

In this work, the rheological behavior of PDEAEMA$_x$-*b*-PNIPAAM$_y$-*b*-PEG$_z$-*b*-PNIPAAM$_y$-*b*-PDEAEMA$_x$ together with small angle light scattering (SALS) was

studied by imposing a small-amplitude oscillatory shear strain, to monitor the sol-gel transition at higher concentration (20.0% w/w). In order to have a better understanding of the polymer system, a steady shear stress was applied on the solutions in lower concentrations (0.5% w/w) and rheological responses were measured as well.

1.3.1 Rheometry

For solution systems, the simplest rheometers impose a shearing flow on the sample and measure the resulting stresses, or alternatively, impose a shearing stress and measure the resulting shearing rate. There are different geometries for producing shearing flows, such as sliding plates, concentric cylinders (Couette flow), cone and plate and parallel disks (Figure 5).

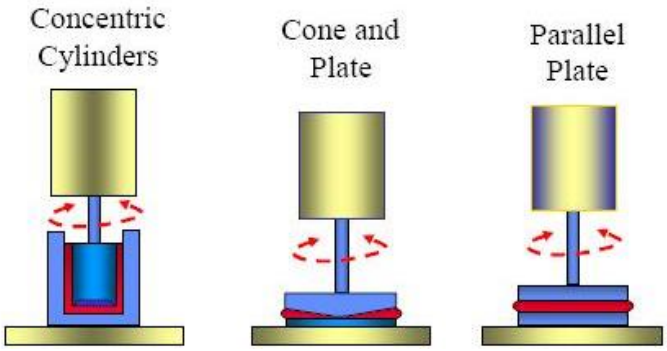

Figure 5- Different geometries for shearing flow rheometers[9]

Each geometry could be the best choice for a special purpose [39]. In this study, cone and plate and parallel disks were used.

In steady shear rate measurements, the applied shear rate in the cone and plate geometry is $\dot{\gamma} = \Omega/\tan\delta$, where Ω is the steady angular rotation speed of the cone or plate (the one is rotating), and the steady-state shear viscosity is the ratio of the steady shear stress σ to the shear rate $\dot{\gamma}$: $\eta=\sigma(\dot{\gamma})/\dot{\gamma}$.

In small-amplitude oscillatory shearing, in cone and plate geometry, the cone oscillates about its axis with an angular velocity that oscillates sinusoidally,

[9] http://plastics.tamu.edu/knowledgebase

$\Omega(t)=\Omega_0 \cos(\omega t)$, where ω is the frequency of oscillation (rad/sec). The shear rate ($\dot{\gamma}$) and shear strain γ are then also sinusoidal functions of time.

In general, the sinusoidally varying stress due to the applied strain (rotation of cone for instance) can be presented as equation 16:

$$\sigma(t)= \gamma_0 [G'(\omega) \sin(\omega t) + G''(\omega) \cos(\omega t)] \qquad \text{Eq.16}$$

where $G'(\omega)$ and $G''(\omega)$ are called storage modulus and loss modulus, respectively. The regime of small amplitude strain in which equation 16 is valid, is called the linear viscoelastic regime [39]. The ratio of G''/G' is called the loss tangent, $\tan \delta$. It has been found that $\tan \delta$ decreases during the gel formation, indicating that the solutions become more and more elastic [40]. In case of sol-gel transition by changing the temperature, frequency-independence of loss tangent, $\tan \delta$ is one of the rheological methods to determine the gel point. The scaling law and the frequency-independence of $\tan \delta$ in the vicinity of the gel point, is expressed by equation 17-a and 17-b:

$$G'(\omega) \sim G''(\omega) \sim \omega^n \quad (0 < n < 1) \qquad \text{Eq. 17-a}$$

$$\tan \delta = G''(\omega)/ G'(\omega) = \tan (n\pi/2) = \text{constant} \qquad \text{Eq. 17-b}$$

where n is the scaling exponent (or critical relaxation exponent). Therefore, the gelation temperature can be determined from a multi-frequency plot of $\tan \delta$ versus temperature [41].

The slopes of G' and G'' values as functions of oscillation frequency provide information on viscoelasticity of the system. For polymeric liquids $G' \sim \omega$, $G'' \sim \omega^2$ and $G' < G''$[42]. In case of forming a gel network at a right concentration of the sample, it has been found that $G' \sim \omega^{n1}$ and $G'' \sim \omega^{n2}$ [43] and a low exponent (i.e., $n_1 < 0.5$) usually indicates a highly ordered 3-D structure inside the gel (e.g., a close hard-sphere packing or a rigid continuous network formation) [44]. For strong cross-linked gels, G' has higher value than G'' ($G' > G''$), the frequency sweep exhibits an almost flat profile, due to the almost infinite lifetime of their network, (G' and G'' independent of the frequency). Finally for the intermediate case of weak gels, G'

has yet higher value than G'' (G'>G'') in the high frequency region, where the lifetime of the network junctions is superior to the measurement time, but this relation reverses in the low frequency region, i.e., for long measurement times. The average relaxation time τ is then a key parameter to determine the lifetime of a network and can be taken as the inverse of the radial frequency (ω= 2πf) at ω_c for which G' and G'' cross (equation 18).

$$\tau = 1/\omega_c(s) \qquad \text{Eq. 18}$$

It has been found that for soft gels G'≈G'' ($n_1 \approx n_2$)[42, 45]. The n_1 exponent is determined from a log-log plot of storage modulus G' versus frequency ω. The higher exponent can be an indication of less organized gel structure [46].

The linear viscoelastic properties of incipient gels can be characterized by the gel strength parameter S [40, 47], that depends on the cross-linking density and the molecular chain flexibility. The gel strength is defined by equation 19:

$$G' = S\omega^n \Gamma(1-n) \cos\delta \qquad \text{Eq.19}$$

where Γ(1-n) is the gamma function.

1.3.2 Physical Gels

Physical gels are three-dimensional networks cross-linked by physical bonds. The binding energy is of the order of thermal energy; therefore crosslinks can be reversibly formed and destroyed by a change in temperature, for instance. If the crosslinks are sufficiently weak to be created and destroyed by the thermal motion of the constituents, the gels are often called thermoreversible gels.

Networks could be perfect or just made by random crosslinking of the primary polymers (Figure 6). In this case the network has free-end chains or dangling chains.

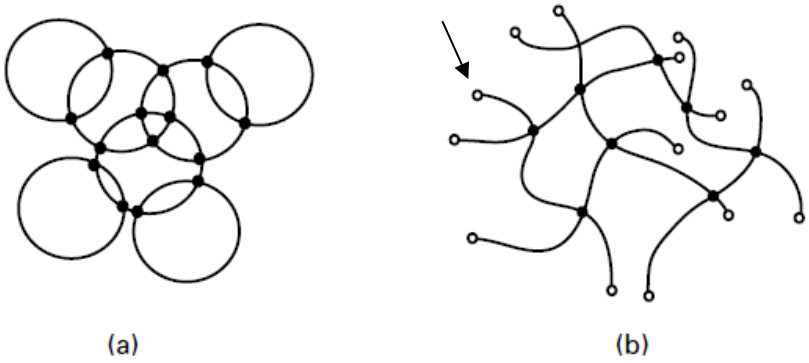

Figure 6- Model networks: (a) perfect network, (b) network made by random cross-linking of primary polymers

The origin of crosslinks depends on the polymer chain properties. Figure 7 shows the various types of physical crosslinks [48].

Hydrogen bonding- H-bonds between polymer chains form pairwise crosslinks and bridge them. The binding energy of an H-bond in a solution is of the order of the thermal energy, so that the bonds may easily break and recombine.

Dipole interaction- If polymers carry dipole moments that are sparsely dispersed along the chains, they are crosslinked by aggregation of the dipole moments.

Hydrophobic association- Water-soluble polymers carrying hydrophobic groups, such as short alkyl chains, fluorocarbon chains, etc., form gels by micellization of the hydrophobic groups in water. Micelles serve as the crosslinks that can dissociate and associate by temperature, external force, added agents, etc.

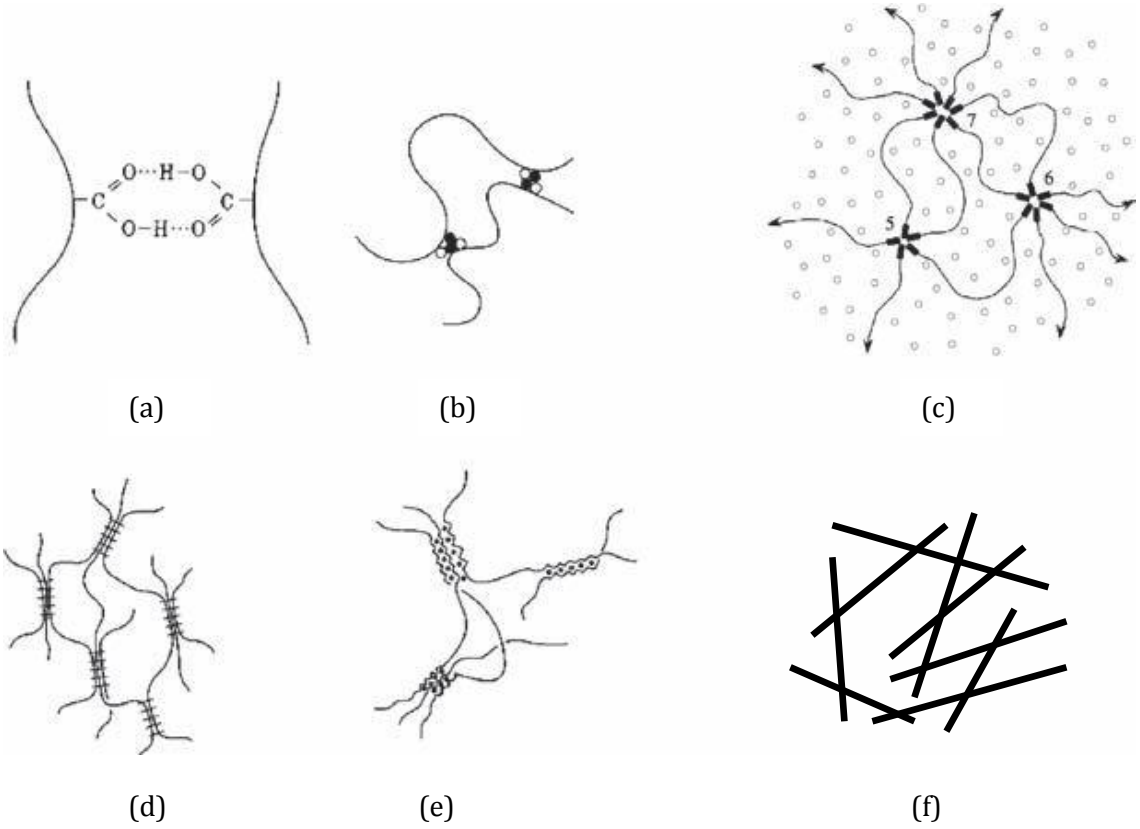

Figure 7- Various types of physical crosslinks: (a) hydrogen bonds, (b) dipole association, (c) micellar formation of hydrophobic groups, (d) microcrystalline junction, (e) ion association and complex formation, (f) entanglements of long rigid polymers.

Gels with microcrystalline junctions- When crystallizable polymers are quenched below their melting point, they often form gels with microcrystals involving many chains at their junctions.

Complex formation- Gels with zipper-like cross-links of sequential H-bonds, with double or triple helices and with egg box-shaped complexes involving ions, may be classified as gels with extended junction zones of complexes. Conformation change of prepolymers is necessary to form such complex junction zones, so that coil‑helix transition often takes place before gelation.

Entanglement- Entanglements of long rigid polymers in concentrated solutions and melts often lead to gel-like rheological properties. The entanglements are created and destroyed by the thermal motion of the polymers or by external force.

1.3.3 Theory of Gelation

There are several experimental theories on gelation; a few of them are briefly described as follows. Each theory includes several simplifying assumptions which might not be valid in real systems [49].

Branching theory- Branching models are based on multifunctional molecules of different types between which covalent bonds are formed to yield a network structure. One of the multifunctional molecules is required to carry at least three functional groups, while the other one can have two functional groups (Flory [50] and Stockmayer [51]).

Percolation theory- Percolation theory describes [52] the random growth of molecular clusters on a 2-dimensional lattice. In random bond percolation, which is one of the most widely used to describe gelation, monomers, occupy sites of a periodic lattice. The network formation is simulated by the formation of bonds between nearest neighbors of lattice sites (Figure 8). Since these bonds are randomly placed between the lattice nodes, intra-molecular reactions are allowed.

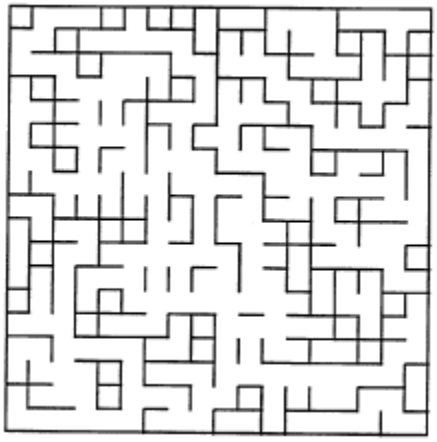

Figure 8- A two-dimensional square lattice, each bond that has been formed is shown as a short line connecting two monomers, while the monomers are not shown

Scaling theory- Scaling theories yield unique scaling relationships with appropriate exponents for molecular (e.g. mean cluster size, size distribution) and bulk properties (e.g. equilibrium modulus) near the gel point.

Fractal theory- Based on the fractal behavior of the polymer gel, several different relationships between the critical exponent n and the fractal dimension d_f have been proposed. The fractal dimension d_f of the polymer cluster is commonly defined by equation 20 [53].

$$R \propto M^{1/df} \qquad \text{Eq. 20}$$

Muthukumar and Winter [54] investigated the behavior of monodisperse polymeric fractals following Rouse chain dynamics, i.e. Gaussian chains (excluded volume fully screened) with fully screened hydrodynamic interactions. They predicted that n and $\overline{d_f}$(the fractal dimension of the polymer if the excluded volume effect is fully screened) are related by equation 21:

$$n = \frac{\overline{d_f}}{2 + \overline{d_f}} \qquad \text{Eq. 21}$$

Muthukumar [55] further investigated the effects of polydispersity, which are important for crosslinking systems. If the excluded volume is not screened, n is related to d_f by equation 22:

$$n = \frac{d_f}{2 + d_f} \qquad \text{Eq. 22}$$

In the case of full screening of excluded volume he obtained equation 23:

$$n = \frac{d_f}{2 + \overline{d_f}} = \frac{d(d+2-2d_f)}{2(d+2-d_f)} \qquad \text{Eq. 23}$$

Especially in the latter case, a small change in the fractal dimension can lead to a significant change in n, and he therefore concluded that n can take values between 0 and 1 (for d_f ranging from 2.5 to 1.25, see Figure 9).

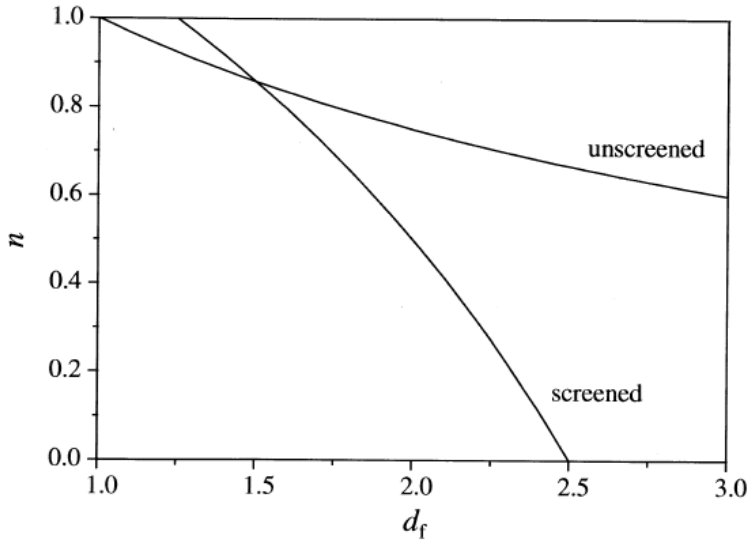

Figure 9- Relation between relaxation exponent n and fractal dimension d& for a three-dimensional network. In case of complete screening of excluded volume, values of 0<n<1 are possible if d_f is chosen between 1.25 and 2.5

1.3.4 Rheo-SALS

In this section, self-assembly and rheological behavior of the polymer systems in aqueous solutions under shear fields are investigated and observed with a combination of rheometry and Small Angle Light Scattering (SALS).

The principle of this method, is applying a shear strain on the sample which is placed in the cell, (in this study) composed of two parallel transparent plates. The shear strain is applied by rotating the lower plate and shear force and normal force from the sample are measured by a stress transducer fixed to the upper plate of the cell. Incident beam goes from the lower plate and after passing the sample, the patterns of the scattered light are recorded by a CCD[10] camera [56].

Figure 10 represents a schematic illustration of Rheo-SALS instrument [57].

[10] Charge Coupled Device

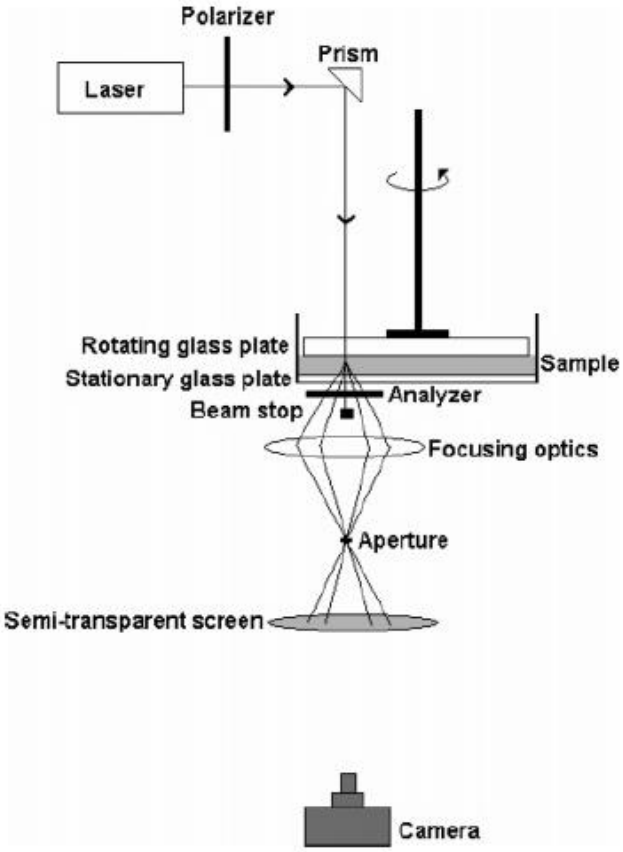

Figure 10- Schematic diagram for a Rheo-SALS apparatus

* * *

In the next section, experimental conditions and instruments for characterization of PDEAEMA$_x$-*b*-PNIPAAM$_y$-*b*-PEG$_z$-*b*-PNIPAAM$_y$-*b*-PDEAEMA$_x$ are elaborated.

2 Experimental

2.1 PDEAEMA$_x$-b-PNIPAAM$_y$-b-PEG$_z$-b-PNIPAAM$_y$-b-PDEAEMA$_x$ Synthesis

The penta-block terpolymers, De$_1$Ni$_1$PEG$_1$, De$_{0.8}$Ni$_{1.2}$PEG$_{2.3}$ and De0.$_1$Ni$_1$PEG$_2$ were synthesized by ATRP[11] procedure; M_n and PDI were measured by both ^{1}H NMR and GPC. The whole synthesis part and M_n and PDI measurements were performed by Dr. Kaizheng Zhu in the Polymer Group, Department of Chemistry, University of Oslo (UiO).

[11] Atom Transfer Radical Polymerization

2.2 Fluorescence Spectroscopy

The formation of micellar structures was confirmed by a fluorescence technique using pyrene as a probe. Steady-state fluorescence spectra were obtained by Infinite® M200 (Tecan Group Ltd.) microplate reader spectrophotometer. Fluorescence emission spectra were recorded at wavelength λ_{em} = 320 nm and excitation wavelength λ_{ex} was set at 310 nm. The intensity ratios of the first to the third vibronic peak (I_1/I_3) in the emission spectra of the monomer pyrene were used to estimate the polarity of the pyrene microenvironment. The steady-state fluorescence spectra of a series of polymer micelle aqueous solutions in PBS (pH 3.0, pH 7.4 and pH 9) with the polymer concentration in the range of 2.5×10^{-11} to 2×10^{-4} g/mL were measured. Pyrene solutions were prepared by adding known amounts of pyrene dissolved in acetone into dry volumetric flasks. After evaporation of the acetone, polymer solutions were added to make a final pyrene concentration of 6.0×10^{-7} M[5, 58] .The solutions were kept overnight at 25 °C to equilibrate pyrene with the polymer solutions. All fluorescence spectra were recorded at 25 °C. By the profile of relative intensity I_{rel}, the intensity ratio of polymer solutions to the solvent I_p/I_s (both have the same concentration of pyrene) as a function of polymer concentration, the critical micelle concentration (CMC) was determined.

2.3 Densitometry

LCST of the solutions was investigated by density measurements. Solution densities were determined with a densitometer DMA 5000 (Anton Paar, Graz), which uses the oscillating-tube technique. The density determination is based on measuring the period of oscillation of a vibrating U-shaped hollow tube that is filled with the sample and using the relationship between the period of oscillation and the density. The densitometer was calibrated daily at 20 °C, using air and water as reference samples. The sample volume needed was approximately 1.5 mL and all measurements were performed with fresh samples at concentration of about 1.0 w/w% (the accurate value of concentrations are considered in the calculations, with a precision of five decimal places). The temperature was

increased from 20 to 50 °C in steps of 1 degree. The measured density in g/cm^3 is converted to apparent specific volume of the polymer by equation 24:

$$v_{polymer} = \left(\frac{1}{c_{polymer}}\right)\left(\frac{1}{\rho_m}\right) - \left(\frac{1 - c_{polymer}}{c_{polymer}}\right)\left(\frac{1}{\rho_s}\right) \qquad \text{Eq. 24}$$

where ρ_m is the measured density of the sample, ρ_S the measured density of solvent, and $C_{polymer}$ the weight fraction of the polymer. In this study, PBS and heavy water (D_2O) at different pH values were used as solvents.

In the case of a copolymer consisting of for example two blocks, B_1 and B_2, assuming additivity of the volume contributions of B_1 and B_2, the apparent specific volume of the copolymer can be estimated as equation 25:

$$v_{polymer} = m_{B1}v_{B1} + m_{B2}v_{B2} \qquad \text{Eq.25}$$

where m_{B1} and m_{B2} are the mass fraction of the two blocks B_1 and B_2, and v_{B1} and v_{B2} are the specific volume (in cm^3/g) of B_1 and B_2 in the polymer, respectively [59]. Apparent specific density $D_{polymer}$ is simply the reciprocal of the apparent specific volume $v_{polymer}$.

2.4 Turbidimetry

The turbidity experiments were conducted on an NK60-CPA cloud point analyzer from Phase Technology, Richmond, BC, Canada. A detailed description of the equipment and determination of turbidities have been given in another study [60]. The apparatus utilizes a scanning diffusive technique to characterize phase changes of the sample with high sensitivity and accuracy. The light beam from an AlGaAs light source, operating at 654 nm, was focused on the measuring sample that was applied onto a specially designed glass plate that was coated with a thin metallic layer of very high reflectivity (mirror). Directly above the sample, an optical system with a light-scattering detector continuously monitored the scattered intensity signal (S) of the sample as it is subjected to prescribed temperature alterations. The relation between the signal and the turbidity (κ) is given by the following empirical relationship $\kappa\ (cm^{-1}) = 9.0 \times 10^{-9}\ S^{3.751}$. The temperature at which the first deviation of the scattered intensity from the baseline occurred was taken as the cloud point (CP) of the considered sample [61].

In these experiments, the heating rate was set to 0.5 °C min^{-1}. The turbidity values were determined for the penta-block terpolymer solutions with the concentrations of 0.5% w/w in both D_2O and PBS and with 20.0% w/w in PBS of different pH values and over a temperature range from 25 to 50 °C.

2.5 Proton Nuclear Magnetic Resonance (^{1}H NMR) Spectroscopy

Change of micelle structure in the polymer solutions at different temperatures and pH values was confirmed by ^{1}H NMR spectroscopy. All ^{1}H NMR spectra were recorded using a Bruker DRX 500 MHz spectrometer. Each penta-block polymer was prepared in the concentration of 0.5% w/w in D_2O and pH was adjusted to 3.0, 7.4 and 9.0 using small drops of 1M DCL and 1M NaOD. The spectra were recorded at 25° C, 37°C and 52°C.

2.6 Zeta (ζ) potential measurements

ζ-potential measurements were performed on a Malvern Zetasizer Nano ZS (Malvern Instruments Ltd., Worcestershire, UK). The ζ- potential was determined from the electrophoretic mobility (U_E) by applying the Henry equation,
$U_E = 2\varepsilon\zeta\, f(Ka)/3\eta$, where the viscosity (η) and the dielectric constant (ε) for pure water were used. The Smoluchowski approximation to Henry's function (f(Ka) = 1.5) was applied. The electrical conductivity was also measured by the Zetasizer Nano ZS. The measurements were conducted for polymer solutions with the concentration of 0.5% w/w in D_2O and PBS in different pH values and over a temperature range from 25 to 60 °C with the heating rate of 0.5 °C min^{-1}. The sample cell used was a dip-cell, including palladium electrodes with 2 mm spacing, one 12 mm glass cell PCS1115 cuvette, and a cap [62].

2.7 Laser Light Scattering (LLS)

Dynamic and Static light scattering (DLS and SLS) experiments were conducted using an ALV/CGS-8F multi-detector version compact goniometer system, with 8 fiber optical detection units, from ALV-GmbH., Langen, Germany. The beam from a Uniphase cylindrical 22 mW HeNe laser, operating at a

wavelength of 632.8 nm with vertically polarized light, was focused on the sample cell (10-mm NMR tubes, Wilmad Glass Co., of the highest quality) through a temperature-controlled cylindrical quartz container (with 2 plane-parallel windows), which is filled with a refractive index matching liquid (cis-decalin). The temperature in the container was controlled to within ±0.01 °C with a heating/cooling circulator. The polymer solutions were filtered in an atmosphere of filtered air through a 5 μm filter (Millipore) directly into pre-cleaned NMR tubes. The correlation function data were recorded continuously with an accumulation time of 3 min. The solutions were prepared in the concentration of 0.5% w/w in D_2O and PBS at different pH values and over a range of temperature from 25 to 60 °C with the heating rate of 0.5 °C min^{-1} and a 10 min equilibrium time in each temperature. The measurements proceeded up to the temperature that the solutions became so turbid, multiple scattering was observed and single scattering no longer existed.

The refractive indices of all samples were measured on a PTR 46 refractometer (Index Instruments, UK) with a wave length of sodium yellow 589 nm and over a range of temperature from 25 to 50 °C with a temperature accuracy of ±0.1 °C.

In DLS, equations 8-12 were used to analyze the correlation functions. In SLS experiments the angular dependence of the reduced time-average scattering intensity, known as the excess Rayleigh ratio, R_Θ, was measured. SLS measurements were carried out with the same optical system as DLS measurements but with a smaller angular step. SLS data were analyzed typically by a Zimm plot. In cases of significant nonlinearity of the Zimm plot, a Berry plot equation was used for the extrapolation. For a dilute solution of concentration c, the Berry equation can be written as equation 26:

$$\left(\frac{Kc}{R_\Theta}\right)^{1/2} = \left(\frac{1}{M_w}\right)^{1/2}\left(1+\frac{<R_g^2>q^2}{6} + A_2M_wc + \ldots\right) \qquad \text{Eq.26}$$

here, $K= 4\pi^2n_s^2(dn/dc)^2/(N_A\lambda_0^4)$, dn/dc is the differential refractive index increment of the solution, N_A is Avogadro's number, M_w is the weight-average molecular weight, $<R_g>$ is the z-average root-mean-square radius of gyration, and A_2 is the second virial coefficient. At low concentrations the effect of A_2 is negligibly

small. Therefore extrapolation to zero concentration was unnecessary. Extrapolation to zero scattering angle yielded the M_w, while the fit of the angular dependence of $Kc/R_\theta(q)$ produced an apparent R_g. The reference solvent used in this study was toluene. The average intensity of scattered light (I) was measured at a wide range of angles and the polymer solvent (D_2O at different pH values) scattering under identical conditions was subtracted from it. The refractive index increment (dn/dc) of the solutions was obtained by linearly fitting of refractive index data in different concentrations [63].

2.8 Small Angle Neutron Scattering (SANS)

The SANS measurements were conducted at JEEP-II reactor in IFE, Norway. A liquid nitrogen cooled 15 cm long Be filter is installed in the beam path to remove fast neutrons (cutoff at a wavelength of λ= 4 Å), and additional 15 cm Bi filter removes the γ radiation. The wavelength was set with the aid of a selector (Dornier), using a high FWHM [12] for the transmitted beam ($\Delta\lambda/\lambda$= 20%) and maximized flux on the sample. The beam divergence was set by an input collimator (18.4 or 12.2 mm diameter) located 2.2 m from the sample, together with a collimator that was fixed to 4.9 mm. The neutron detector was a 128 × 128 pixel, 59 cm active diameter, ^{3}He-filled RISØ-type detector, which is mounted on rails inside an evacuated detector chamber. The distance varied from 1.0 to 3.4 m and the wavelength between 5.1 and 10.2 Å, giving a wavevector range from 0.008 to 0.3 $Å^{-1}$. The wavevector q is given by $q = (4\pi/\lambda) \sin(\theta/2)$, where θ is the scattering angle. The polymer solutions were held in 2 mm quartz cuvettes, which were equipped with stoppers. The measuring cells were placed onto a cooper base for good thermal contact and mounted in the sample chamber. The experiments were carried out at different temperatures in the range 25-50 °C (temperature controlled to within (0.1 °C). In all the SANS measurements, deuterium oxide was used as a solvent instead of light water to obtain good contrast and low background for the neutron-scattering experiments. Standard reductions of the scattering data, including transmission corrections, were conducted by

[12] Full Width Half Maximum

incorporating data collected from empty cuvette, beam without cuvette, and blocked-beam background.

The penta-block terpolymers solutions were prepared in D_2O with the concentrations of 0.5% w/w and 20.0% w/w at different pH values. pH were adjusted with small drops of 1M HCL and 1M KOH in D_2O, assuming a negligible alteration of the contrast.

2.9 Rheometry and Rheo-SALS

Steady shear viscosity measurements were performed on a Paar-Physica MCR 300 rheometer using a cone-and-plate geometry, with a cone angle of 1° and a diameter of 75 mm. The samples were introduced onto the plate, and to prevent evaporation of the solvent, the free surface of the sample was always covered with a thin layer of low viscosity silicone oil. (The viscoelastic response of the samples is not observed to be affected by this layer.) The measuring unit is equipped with a temperature unit (Peltier plate) that provides a rapid change of the temperature and gives an accurate temperature control (±0.05 °C) over an extended time for all the temperatures considered in this work.

For these experiments, the penta-block solutions with the concentrations of 0.5% w/w in PBS with different pH values were prepared. Firstly, viscosity-temperature profile over a range of temperature from 25 to 60 °C with the heating rate of 0.5 °C min^{-1} in a low shear rate (1 s^{-1}) and then viscosity-shear rate profile in a few selected temperatures from the first experiments were investigated over a range of shear rate from 0.001 to 1000 s^{-1}.

Rheological and Small Angle Light Scattering (Rheo-SALS) measurements were conducted on a Paar-Physica MCR 300 plate-plate rheometer. Small angle light scattering and oscillatory shear measurements were performed simultaneously. The plate diameter was 43 mm and the gap between the plates 1.0 mm. The small distance between the plates reduces the effect of multiple scattering when the sample becomes turbid at elevated temperatures.

A 10 mW diode laser operating at a wavelength of 658 nm was used as the light source allowing an approximate accessible scattering wavevector (q) range between $q = 4 \times 10^{-4}$ nm^{-1} and $q = 2 \times 10^{-3}$ nm^{-1}; here q is defined as $q = (4\pi/\lambda) \sin(\theta/2)$, where λ is the wavelength of the incident beam and θ is the scattering angle.

Two-dimensional pictures were captured with a CCD camera (driver LuCam V. 3.8) every 120th seconds. A detailed description of the Rheo-SALS set-up has been given in another study [57].

Experiments were conducted on the solutions of 20.0% w/w in PBS of different pH values over a range of temperature from 25 to 60 °C with the heating rate of 0.5 °C min^{-1} under an increasing angular frequency from 0.01 rad/s to 100 rad/s with 10% amplitude for shear strain.

3 Results and Discussion

3.1 Fluorescence Spectroscopy

Self-assembly of block polymers into micellar structures requires certain physical-thermodynamical circumstances. In this work, the critical micelle concentration (CMC) of the ABCBA penta-block terpolymers was determined by fluorescence spectroscopy, using pyrene as the probe. The effects of block length of the polymers, pH and ionic strength of the PBS used as the solvent were investigated. Figure 11 shows the variation of the fluorescence relative intensity as a function of the polymer concentration at different pH values.

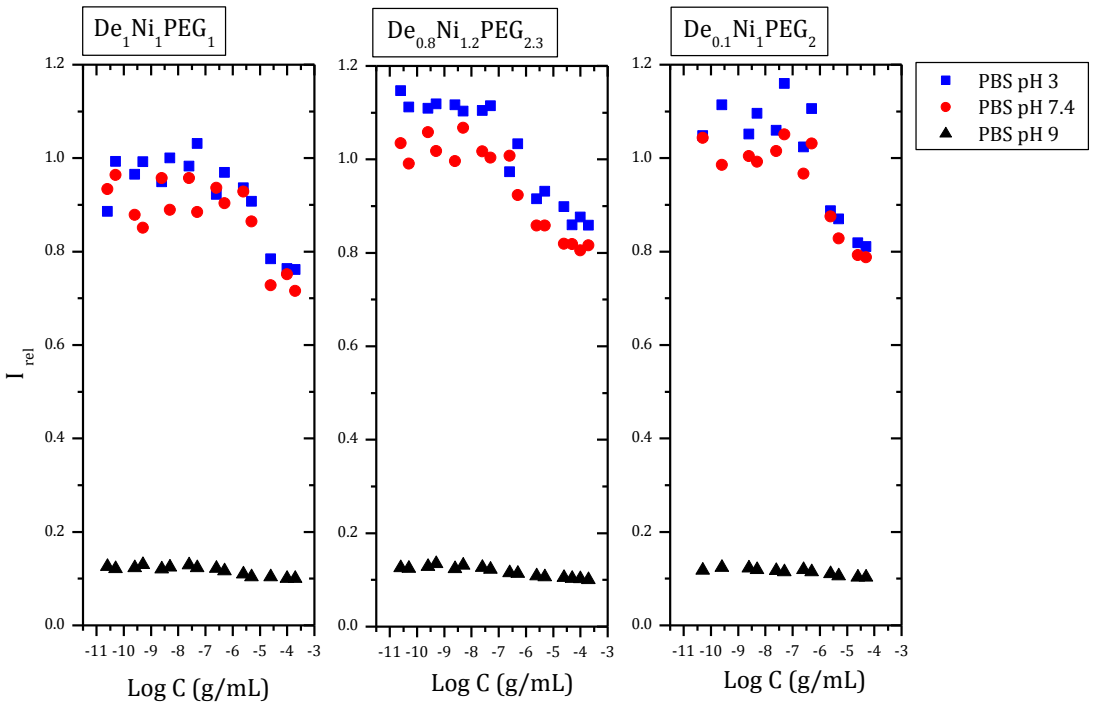

Figure 11 – Fluorescence spectra of ABCBA penta-block terpolymers

It is clear that the relative intensity at higher pH is lower and at lower pH exhibits higher values. The difference is ascribed to protonation/deprotonation state of PDEAEMA at different pH values [64]. At PBS pH 3 and PBS 7.4 the PDEAEMA block in PDEAEMA$_x$-*b*-PNIPAAM$_y$-*b*-PEG$_z$-*b*-PNIPAAM$_y$-*b*-PDEAEMA$_x$, is protonated, while at PBS pH 9 it becomes deprotonated and hydrophobic. The deprotonation is ascertained from pyrene interaction within the ABCBA penta-block terpolymer and consequently the significant change of the relative intensity of fluorescence spectra by changing the pH from 3 and 7.4 to 9. As it is well-accepted, pyrene as one of the most commonly used polarity-sensitive chromophores, is solubilized favorably within the hydrophobic micro-environment (Figure 12) [65]. At pH 3 and 7.4, pyrene is located on the partially hydrophobic blocks within the ABCBA penta-block terpolymer, while at pH 9, PDEAEMA blocks become fully hydrophobic and pyrene is bound to the hydrophobic blocks of the pre-micellar associations or the collapsed core of the micelles at higher concentrations.

Figure 13 demonstrates CMC determination at different pH values at a close range. It has been indicated that pyrene exhibits five well-resolved vibronic bands between 370 and 400 nm, and the intensity ratio of the first vibronic band to the third (I_1/I_3) is significantly dependent on its local polarity [66].

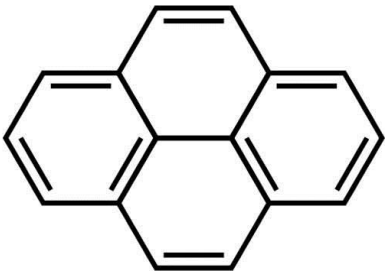

Figure 12 – Structure of pyrene , C_6H_{10}

At the concentrations below CMC, pyrene is located on the hydrophilic unimers or semi-hydrophilic structures; as the chains associate into the micelles, pyrene is transferred to the hydrophobic segments within the micelles, therefore I_{rel} (I_1/I_3) decreases rapidly; the turning point is considered as CMC. The CMC values were summarized in table 5. The expected trend is that by increasing pH, CMC decreases; this was followed in all the three polymers at from pH 7.4 to pH 9, however pH 3, did not follow the trend. $De_{0.8}Ni_{1.2}PEG_{2.3}$ with the highest M_n, showed the lowest CMC, while $De_{0.1}Ni_1PEG_2$ with lower M_n in comparison to $De_1Ni_1PEG_1$ showed a lower CMC. It can be inferred that PEG contribution within the penta-terpolymer has a significant role in the micelle formation. Compared to the relative intensity's amplitude in figure 13, $De_{0.1}Ni_1PEG_2$ surprisingly suggested a higher tendency to form aggregation at pH 9 than the other two polymers; at pH 3 and 7.4 it had still lower amplitude than $De_{0.8}Ni_{1.2}PEG_{2.3}$ and almost the same amplitude in comparison to $De_1Ni_1PEG_1$. This conjecture will be discussed further in 3.6 Laser Light Scattering, and propounds the existence of aggregation-like structure in $De_{0.1}Ni_1PEG_2$ before CMC, without forming a classic micelle. Therefore the value reported in the figure 13 for $De_{0.1}Ni_1PEG_2$ should probably not be considered as the correct CMC for this polymer. It is worth pointing out that the tendency to form aggregation, generally increase in the salt solution than in the pure water. The formed aggregates might be misleading in the interpretation of CMC. Polydispersity of the polymer chains can also contribute to misleading information in case of this polymer. The existence of chains with different sizes, tetra-blocks, tri-blocks and di-blocks in the solution change the micellization process. Fluorescence spectroscopy fundamentally requires precisely defined conditions to give reliable results.

ABCBA penta-block terpolymer	CMC (g/mL)		M_n (g/mol)
$De_1Ni_1PEG_1$ Block lengths: 34/58/34/58/34	pH 3 pH 7.4 pH 9	1.87×10^{-6} 2.45×10^{-6} 1.74×10^{-7}	27000
$De_{0.8}Ni_{1.2}PEG_{2.3}$ Block lengths: 27/68/77/68/27	pH 3 pH 7.4 pH 9	2.88×10^{-8} 1.12×10^{-7} 2.05×10^{-8}	29000
*$De_{0.1}Ni_1PEG_2$ Block lengths: 2/57/68/57/2	pH 3 pH 7.4 pH 9	6.92×10^{-7} 8.41×10^{-7} 1.58×10^{-7}	17000

Table 5- CMC results for penta-block terpolymers (* this is just a representation of the results; not all CMC values reported here are acceptable- see the argument)

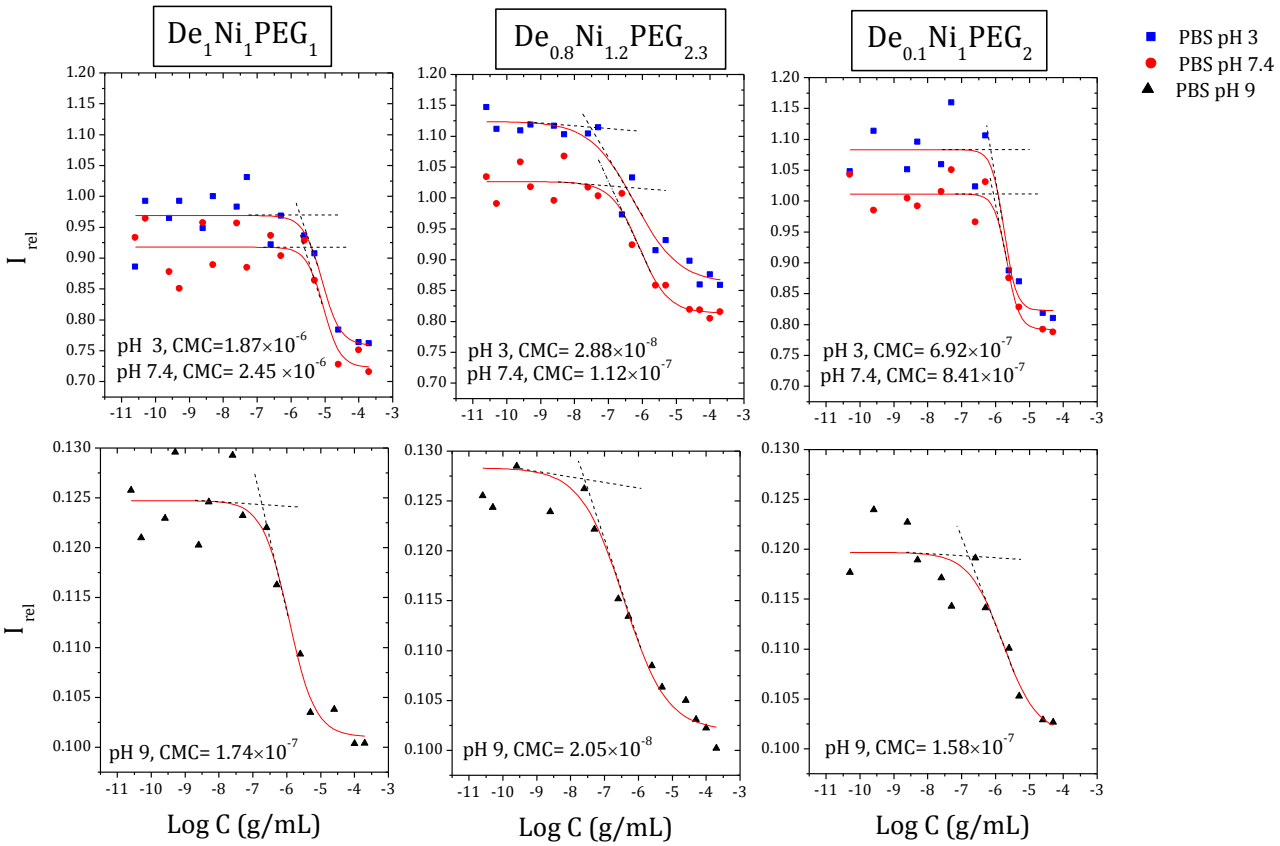

Figure 13 – CMC determination by changing the fluorescence relative intensity

Considering ionic strength[13] [67]of the PBS in different solutions, 0.025 M, 0.189 M and 0.297 M for PBS pH 3, PBS pH 7.4 and PBS pH 9, respectively, the salt screening effect favorably changes with pH increase. In general, as the ionic strength increases, repulsive electrostatic interactions are screened, resulting in polymer chains collapse. This will be discussed further in 3.2 Densitometry.

3.2 Densitometry

Density measurements of ABCBA penta-block terpolymers at different pH values and over a temperature range from 20 °C to 50 °C in D_2O as the solvent are shown in figure 14-a and 14-b.

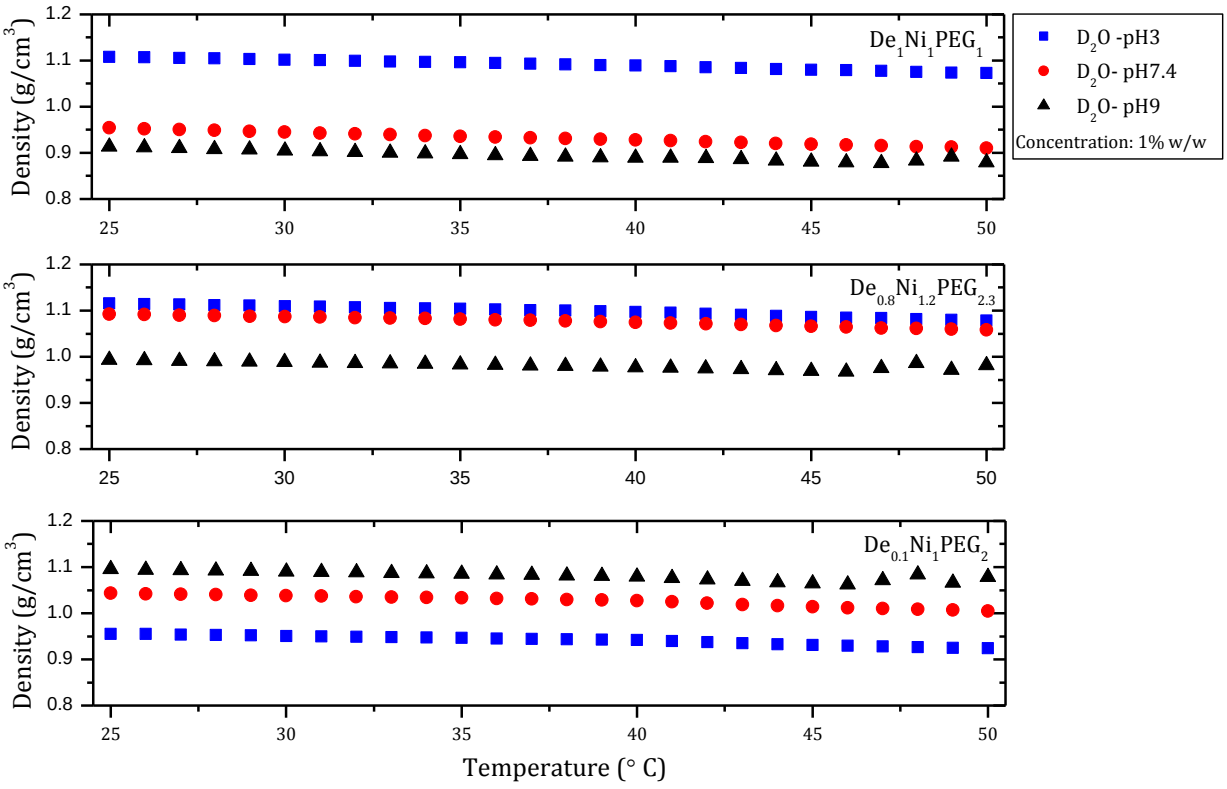

Figure 14-a – Density measurements in D_2O, pH effect

[13] Ionic strength is calculated with this formula : $I = \frac{1}{2}\sum_{i=1}^{n} m_i z_i^2$

where z_i and m_i are the charge and molality of the i^{th} ion, respectively.

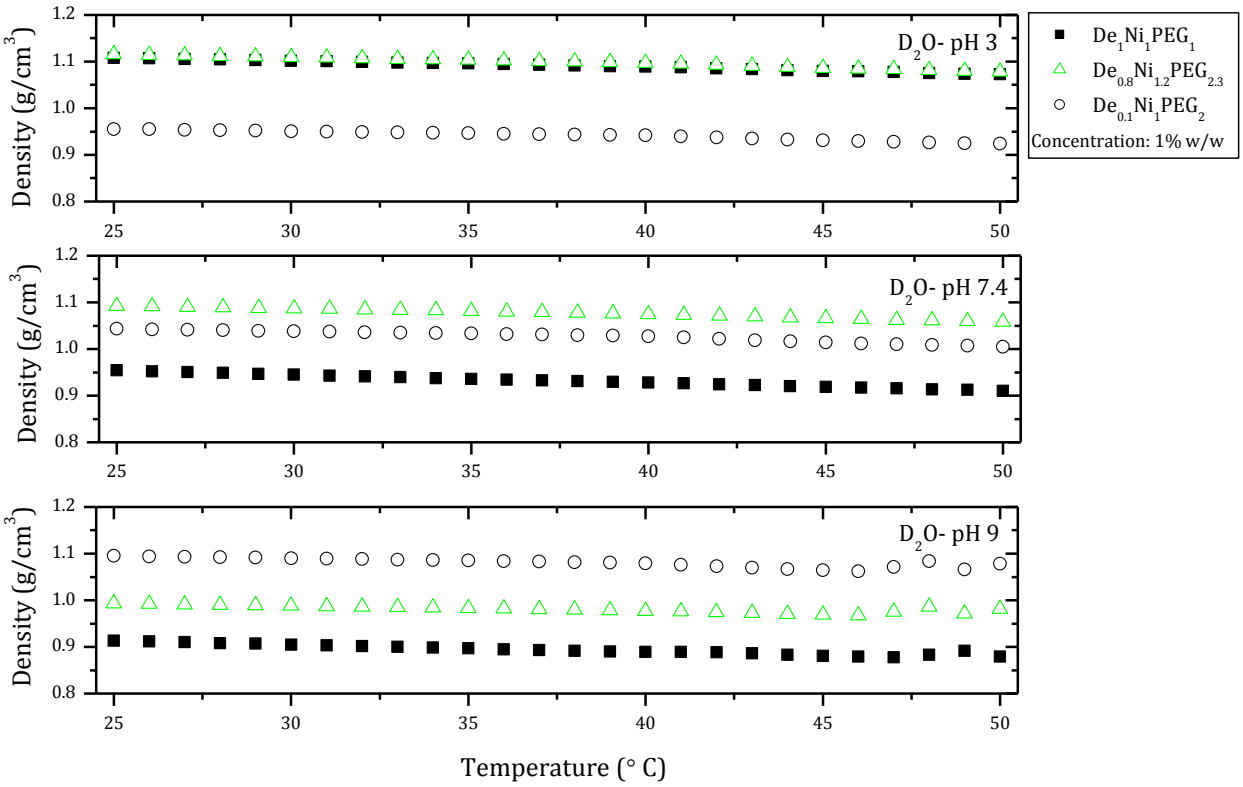

Figure 14-b – Density measurements in D_2O, block length effect

The general trend for $De_1Ni_1PEG_1$ and $De_{0.8}Ni_{1.2}PEG_{2.3}$ indicates higher specific densities for $De_{0.8}Ni_{1.2}PEG_{2.3}$ (lower specific volume) and also suggests that by increasing pH, specific volume of penta-block terpolymers increases. The higher specific density can be attributed to the larger perturbation of water molecules in the vicinity of the polymer chains at lower pH or in case of a shorter PDEAEMA (pH-responsive block) within the penta-block terpolymers, while rising pH results in hydrophobicity of the PDEAEMA block, so PDEAEMA tends to form the core of the micelle, and the remaining water in the core which is now in a disorder state makes a higher specific volume [59]. However, this doesn't seem to be the case for $De_{0.1}Ni_1PEG_2$.

Figure 15-a, 15-b and 15-c show density measurements on different scales to magnify transition temperature (Θ_{tr}) of the penta-block terpolymers. Θ_{tr} is considered to be the first temperature that specific density falls by increasing temperature.

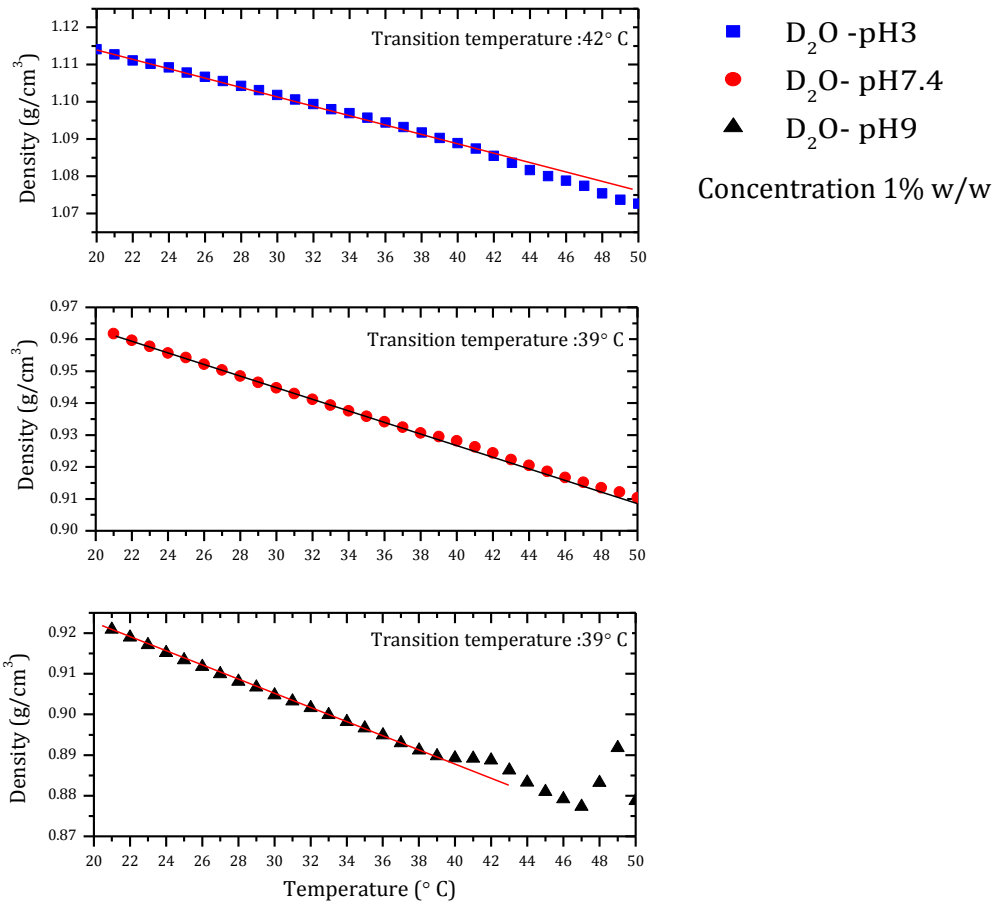

Fig.15-a – Density measurements, $De_1Ni_1PEG_1$

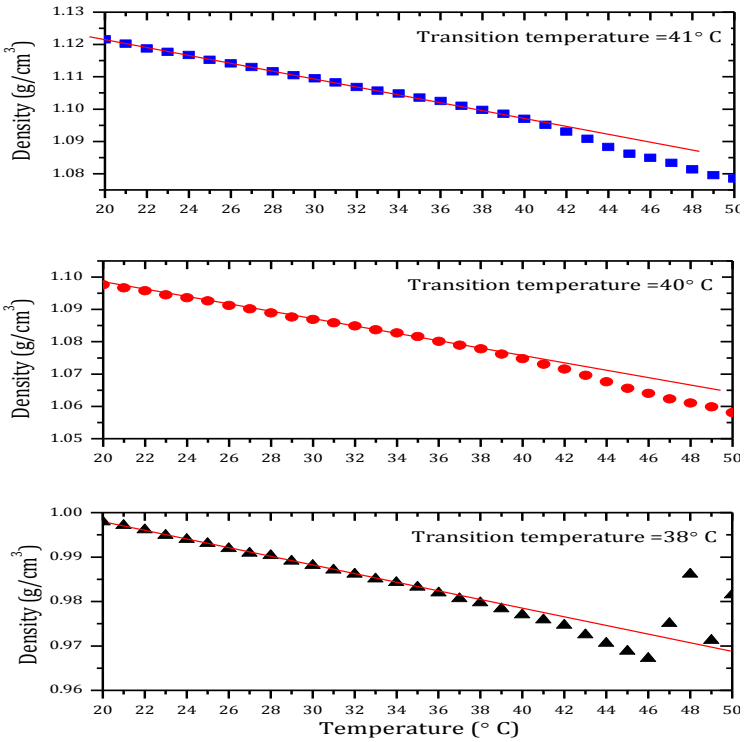

Figure 15-b – Density measurements, $De_{0.8}Ni_{1.2}PEG_{2.3}$

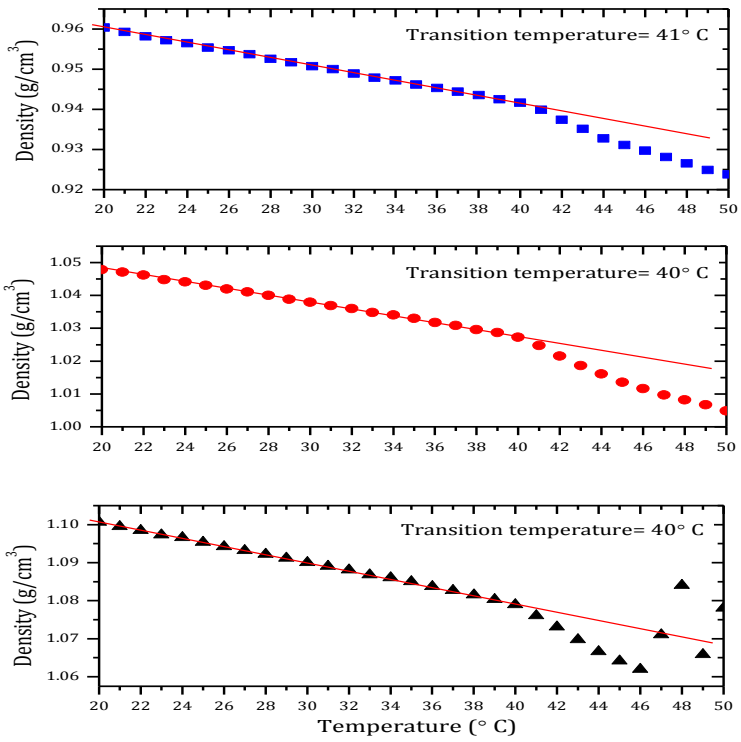

Figure 15-c – Density measurements, $De_{0.1}Ni_1PEG_2$

Transition temperatures (Θ_{tr}) were summarized in table 6.

ABCBA penta-block terpolymer	pH	Θ_{tr} (°C) D_2O	Θ_{tr} (°C) PBS
$De_1Ni_1PEG_1$	pH 3	42	40
Block lengths: 34/58/34/58/34	pH 7.4	39	38
	pH 9	39	-
$De_{0.8}Ni_{1.2}PEG_{2.3}$	pH 3	41	40
Block lengths: 27/68/77/68/27	pH 7.4	40	38
	pH 9	39	-
$De_{0.1}Ni_1PEG_2$	pH 3	41	39
Block lengths: 2/57/68/57/2	pH 7.4	40	37
	pH 9	40	-

Table 6- Transition temperatures of penta-block terpolymers from densitometry

Based on the information from table 6, Θ_{tr} for the three penta-block terpolymers at a same pH was almost unchanged, which is plausible since the thermoresponsive block's length (PNIPAAM) was fixed; on the other hand, observation a transition temperature by heating up the sample, basically originates from disorder in water molecules in the vicinity of polymer chains which causes a rise in the polymer specific volume. In other words, as the temperature increased, the solvent quality became poorer, the strong hydrogen bond between PNIPAAM and water faded away, the amide group of PNIPAAM became dehydrated and this led to the large density changes.

Density measurements in phosphate buffer solutions showed a similar trend for Θ_{tr} (table 6). Figure 16 shows Θ_{tr} for the polymers. At pH 9 and higher temperatures large bubbles were formed and caused errors in the measurements, therefore data were not reported in this case. Due to the salt screening effect, and the electrostatic repulsion diminishing, polymer chains collapse was manifested at lower temperatures; in addition, hydrogen bonds among water molecules were disrupted in the presence of salt ions, i.e., water molecules would have a higher mobility around the polymer chains and that leads to a higher value of density in PBS in comparison to heavy water (Figure 17). Furthermore, since the mass of deuterium is larger than that of hydrogen, the hydrogen bonds are stronger in D_2O

than in H_2O at a same temperature and this caused a reduced interaction between the polymer chain and D_2O molecules and consequently a more disordered state of water molecules around the polymer chain in D_2O than in H_2O (higher specific volume of polymer in D_2O than in H_2O) [59].

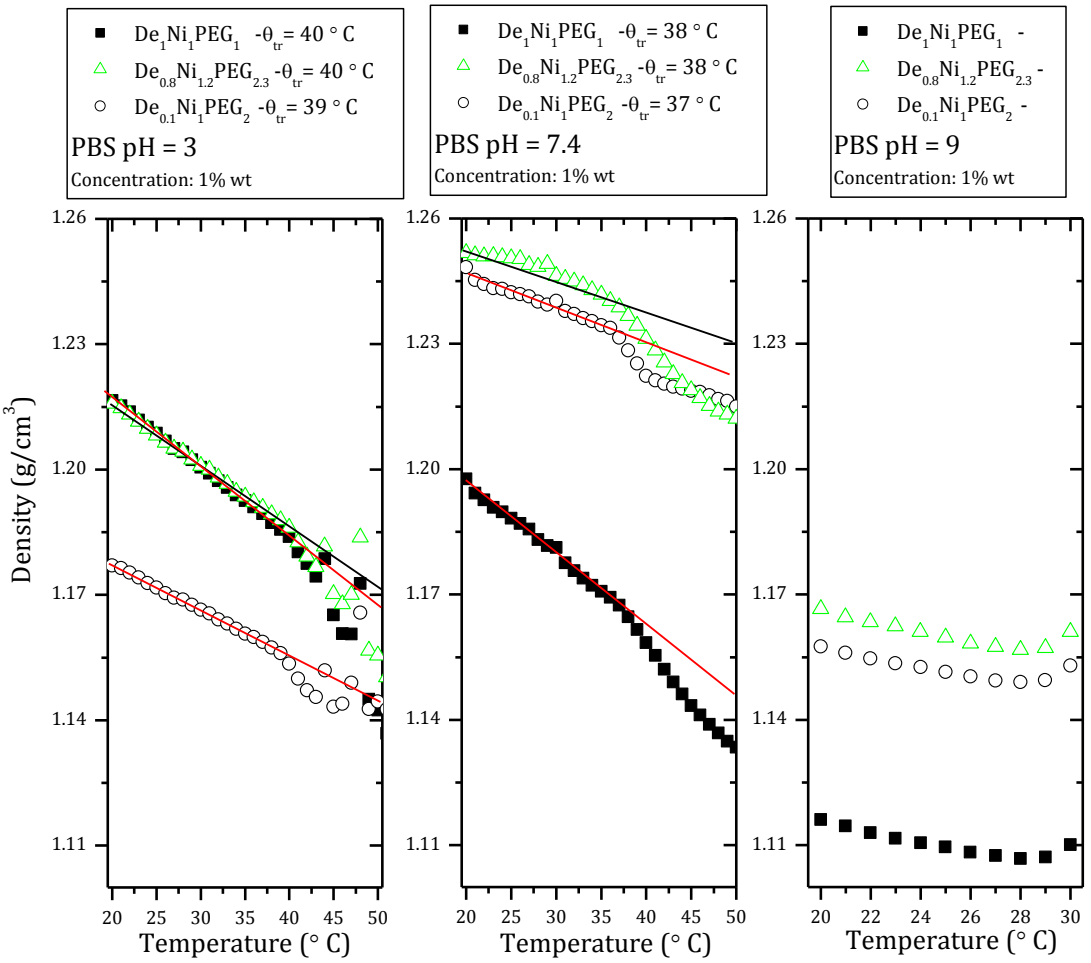

Figure 16 – Density measurements in PBS, concentration 1% w/w

Knowing the specific volume of each block provides an understanding of the composed block polymer's behavior. Specific volume of PEG has been reported in another research [59], for PNIPAAM, density measurement was performed on its homopolymer, and having the specific volume of PDEAEMA$_x$-*b*-PNIPAAM$_y$-*b*-PEG$_z$-*b*-PNIPAAM$_y$-*b*-PDEAEMA$_x$, approximate specific volume of PDEAEMA was calculated, since measurements for PEG and PNIPAAM were performed in H_2O and for the penta-block terpolymer was performed in D_2O; therefore the real specific

volume value for PDEAEMA would be slightly lower than what was reported here. All data and results were summarized in table 7.

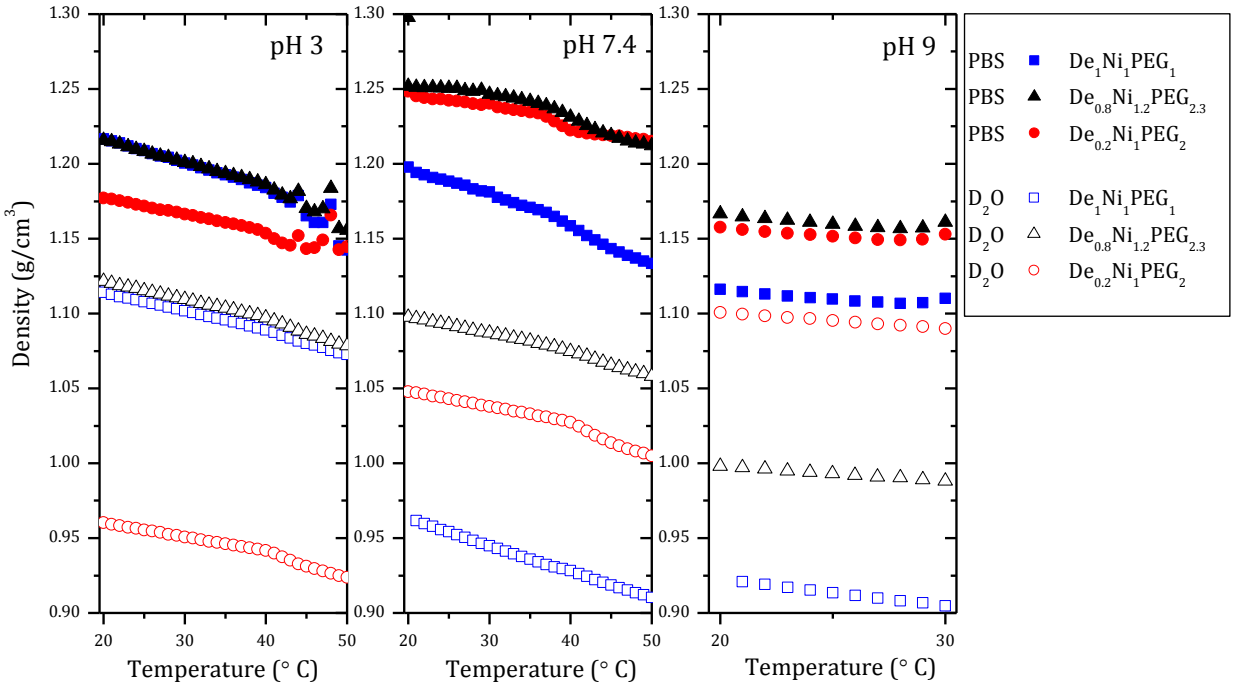

Figure 17 – Summary of density measurements in PBS and D_2O

Specific volume of PDEAEMA was calculated for $De_1Ni_1PEG_1$ and $De_{0.8}Ni_{1.2}PEG_{2.3}$ (since these two polymers had exhibited an expected trend in density measurements) and the average value was presented.

Another advantage of knowing the specific volume is that scattering length density (SLD) of the polymer can be calculated. SLD from a molecule with x_i, atoms i and molecular volume v_p is defined by equation 27:

$$k_p = \frac{\sum_i x_i b_i}{v_P} \qquad \text{Eq. 27}$$

b_i is the coherent neutron scattering length of atom i and its values are experimentally determined and tabulated [68-69]. For some selected atoms b_i values were given in the table 8. Calculating an accurate SLD is not facile; for PNIPAAM and PEG, it has been reported to be 0.87×10^{10} cm^{-2} [70-71] and 0.64×10^{10} cm^{-2} [72] respectively, here knowing the specific volume of PDEAEMA at 25 °C and neutral pH , SLD for PDEAEMA was calculated.

Temperature (° C)	$v_{PNIPAAM}$ (cm^3/g)	v_{PEG} (cm^3/g)	*$v_{PDEAEMA}$ [14] from $De_1Ni_1PEG_1$ (cm^3/g)	*$v_{PDEAEMA}$ from $De_{0.8}Ni_{1.2}PEG_{2.3}$ (cm^3/g)	**$v_{PDEAEMA}$ [15] average (cm^3/g)
20	0.877033	0.8337	1.424266	1.110012	1.267139
25	0.880626	0.8383	1.450581	1.130941	1.290761
30	0.884416	0.8426	1.484498	1.15494	1.319719
35	0.898662	0.8469	1.517187	1.177439	1.347313
40	0.904575	0.8511	1.545558	1.206902	1.37623
45	0.904673	0.8553	1.582068	1.247157	1.414613
50	0.907577	0.8595	1.613622	1.280376	1.446999

Table 7 – Specific volume of PNIPAAM (in water neutral pH), PEG (from previous works) and PDEAEMA calculated from the penta-block terpolymer measurements

atom	bi (10^{-15} m)
^1H	-3.739
C	+6.646
N	+9.36
O	+5.803

Table 8 – Scattering length density of selected atoms

$k_{PDEAEMA}= [(10\times6.646) - (19\times3.739) + (2\times5.803) + (1\times9.36)] \times 10^{-13} \times N_A/ (1.290761\times M_{monomer})= 0.4132 \times 10^{10}\ cm^{-2}$

where N_A (Avogadro's number) and $M_{monomer}$ for DEAEMA are 6.022×10^{23} and 185 g/mol respectively. The calculated SLD is comparable with $0.4844 \times 10^{10}\ cm^{-2}$

[14] Since density measurement is a highly sensitive experiment, a slight difference on the concentrations causes a noticeable difference in the density. That explains the difference of vPDEAEMA from $De_1Ni_1PEG_1$ and $De_{0.8}Ni_{1.2}PEG_{2.3}$

[15] Since $De_{0.1}Ni_1PEG_2$ did not represent the similar trend as the other two polymers, it was not considered in calculation of specific volume, to avoid complexity and producing probable errors.

that has been reported for SLD of PDEAEMA with a bulk density of 1.035 gcm^{-3} [73].

3.3 Turbidimetry

For block polymers with a temperature responsive block, turbidity measurement is a valuable asset to monitor the transition temperature, where the turbidity of the sample undergoes a remarkable change. A rise of turbidity indicates the growth of the hydrophobic associations among the present micelles or the loose assembly of chains. A comparison of turbidity data at different pH values for the three penta-block terpolymers was demonstrated in figure 18.

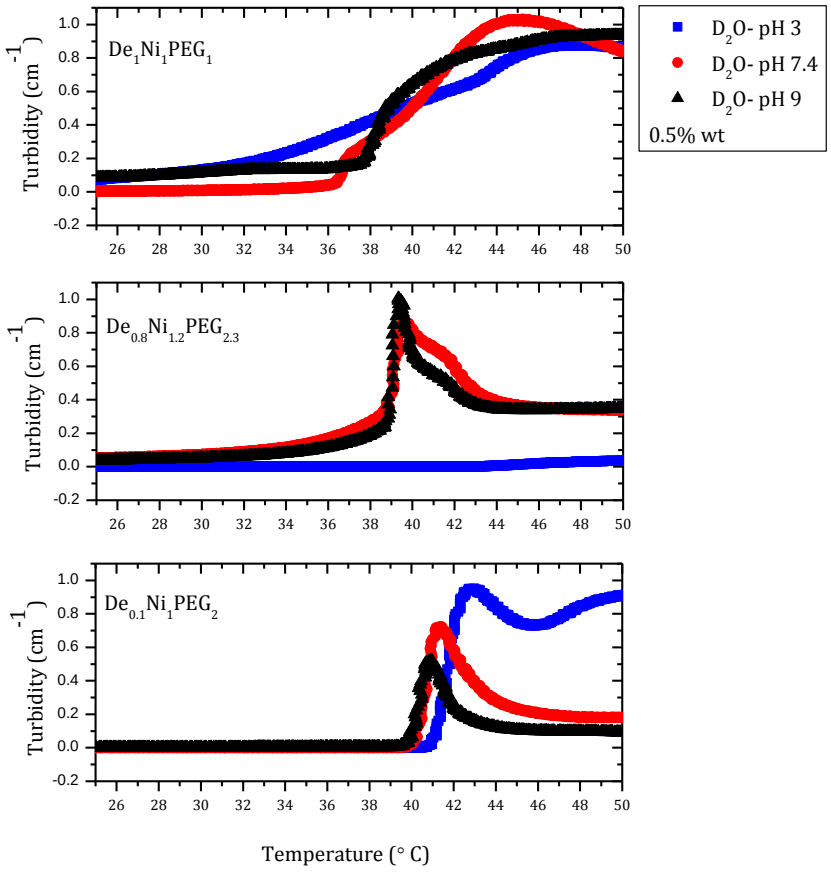

Figure 18-a – Turbidity measurements in D_2O- pH effect

The first temperature at which turbidity rises sharply was considered as the cloud point (CP). In case of $De_1Ni_1PEG_1$ that turbidity gradually increased, the turning point of the plot where the convexity changed was considered as the cloud point (CP); this consideration, in comparison to the other experiments was reasonable. For $De_{0.8}Ni_{1.2}PEG_{2.3}$ at pH 3, the sharp rise was not clear on the scale shown in

figure 18-a; turbidity measurements of these two samples were demonstrated in figure 19. A comparison between figure 18-a and figure 14-a suggests a reasonable trend. As in density measurements for $De_1Ni_1PEG_1$ and $De_{0.8}Ni_{1.2}PEG_{2.3}$ samples at lower pH showed lower specific volume (higher density), in turbidity measurements samples at lower pH showed a relatively lower turbidity. However a reverse trend was observed for $De_{0.1}Ni_1PEG_2$ again here.

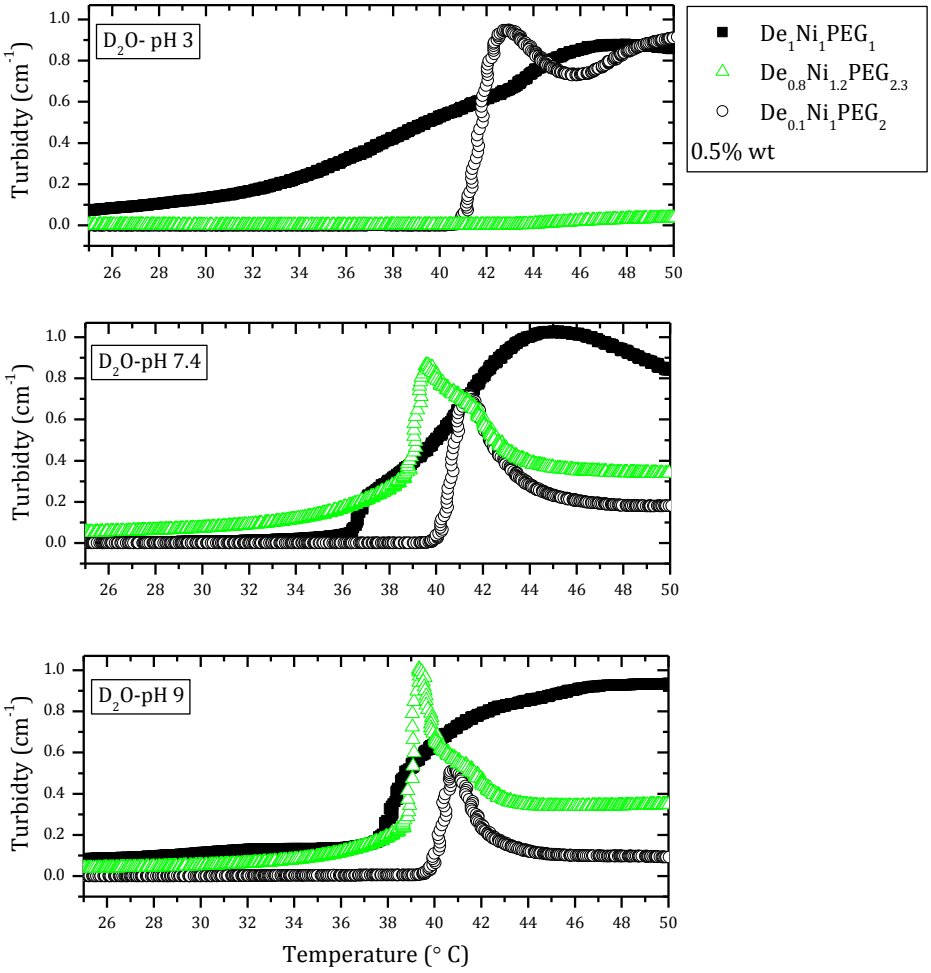

Figure 18-b – Turbidity measurements in D_2O- block length effect

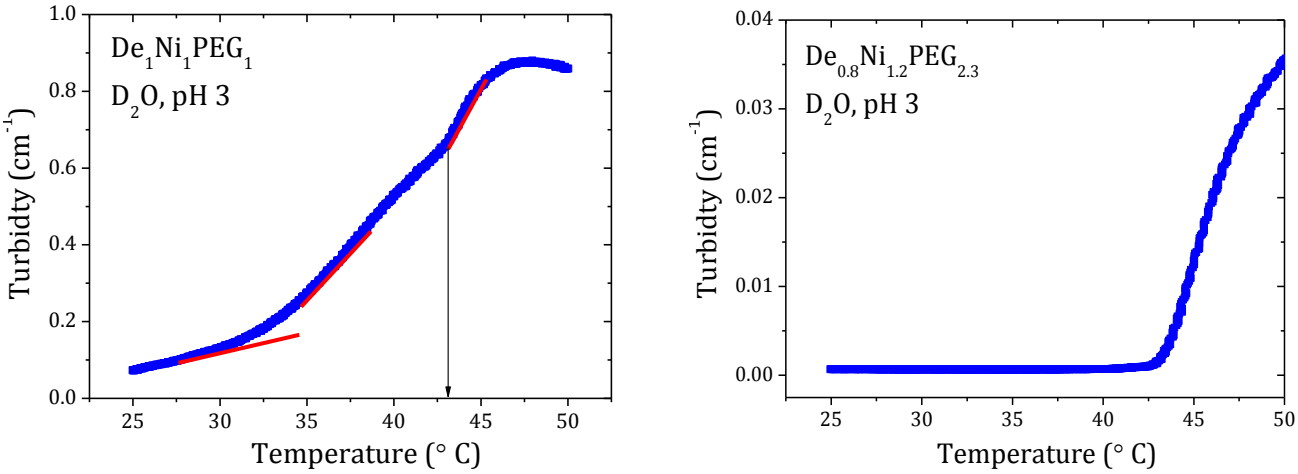

Figure 19 – Clear view of turbidity measurements of $De_1Ni_1PEG_1$ and $De_{0.8}Ni_{1.2}PEG_{2.3}$

A comparison between figure 18-b and figure 14-b displayed the similar trend, although in this case $De_{0.8}Ni_{1.2}PEG_{2.3}$ and $De_{0.1}Ni_1PEG_2$ exhibited a similar pattern of turbidity change and $De_1Ni_1PEG_1$ didn't tend to show a sharp rise of turbidity, especially at low pH. The gradual rise in turbidity by heating up the samples indicates the formation of PNIPAAM hydrophobic structures that arrange in micelles or intermicellar structures in a way that make the least contact with water. In case of $De_{0.8}Ni_{1.2}PEG_{2.3}$ and $De_{0.1}Ni_1PEG_2$, a peak in turbidity signal is observed. This could be ascribed to the longer PEG length in these two polymers than in $De_1Ni_1PEG_1$[61]; at temperatures beyond the peak, with the long PEG chains, the huge hydrophobic structured penetrate each other and a network of bridged structures is developed. As the temperature increases, the hydrophobic microdomains are evenly distributed in the network and this homogeneous network shows a lower turbidity.

Turbidity measurements in PBS in different solutions and two different concentrations, i.e., 0.5% w/w and 20% w/w, were displayed in figure 20 and figure 21. Considering the most frequently investigated pH values in drug delivery applications, pH 3 and pH 7.4 were selected to study at high concentrations. Clearly, turbidity signal for samples at higher concentrations was stronger, while cloud points appeared at almost the same temperatures. This is a result of the

formation of inter-micellar structures at higher concentrations. Transition point, or, cloud point in this case results were given in the table 9.

According to figure 20 patterns in turbidity change at pH 3, 5 and 6 in each penta-block terpolymer are analogous, while at pH 7.5 the pattern begins to change and it is similar to the pattern at pH 9. This suggests that the critical pH to observe inter-chain hydrophobical associations is between 6 and 7.4 ($6 < pH_{critical} \leqslant 7.4$). Considering ionic strength of phosphate buffer solutions (table 10), charge screening effect is expected to act in conformity with pH increasing effect, however samples at pH 6 and in particular $De_1Ni_1PEG_1$ at pH values below 6 didn't follow the expected behavior (see cloud point table 9).

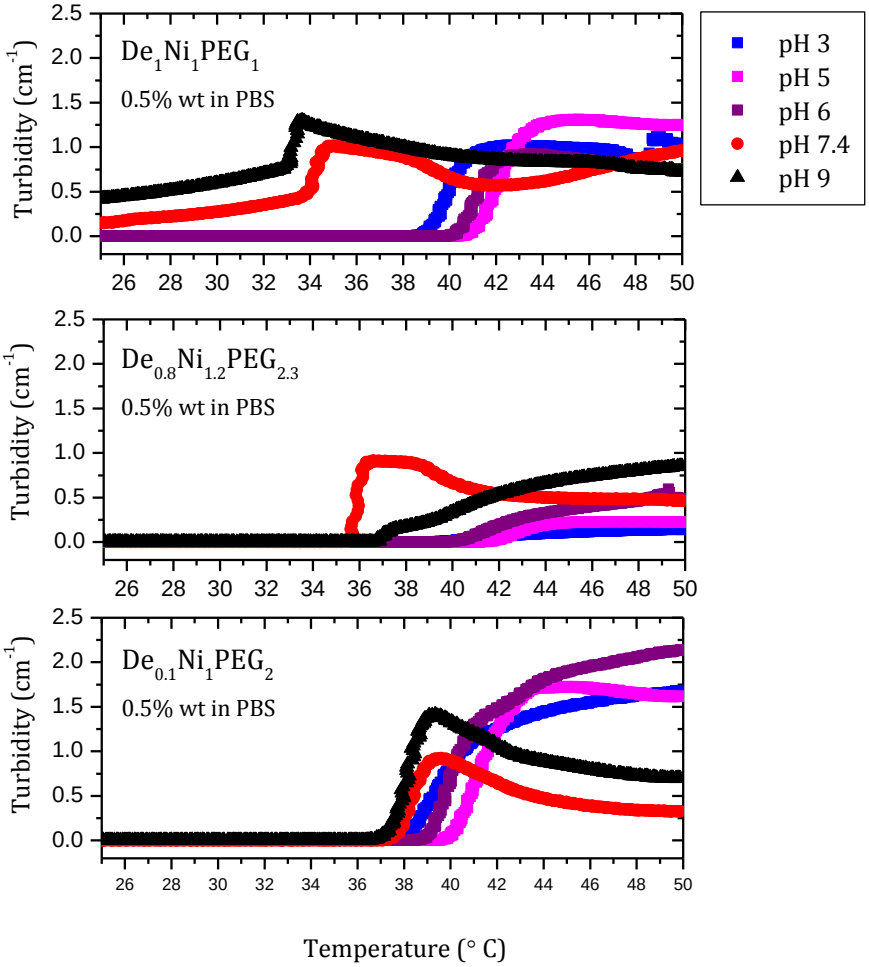

Figure 20 – Turbidity measurements in PBS at different pH values, concentration 0.5% w/w

According to table 9, by increasing pH of solutions, cloud point of samples was observed at lower temperatures, but not when the ionic strength value was lower. A comparison between figure18-a and figure 20 showed that turbidity

signals at buffer solutions were relatively stronger than they were in D_2O. This is presumably due to the hydrogen bond strength that is weakened in salt solutions; in addition in the presence of salt ions charge density on the polymer chains are screened and result in hydrophobic associations at lower temperatures and relatively weaker turbidity signals.

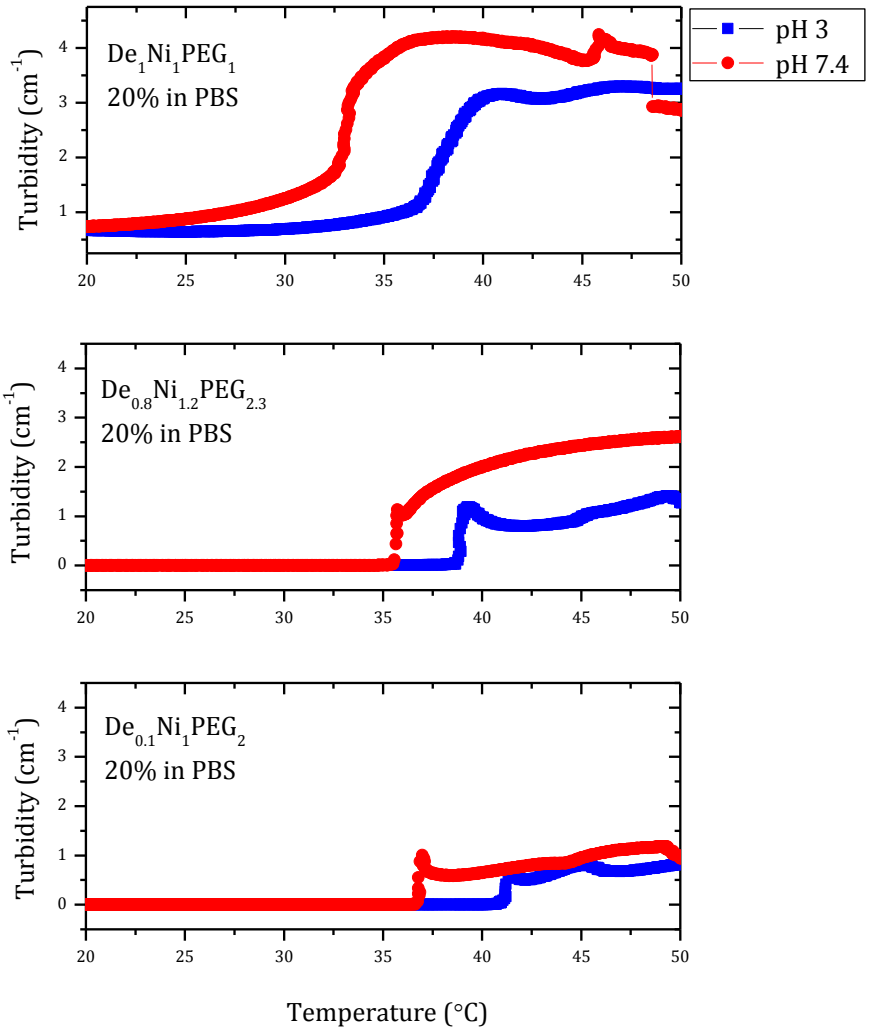

Figure 21 – Turbidity measurements in PBS at selected pH values, concentration 20% w/w

By collating cloud points of the penta-block terpolymers at the same conditions, this could be inferred that since the temperature responsive block in all the three polymers have almost the same length, the cloud points didn't change significantly, while at a higher concentration (20% w/w) the cloud point difference in the three polymers became more noticeable, therefore at higher concentrations, knowing the accurate block length matters in designing a polymer with a desired cloud point. On the other hand, the longer PEG block in $De_{0.8}Ni_{1.2}PEG_{2.3}$ and

$De_{0.1}Ni_1PEG_2$ make the polymer chains more flexible than the chains in $De_1Ni_1PEG_1$ [61] that form a fairly homogenous network by bridging among the micelles, therefore in the former penta-block terpolymers turbidity signals are relatively weaker and cloud points are higher than the latter (Figure 21).

ABCBA penta-block terpolymer	pH	CP(°C) D_2O 0.5% w/w	CP(°C) PBS 0.5% w/w	CP(°C) PBS 20% w/w
$De_1Ni_1PEG_1$	pH 3	43	36	37
Block lengths: 34/58/34/58/34	pH 5	-	42	-
	pH 6	-	40	-
	pH 7.4	37	35	33
	pH 9	37	37	-
$De_{0.8}Ni_{1.2}PEG_{2.3}$	pH 3	43	39	39
Block lengths: 27/68/77/68/27	pH 5	-	42	-
	pH 6	-	40	-
	pH 7.4	39	35	35
	pH 9	39	37	-
$De_{0.1}Ni_1PEG_2$	pH 3	41	38	41
Block lengths: 2/57/68/57/2	pH 5	-	40	-
	pH 6	-	39	-
	pH 7.4	40	37	37
	pH 9	40	37	-

Table 9 – Cloud point data

pH of PBS	Ionic strength (M)
3	0.025
5	0.02
6	0.056
7.4	0.189
9	0.297

Table 10 – Ionic strength of PBS used in experiment

3.4 Proton Nuclear Magnetic Resonance (^{1}H NMR) Spectroscopy

Schizophrenic self-assembly of PDEAEMA$_x$-*b*-PNIPAAM$_y$-*b*-PEG$_z$-*b*-PNIPAAM$_y$-*b*-PDEAEMA$_x$ was confirmed by ^{1}H NMR. Figure 22 shows the temperature- and pH- dependent ^{1}H NMR spectra for De$_{0.8}$Ni$_{1.2}$PEG$_{2.3}$ at D_2O and concentration of 0.5% w/w

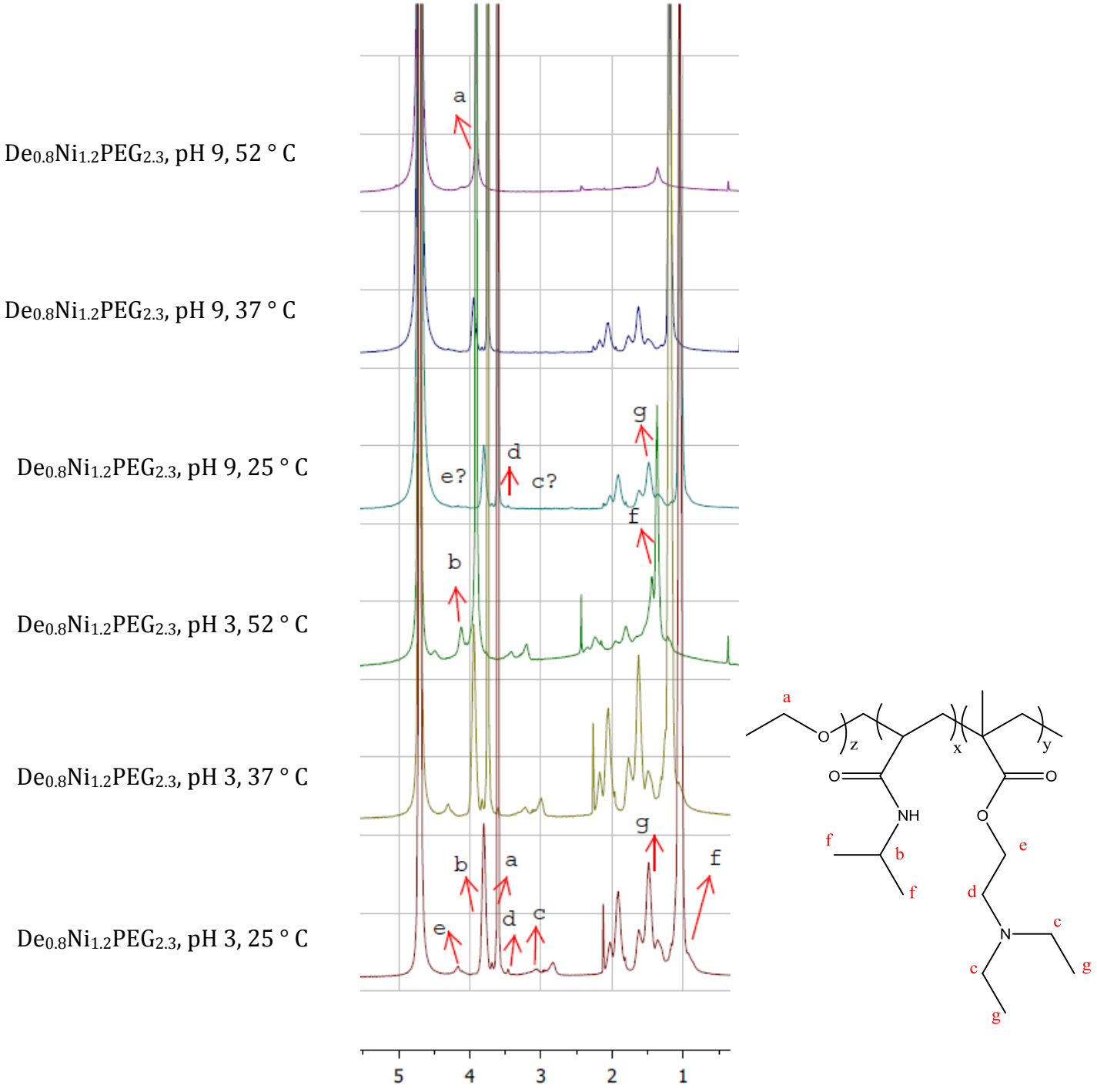

Figure 22 – ^{1}H NMR spectra of De$_{0.8}$Ni$_{1.2}$PEG$_{2.3}$ in D_2O at different temperatures and pH values

According to figure 22 at pH 3 (below pK_a of PDEAEMA) and 25° C (below LCST of PNIPAAM) , since all the characteristic peaks for PDEAEMA, PNIPAAM and PEG are visible, all blocks are relatively hydrophilic to be molecularly soluble in the solvent (D_2O), however they have been hydrophobic enough to form the micelles (see table 5). At pH 3 and 52 °C, the intensity of PNIPAAM characteristic peaks were significantly reduced, indicating a micellar structure with PNIPAAM in the core and well-solvated hybrid PEG/PDEAEMA coronas, although corresponding peaks for PDEAEMA were also attenuated. It has been found earlier that PDEAEMA shows a temperature responsive behavior too [24], therefore this also can be taken into consideration in analyzing the data. At pH 9 and 25 °C, due to the deprotonation and collapse of PDEAEMA chains, peaks “g” and “d” were significantly attenuated and peaks “e” and “c” almost disappeared, implying a micellar structure with PDEAEMA in the core, PNIPAAM in the corona and PEG in the shell. By increasing both pH and temperature to 9 and 52, respectively, except for PEG that exhibited a weaker peak in comparison with other conditions, all other peaks became almost invisible, suggesting a micellar structure/aggregation or clusters with PNIPAAM and PDEAEMA in the core with probably a loose assembly of PEG chains around.

The ^{1}H NMR spectra repeated the same patterns for $De_1Ni_1PEG_1$ and $De_{0.1}Ni_1PEG_2$. By comparing the spectra of the three penta-block terpolymers at the same condition (Figure 23), no conspicuous changes in the peak intensities were observed, therefore drawing a decisive conclusion on how different the micelles would be in each penta-block terpolymer requires a thorough investigation with other experiments and methods. However since $De_{0.1}Ni_1PEG_2$ showed relatively stronger peaks than $De_1Ni_1PEG_1$ and $De_{0.8}Ni_{1.2}PEG_{2.3}$ under any conditions, it could be inferred that this polymer was dissolved more effectively in D_2O in comparison with $De_1Ni_1PEG_1$ and $De_{0.8}Ni_{1.2}PEG_{2.3}$. This does not oppose the conjecture in 3.1 Fluorescence Spectroscopy; it will be disclosed in 3.6 Laser Light Scattering, that $De_{0.1}Ni_1PEG_2$, due to the relatively high polydispersity, shows at least two regimes of size, one for unimers with a high solubility in water as it was shown in ^{1}H NMR spectra, the other for cluster-like structures which contributed to the solution turbidity, or at very low concentrations to the change of the fluorescence spectra.

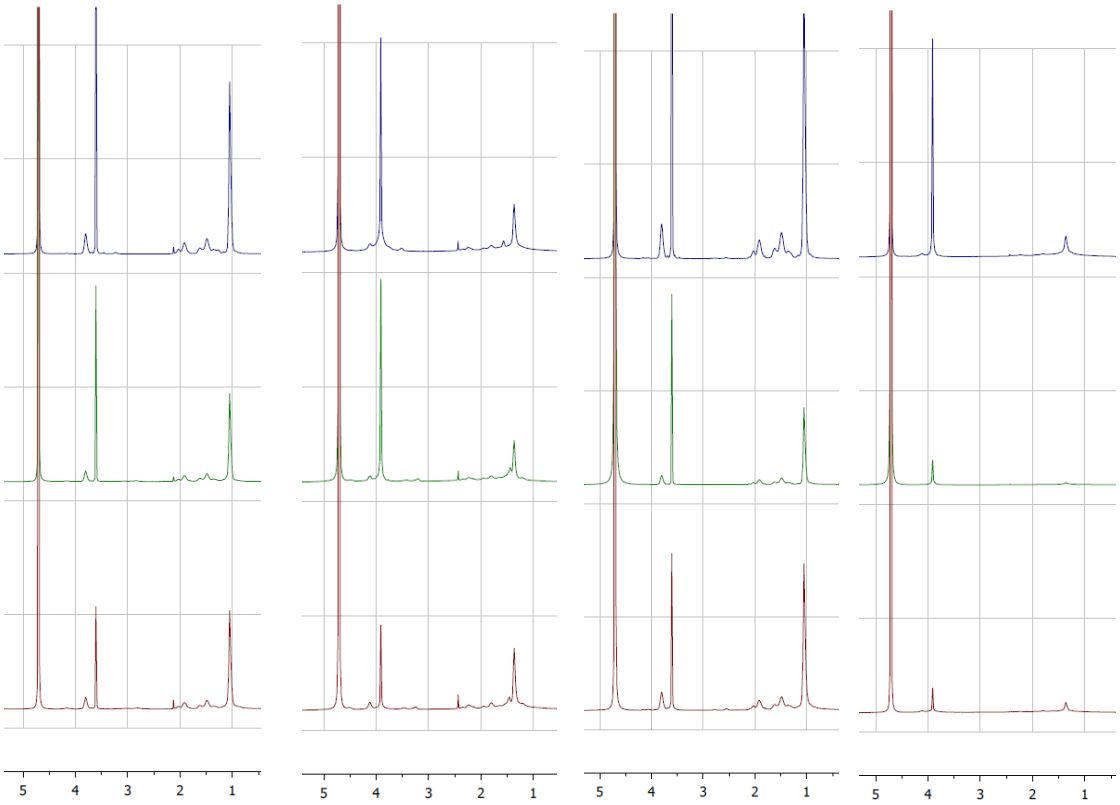

Figure 23–Comparison of ^{1}H NMR spectra of the penta-block terpolymer in D_2O at different temperatures and pH values/ $De_{0.1}Ni_1PEG_2$: blue, $De_{0.8}Ni_{1.2}PEG_{2.3}$: green, $De_1Ni_1PEG_1$: red

3.5 Zeta (ζ) potential measurements

In order to investigate the surface charge of the micelles at different temperatures and pH values, ζ-potential measurements were performed. Measurements proceeded up to the temperature or pH where quality and accuracy of the results determined by the instrument was satisfactory and the polymer solutions were in a homogenous state. The results were summarized in table 11; with D_2O, samples were prepared only at pH values 3, 7.4 and 9.

Based on the information in table 11, at pH 3 in D_2O, ζ-potential value increases with increasing temperature, confirming the postulate made from ^{1}H NMR spectra, i.e., the penta-block terpolymer is reaching its LCST, PNIPAAM chain is diffusing into the core of micelle and exposing PDEAEMA and PEG to the continuous aqueous phase [74]. Since it is below pK_a of PDEAEMA, the chains are protonated and this gives a positive charge to the micelle. However $De_{0.1}Ni_1PEG_2$ did not

completely follow this pattern; this could possibly concern the short PDEAEMA length which can not stick out of the micelle surface. Nevertheless, even at high temperatures in which measurement stopped due to the low quality, no sediments were observed, implying electrostatic stability of the micellar structures. At pH 3 and low temperatures, micelles were positively charged; this could suggest that the PDEAEMA block dominantly exists on the surface of the micelles. At pH 9 in D_2O, micelles possessed a negligible positive charge at low temperatures, indicating that PDEAEMA was diffusing into the core of micelles, as temperature gradually rose, it turned to negative charge, implying the existence of hydrated neutral, or more precisely negative PEG chains [75] around the structure with some contribution of PNIPAAM chains; it is worth to mention that PNIPAAM has a slightly negative charge [76]. This is consistent with the hypothesis made in ^{1}H NMR section. On the other hand, in buffer solutions, at pH 3, by increasing temperature, ζ-potential remained almost constant and the ζ-potential values at pH 3, 5 and 6 were almost the same at a constant temperature for each polymer, suggesting an equal screening effect of buffer solutions, while at pH 7.4 and 9, due to the high conductivity of the solution which was a consequence of presence of the salt ions, measurement with a satisfactory quality became impossible and therefore no data were reported. It could be hypothesized that regarding the ionic strength of PBS pH 7.4 (in comparison with the ionic strength of PBS pH 3, 5 and 6), ζ-potential values at pH 7.4 and 9 would have been probably negative even at low temperatures. Typically charged chains like polyelectrolytes are sensitive to changes in pH, which determines the degree of dissociation, and also to changes of ionic strength which affects the Debye screening length [76]; PBS 7.4 and 9 due to the higher ionic strength shielded the charges more effectively, and at higher temperature this caused instability of the micellar structure and a clear phase separation, as the steric hindrance provided by PEG block was not able to sustain the collapsed PNIPAAM and PDEAEMA chains ; this was yet another reason why the ζ-potential measurements were unsuccessful at these two pH values. Figure 24 illustrates a typical measurement with good quality and one with bad quality.

		Mean (mV)	Area (%)	Width (mV)
Zeta Potential (mV): 18.4	**Peak 1:**	18.4	100.0	5.66
Zeta Deviation (mV): 5.66	**Peak 2:**	0.00	0.0	0.00
Conductivity (mS/cm): 0.0451	**Peak 3:**	0.00	0.0	0.00
Result quality Good				

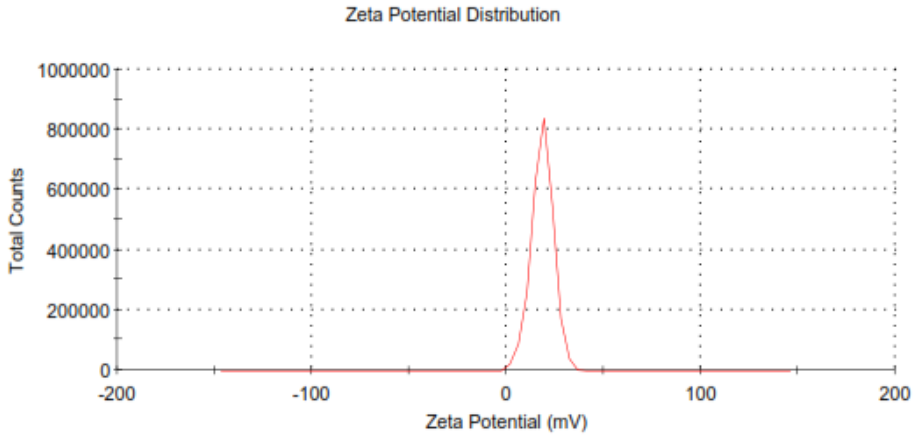

a

		Mean (mV)	Area (%)	Width (mV)
Zeta Potential (mV): 24.7	**Peak 1:**	29.4	23.0	6.58
Zeta Deviation (mV): 39.6	**Peak 2:**	47.0	18.9	5.75
Conductivity (mS/cm): 0.0661	**Peak 3:**	-4.15	12.4	6.89
Result quality See result quality report				

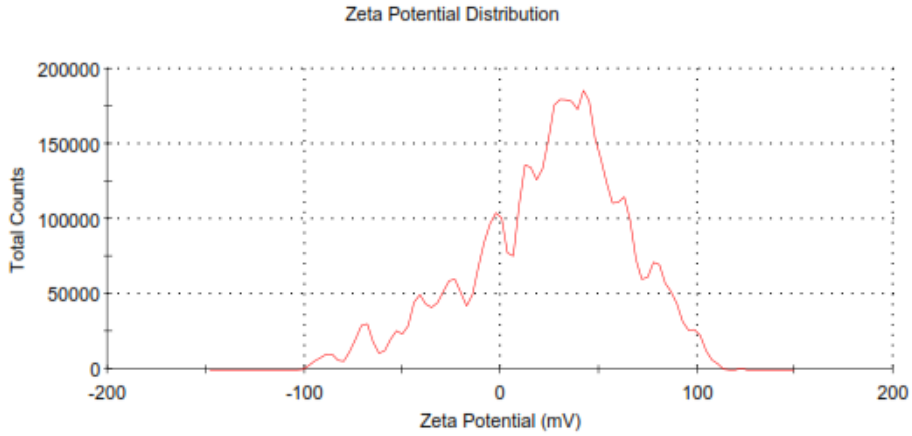

b

Figure 24 –Zeta-potential distributions for $De_{0.8}Ni_{1.2}PEG_{2.3}$ pH 3, D_2O, a- 25 °C good quality, b- 43 °C unsuccessful measurement

ABCBA polymer	Temperature (° C)	ζ (mV) pH 3		ζ (mV) pH 5		ζ (mV) pH 6		ζ (mV)* pH 7.4		ζ (mV)* pH 9	
$De_1Ni_1PEG_1$ 34/58/34/58/34		D_2O	PBS	D_2O	PBS	D_2O	PBS	D_2O	PBS	D_2O	PBS
	25	11.1	12.4		11.1		11.4	3.85	-	0.02	-
	28	12.2	12.9		11.1		10.0	5.84	-	-	-
	31	12.9	12.8		11.9		11.0	4.84	-	-	-
	34	13.7	12.7		11.4		7.59	-	-	-	-
	37	13.9	9.16		7.43		-	-	-	-	-
$De_{0.8}Ni_{1.2}PEG_{2.3}$ 27/68/77/68/27											
	25	17.8	12.6		10.4		10.1	1.09	-	1.64	-
	28	18.6	12.4		10.6		11.1	-1.37	-	2.45	-
	31	19.5	12.6		7.05		10.9	-3.42	-	0.46	-
	34	21.3	12.6		-		8.48	-4.34	-	-0.67	-
	37	21.1	-		-		-	-1.76	-		-
	40	-	-		-		-	-3.4	-		-
$De_{0.1}Ni_1PEG_2$ 2/57/68/57/2											
	25	15.8	16		12.1		7.91	7.68	-	-2.91	-
	28	16.5	16.3		12		7.72	12.0	-	4.23	-
	31	20.3	9.15		11.3		3.94	12.6	-	-3.87	-
	34	20.2	-		-		4.93	-5.06	-	-4.41	-
	37	19.9	-		-		-	-9.11	-	-3.29	-
	40	18.2	-		-		-	-3.94	-	-6.10	-
	43	10.8	-		-		-	-	-	-	-

Table 11 – ζ-potential of the penta-block terpolymers, concentration 0.5% w/w (block lengths of each polymer was written below)
* ζ-potential measurements in PBS pH 7.4 and 9 were unsuccessful

According to the information in table 11, at a constant pH and temperature, $De_{0.8}Ni_{1.2}PEG_{2.3}$ in D_2O propounded the highest stability due to the stronger electrostatic repulsion; as the solvents turned to PBS, this polymer experienced

charge inversion at lower temperatures, implying the highest level of screening effect. This could delicately signify that the PDEAEMA block in $De_{0.8}Ni_{1.2}PEG_{2.3}$ lies relatively farther, toward the surface of the micelle, in comparison to $De_1Ni_1PEG_1$ and $De_{0.1}Ni_1PEG_2$.

3.6 Laser Light Scattering (LLS)

3.6.1 Dynamic Light Scattering (DLS)

A spherical core-shell model had been proposed for $PDEAEMA_x$-*b*-$PNIPAAM_y$-*b*-PEG_z-*b*-$PNIPAAM_y$-*b*-$PDEAEMA_x$ [7] which was a reasonable presumption in this work; although in 3.6.2 SANS this model was confirmed. In DLS, size of the micelles and their temperature and pH-dependency were investigated with multi-angle Dynamic Light Scattering (DLS). Figure 25 shows a typical example of the first-order electric field correlation function vs. time at different angles. The average hydrodynamic radius for the single mode correlation function in the figure and b, the stretching parameter close to 1, are describing a monodisperse system. The curves in the inner graph, i.e., $g^1(t)$-q^2t which are almost masked by each other at different angles, are an indicative of a diffusive system.

In particular, as it was mentioned in 1.2.2 DLS, the decay rate (τ^{-1}) (τ, the relaxation time) as a function of q^2 discloses the diffusivity of the system. Figure 26 shows a typical example of the angular dependency of the decay rate for the system demonstrated in figure 25. The linear correlation coefficient, R close to 1 indicates an adequate diffusivity of the system. The slope of this plot represents the apparent diffusion coefficient D, which in diffusive systems is not dependent on the scattering angle.

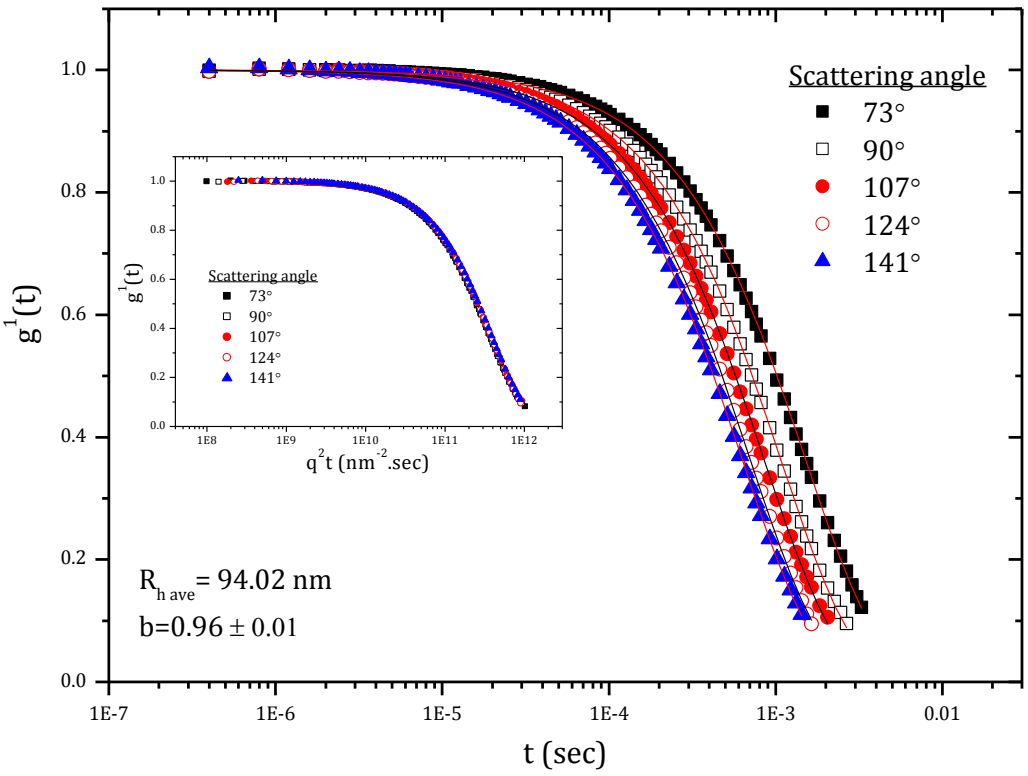

Figure 25 – First-order electric field correlation function vs. time- $De_{0.8}Ni_{1.2}PEG_{2.3}$ (0.5% w/w) in D_2O at pH 3, 25 °C

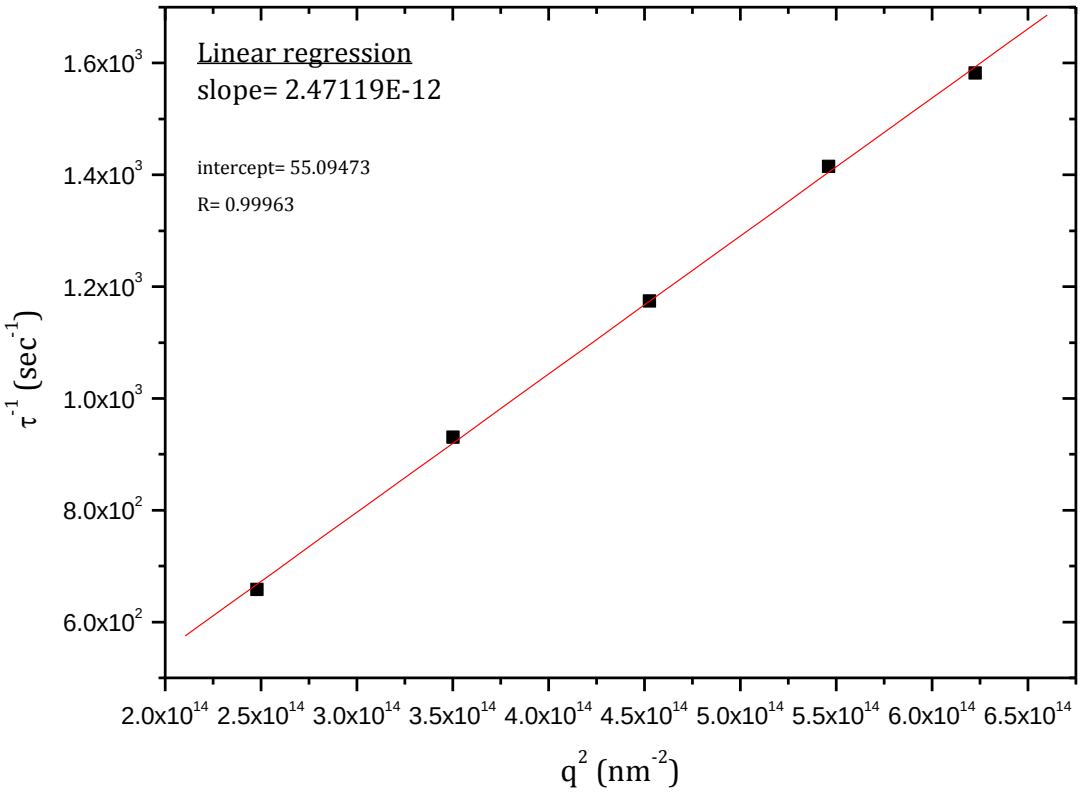

Figure 26 – Decay rate (τ^{-1}) as a function of q^2- $De_{0.8}Ni_{1.2}PEG_{2.3}$ (0.5% w/w) in D_2O at pH 3, 25 °C

As the micellar structures showed a temperature dependency, figure 27 shows $g^1(t)$-t and τ^{-1}-q^2 for the same polymer, i.e., $De_{0.8}Ni_{1.2}PEG_{2.3}$ (0.5% wt) in D_2O at pH 3, and a higher temperature 45 °C. By comparing figures 26 and 27, the system at high temperatures exhibited a polydispersity (b= 0.86 ± 0.01); in the inner graph ($g^1(t)$-q^2t), a slight deviation of curves were observed, and a lower R (0.99678) suggested a relatively lower diffusivity of the system at higher temperature. In addition, $R_{h\ ave}$ became 1.5 times larger. However the correlation function has still single mode.

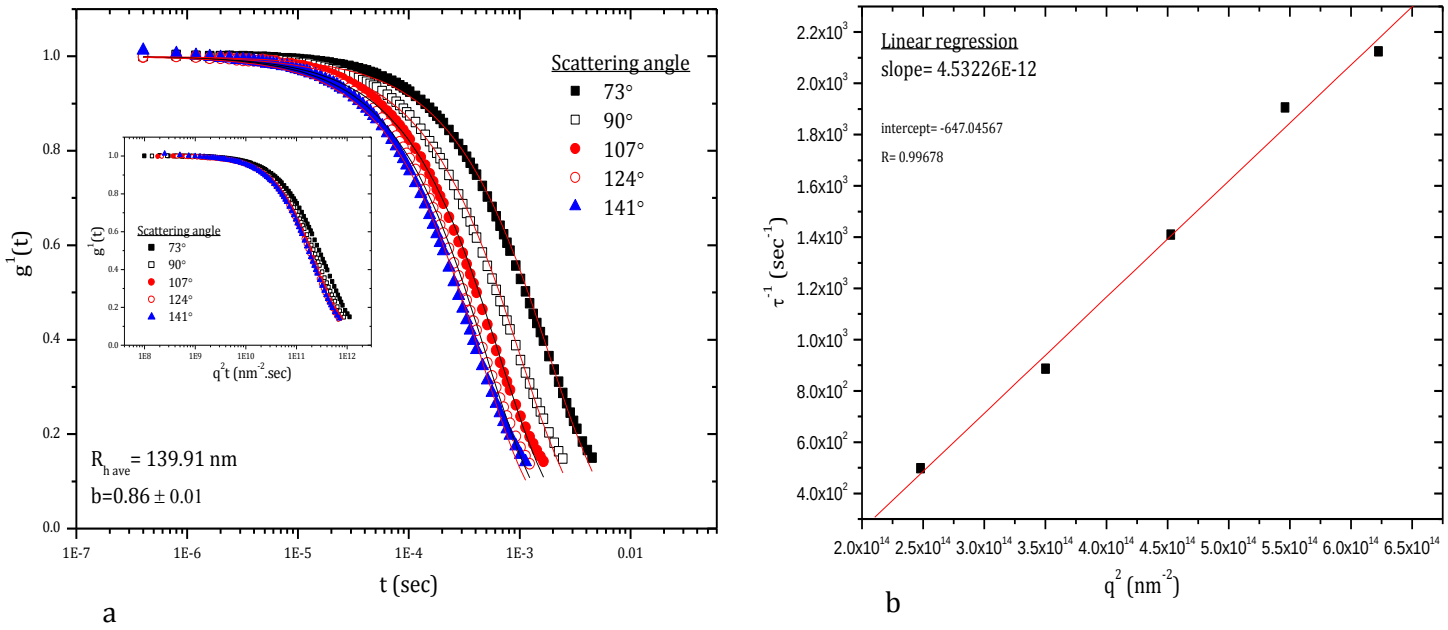

Figure 27 – a- $g^1(t)$-t , b- τ^{-1}-q^2 - $De_{0.8}Ni_{1.2}PEG_{2.3}$ (0.5% w/w) in D_2O at pH 3, 45 °C

The micellar structure showed also a pH-dependency behavior. Figure 28 illustrates temperature dependency of $g^1(t)$-t for $De_{0.8}Ni_{1.2}PEG_{2.3}$ (0.5% w/w) in D_2O at pH 3 and 9, at scattering angle 90°. All measurements were reported up to the temperature that the solutions reached a level of turbidity which caused multiple scattering; for $De_{0.8}Ni_{1.2}PEG_{2.3}$ at pH 9, it was 43 °C, while at pH 3, it was 45 °C.

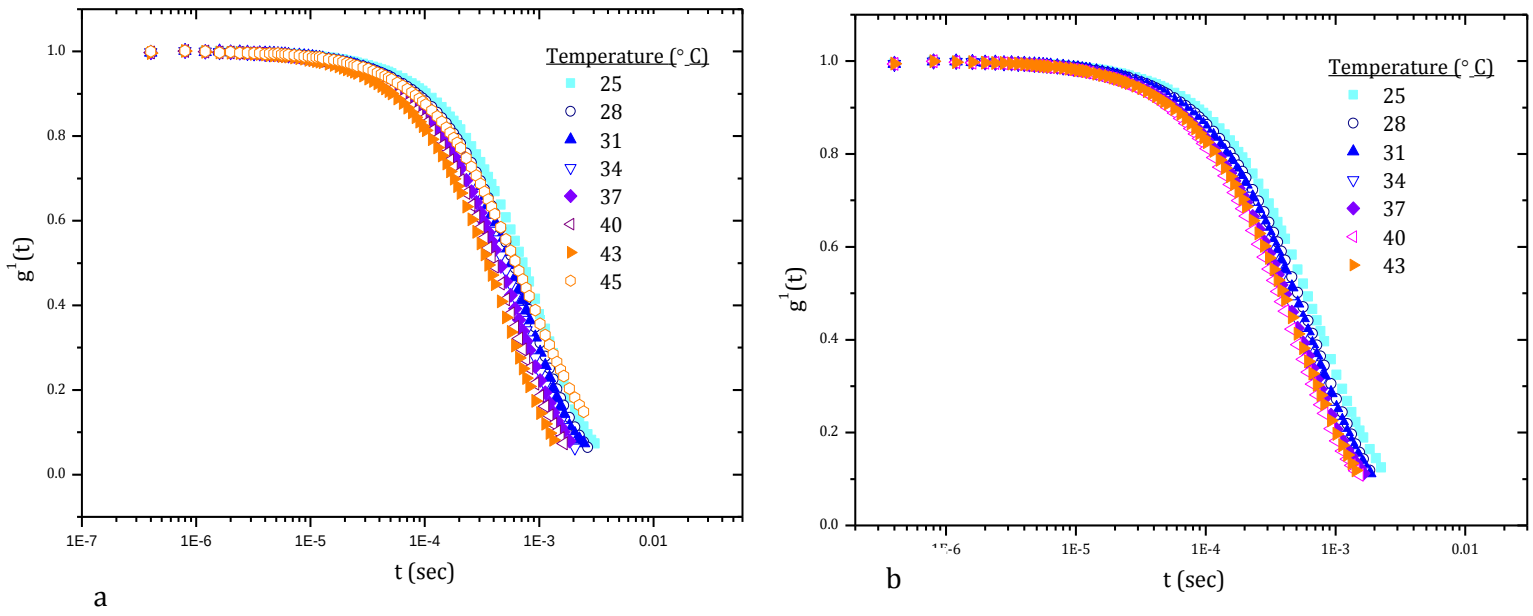

Figure 28 – $g^1(t)$-t - $De_{0.8}Ni_{1.2}PEG_{2.3}$ (0.5% w/w) in D_2O at scattering angle 90°, a- pH 3, b- pH 9

Figure 29 shows the pH-dependency of $g^1(t)$-t for $De_{0.8}Ni_{1.2}PEG_{2.3}$ (0.5% wt) in D_2O at 25 °C and 40 °C, at scattering angle 90°.

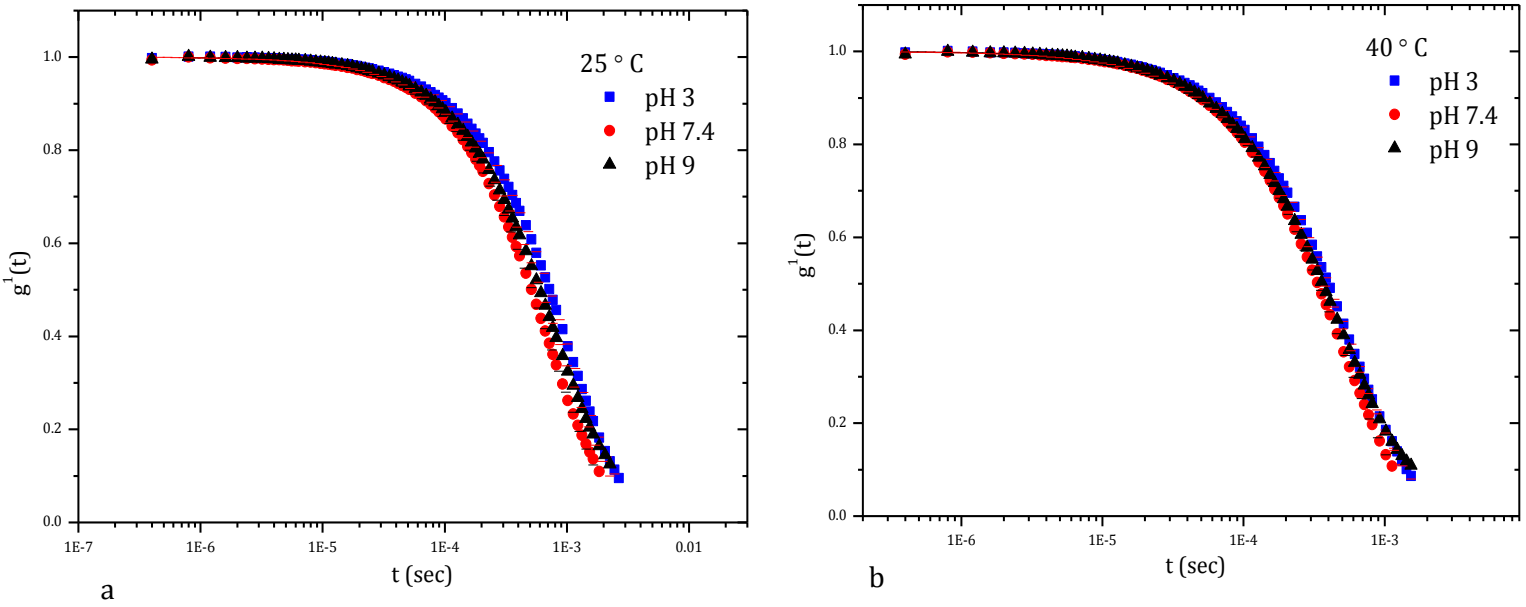

Figure 29 – $g^1(t)$-t - $De_{0.8}Ni_{1.2}PEG_{2.3}$ (0.5% w/w) in D_2O at scattering angle 90°, a- 25 °C, b- 40 °C

Figure 30 compares $g^1(t)$-t for the three penta-block terpolymers at the extreme conditions, i.e., low temperature- low pH, low temperature- high pH, high temperature-low pH, and high temperature-high pH.

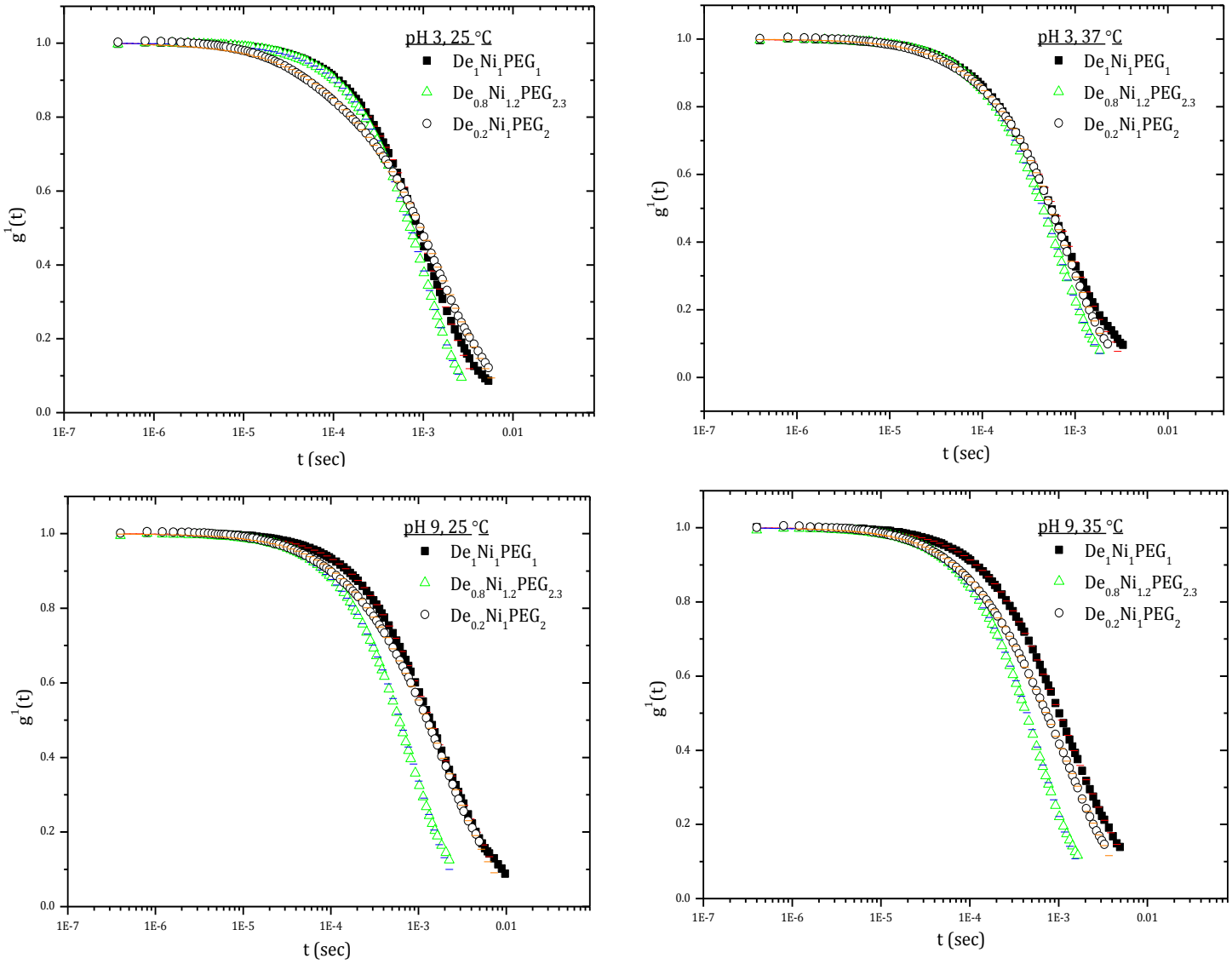

Figure 30 – $g^1(t)$-t – penta-block terpolymers (0.5% w/w) in D_2O at scattering angle 90°

In order to investigate the solvent effect, q^2-dependency of decay rate (τ^{-1}) for the penta-block terpolymers in D_2O and PBS at different pH values were displayed in figures 31-a, -b, -c. In general, solutions in PBS reached the multiple scattering state at lower temperatures in comparison with in D_2O under the same conditions and indicated bimodal correlation functions; furthermore the lower value of the linear correlation coefficient R, suggested a less diffusivity of solution

in PBS than in D_2O, especially for $De_{0.1}Ni_1PEG_2$. In particular, monodisperse spherical particles are expected to yield a linear dependency of the decay rate with q^2 with zero intercept [63].

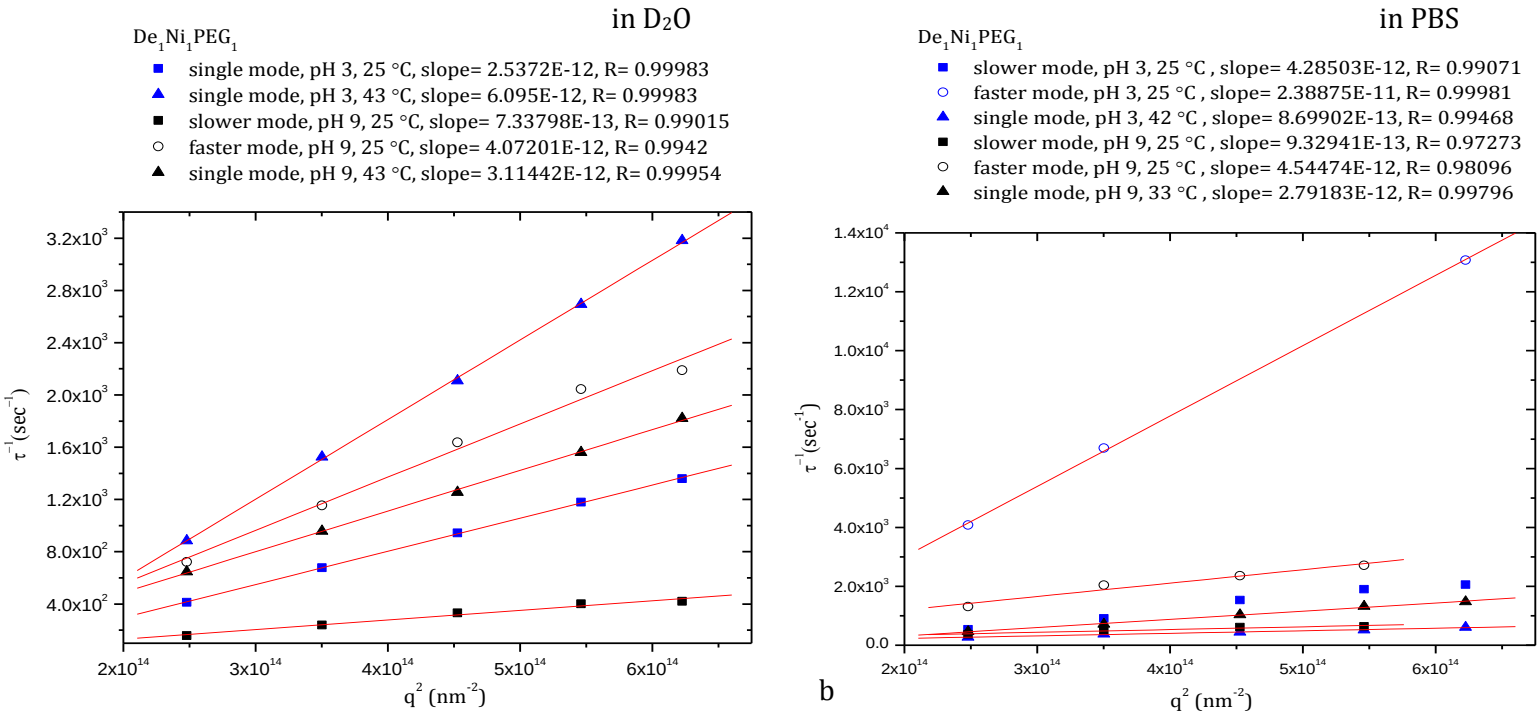

Figure 31-a – Decay rate (τ^{-1}) as a function of q^2- $De_1Ni_1PEG_1$ (0.5% w/w)

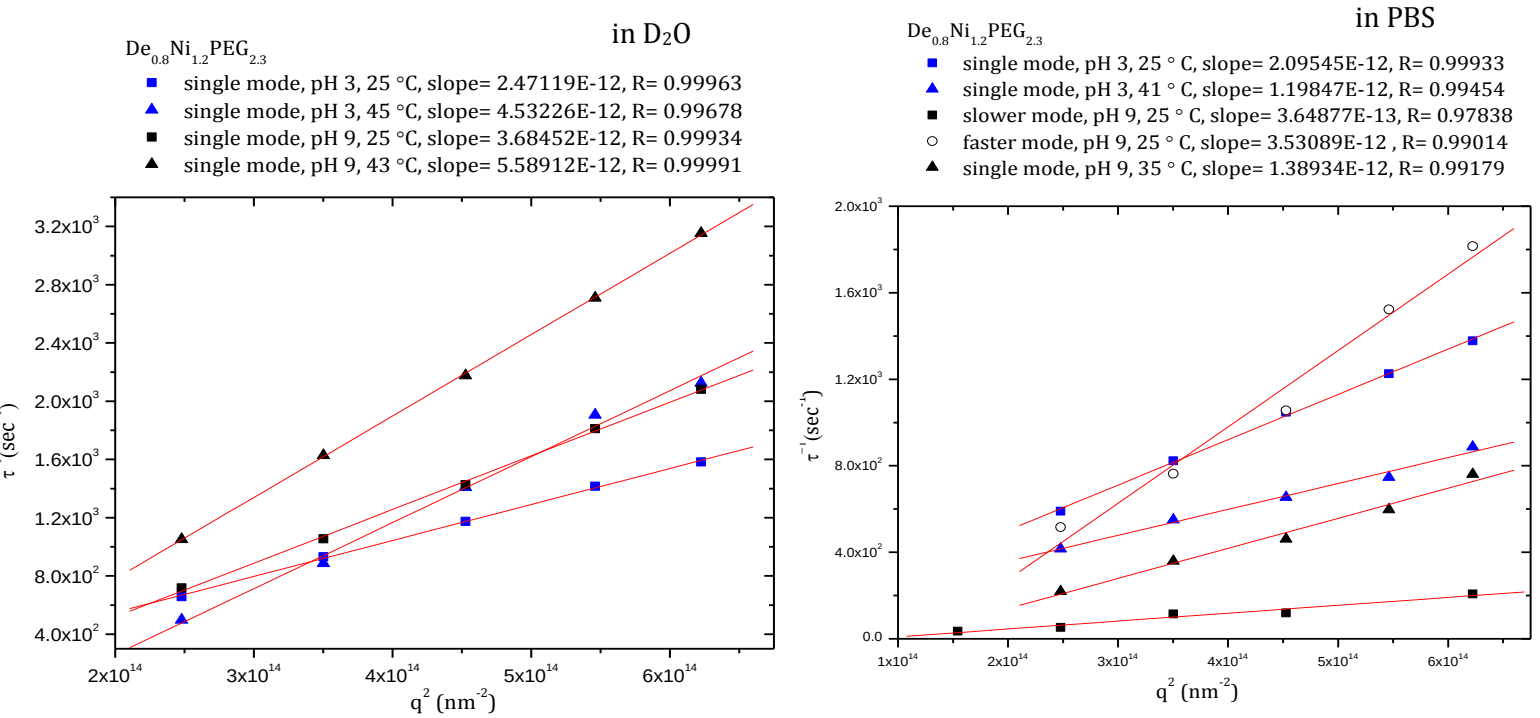

Figure 31-b – Decay rate (τ^{-1}) as a function of q^2- $De_{0.8}Ni_{1.2}PEG_{2.3}$ (0.5% w/w)

In bimodal correlation functions, which are defined for systems with two relaxation modes, D_s the apparent diffusion coefficient for slower mode (larger hydrodynamic radius) has a smaller value than D_f the apparent diffusion coefficient for faster mode (smaller hydrodynamic radius).

In some cases estimating of R_h for the slower mode is misleading, as this mode was found to have a strong dependence of diffusion coefficient on the scattering angle. This usually comes along with a lowered amplitude of correlation function (~ 80%) and a reduced stretching parameter b ~ 0.7[63]. Hydrodynamic radii of the micelles were obtained with the Stokes–Einstein equation (Eq.12-a, 12-b) and were tabulated in table 12. In some bimodal systems with a relatively lower b, e.g., $De_{0.1}Ni_1PEG_2$ at pH 3 and 9, hydrodynamic radius for slower mode should be reported conservatively. Based on the information in the table 12, polymer solutions in PBS developed bimodal size systems; this could be attributed to the charge screening effect of the salt solutions, as it leads to the micelles stickiness and aggregation in the form of larger micelles in case of $De_{0.8}Ni_{1.2}PEG_{2.3}$ and a collapse in case of $De_1Ni_1PEG_1$ and $De_{0.1}Ni_1PEG_2$; as $De_{0.8}Ni_{1.2}PEG_{2.3}$ has a longer PEG block in comparison to $De_1Ni_1PEG_1$ and longer PDEAEMA block as it is

in D_2O

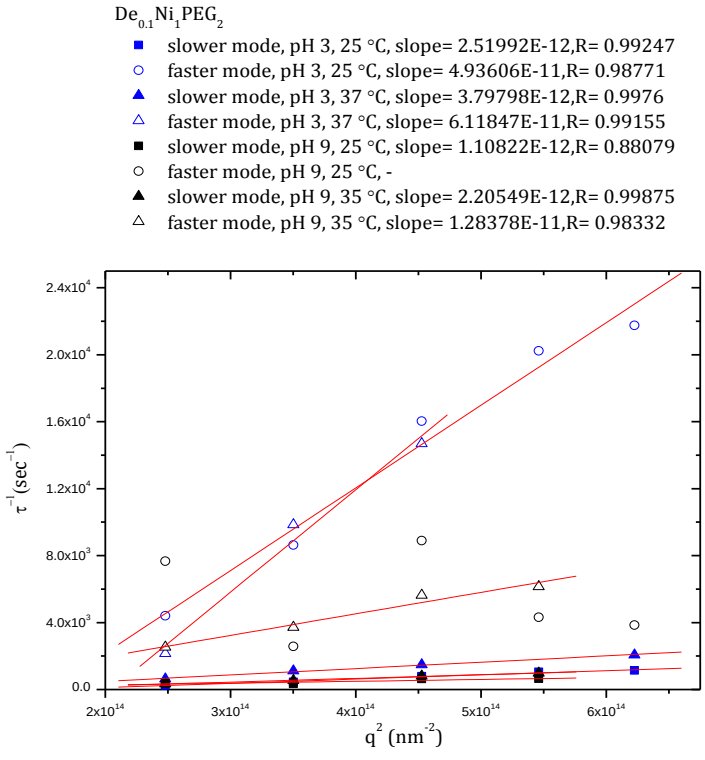

in PBS

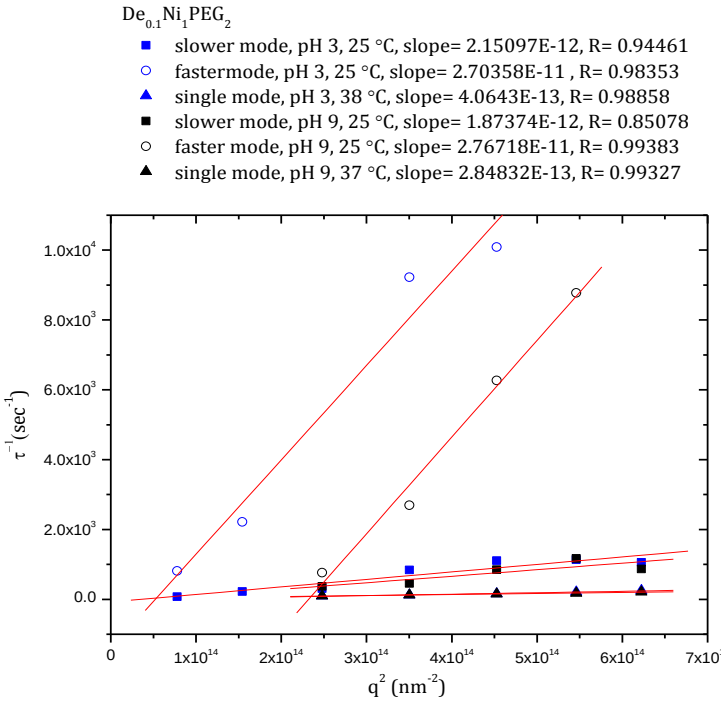

Figure 31-c – Decay rate (τ^{-1}) as a function of q^2- $De_{0.1}Ni_1$ PEG_2 (0.5% w/w)

ABCBA polymer	Temperature (° C)	R_h (nm) pH 3			R_h (nm) pH 7.4			R_h (nm) pH 9			
$De_1Ni_1PEG_1$ 34/58/34/58/34		D_2O	PBS		D_2O	PBS		D_2O		PBS	
	25	123	12	85	177	35		72	355	50	199
b (±0.01)		0.86		0.79	0.81	0.90			0.83		0.92
	30	121	14	99	180	31		68	323	51	186
b (±0.01)		0.87		0.75	0.84	0.96			0.91		0.89
	32	123	13	96	183	33		67	306	50	200
b (±0.01)		0.85		0.77	0.84	0.98			0.90		0.89
	35	116	18	160	175	149		70	340	138	
b (±0.01)		0.85		0.74	0.83	0.85			0.89	0.86	
	37	117	14	105	170			61	301		
b (±0.01)		0.83		0.77	0.83				0.92		
	40	106	31	190				60	285		
b (±0.01)		0.83		0.77					0.94		
	43	84	364					135			
b (±0.01)		0.86	0.86					0.93			
$De_{0.8}Ni_{1.2}PEG_{2.3}$ 27/68/77/68/27											
	25	94	107		65	64	320	78		101	861
b (±0.01)		0.96	0.94		0.97		0.86	0.94			0.86
	30	87	108		61	60	292	78		107	652
b (±0.01)		0.96	0.95		0.97		0.86	0.93			0.85
	32	85	106		62	57	278	77		96	595
b (±0.01)		0.96	0.96		0.96		0.91	0.93			0.86
	35	79	109		59	64	263	74		303	
b (±0.01)		097	0.94		0.97		0.87	0.93		0.84	
	37	78	120		57			74			
b (±0.01)		0.96	0.93		0.97			0.92			
	40	73	241		61			72			
b (±0.01)		0.96	0.99		0.97			0.91			

b (±0.01)	43	68 0.98								79 0.93			
b (±0.01)	45	140 0.86											
$De_{0.1}Ni_1PEG_2$ 2/57/68/57/2													
b (±0.01)	25	9	168 0.77	24	132 0.74	28	198 0.79	21	160 0.74	25	222 0.76	33	155 0.74
b (±0.01)	30	9	172 0.72	26	160 0.76	25	189 0.82	18	140 0.74	27	212 0.83	25	151 0.79
b (±0.01)	32	8	153 0.76	36	136 0.77	24	186 0.83	17	153 0.93	30	257 0.99	23	150 0.80
b (±0.01)	35	17	162 0.94	198 0.89		30	122 0.86	32	343 0.85	30	206 0.79	47	486 0.73
b (±0.01)	37	18	108 0.88	839 0.90		34	158 0.81	523 0.77				954 0.98	

Table 12 – $R_{h\ ave}$ of PDEAEMA$_x$-*b*-PNIPAAM$_y$-*b*-PEG$_z$-*b*-PNIPAAM$_y$-*b*-PDEAEMA$_x$, 0.5% wt

compared to $De_1Ni_1PEG_1$. In this regard, PEG length seems to have a profound impact on the micelle size. A comparison of correlation function in D_2O and PBS was represented in figure 32; clearly relaxation time for larger micelles was longer. On the other hand, in case of $De_{0.1}Ni_1PEG_2$ which in all cases represented a bimodal system, it is believed to have highest polydispersity in comparison to other polymers. According to ^1H NMR spectra this polymer showed the highest solubility in the aqueous solution, therefore parts of the polymer are unimers and parts of the chains cluster-like structures which give a broad size distribution to this polymer.

As a general trend, under the same conditions, micelles at higher pH had a larger size; it can be related to the enhanced deprotonation of PDEAEMA blocks at pH higher than the pK_a; as PDEAEMA is the outermost block within the penta-block terpolymer, chain diffusion to the core of micelles, considering relatively

hydrophilic PEG and PNIPAAM chains spreading in the aqueous solution makes the structure larger. At a constant pH, in D_2O with increasing temperature micelles shrink, while in PBS micelles had a tendency to aggregate. It can be postulated that in the absence of salt ions, PNIPAAM chain collapse results in smaller micelles, although in PBS with increasing temperature, the competitive mechanism of charge screening, dominates collapse of PNIPAAM chains.

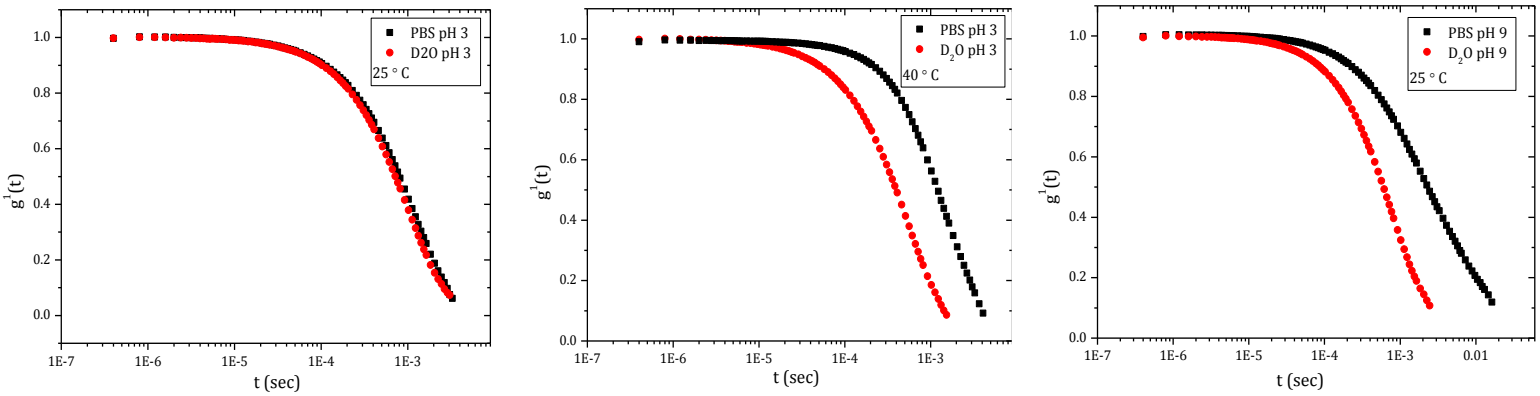

Figure 32 – Correlation function of $De_{0.8}Ni_{1.2}PEG_{2.3}$, 0.5% wt, at angle 90°

Among the three polymer systems, $De_{0.8}Ni_{1.2}PEG_{2.3}$ showed the highest stretching parameter in D_2O, indicating a monodisperse system, however in PBS with bimodal correlation functions, the stretching parameter b decreased, suggesting either polydispersity or various slower processes in the system such as relaxation of unfolded chains [63]. $De_{0.8}Ni_{1.2}PEG_{2.3}$ interestingly formed the smallest micelles in D_2O and the largest micelles in PBS, in comparison to $De_1Ni_1PEG_1$ and $De_{0.1}Ni_1PEG_2$. Although this is not unreasonable; based on the argument proposed in 3.5 ζ-potential measurements, the position of PDEAEMA block in $De_{0.8}Ni_{1.2}PEG_{2.3}$ avoid aggregation of polymer chains into the micelle, in comparison to the other two polymers; as the solvent turns to PBS, due to the charge screening effect, the inverse situation attracts more chains into the micelles, and this makes the micelle larger. At pH 7.4 and 9, by surfaces charge screening, $De_{0.8}Ni_{1.2}PEG_{2.3}$ solution turns to a relatively polydisperse system.

3.6.2 Static Light Scattering (SLS)

Geometrical conformation of the micelles and their temperature and pH-dependency were investigated with Static Light Scattering (SLS). A series of SLS measurements were carried out at different pH values (in D_2O) and temperatures to investigate the shape and apparent molecular weight of the micelles. Berry equation was used to analyze the averaged intensity of the scattered light. The z average radius of gyration R_{gz}, and the molecular weight of the micelles M_w were obtained from linear fitting in a low-q range (Guinier regime) on the $(Kc/R_\Theta)^{0.5}$ vs q^2 plot (or $(I)^{-0.5}$ vs q^2). At low concentration (0.5% w/w) and Guinier regime ($qR_g< 1$) the size of the micelle is a matter of interest, therefore inter-micelle interactions ($qR_g >1$) and multiple scattering was not considered in this study. Figure 33 shows a typical linear fitting on $(Kc/R_\Theta)^{0.5}$ vs q^2.

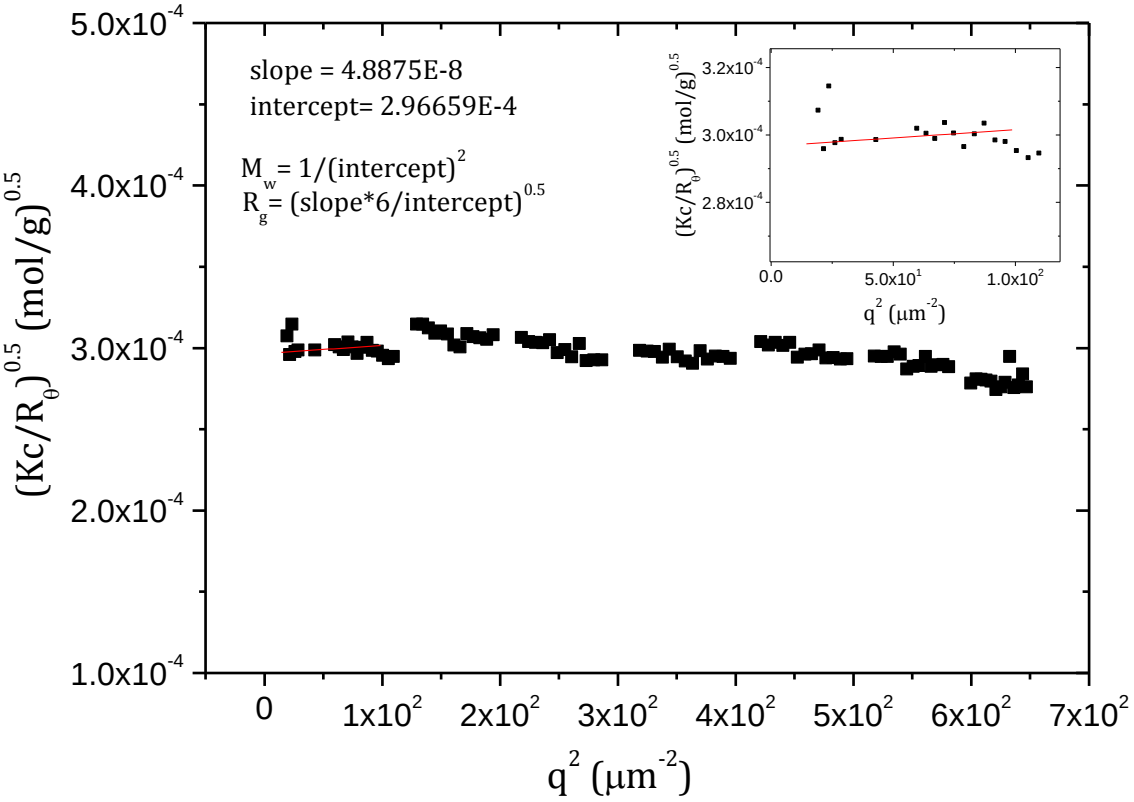

Figure 33 – Berry plot for $De_{0.8}Ni_{1.2}PEG_{2.3}$ in D_2O, at pH 3, 25 °C

Strong interactions among micelles may be identified by a negative initial slope of $(Kc/R_\Theta)^{0.5}$ vs q^2, which was not the case for polymer solutions in this study. Although in order to see in which concentration regime the analyses were carried out, overlap concentration, $c^*= 3M_w/(4\pi N_A R_g^3)$ was calculated from the average

values of M_w and R_g from table 13 [77] as followed in the same table. For $De_1Ni_1PEG_1$ unreasonable c* were obtained which were much lower than 0.005 g ml^{-1}. This does not indicate a semi-dilute regime, since according to DLS results (table 12) $De_{0.1}Ni_1PEG_2$, exhibited a bimodal system, furthermore the sharp slope at the lowest q-range obtained from SLS ($(Kc/R\Theta)^{0.5}$ vs q^2), led to the large R_g belonging to the larger structures which in SLS can not be separated from the smaller structures detected in DLS, therefore overlap concentration calculated with this R_g could be misleading, since it does not represent the overlap concentration of the individual micelles. This also explains the lower temperature at which multiple scattering happened in $De_{0.1}Ni_1PEG_2$ in comparison with the other polymers. A similar argument explains the wrong c* value for $De_1Ni_1PEG_1$. Although in this case, the calculated c* was slightly lower than 0.005 g ml^{-1} and the cluster formation issue was not as serious as it was for $De_{0.1}Ni_1PEG_2$. Nevertheless, inter-cluster or inter-chain interaction parameters were not calculated in this study.

Figure 34 shows the difference in the scattering pattern of the three polymers at 25 °C and pH 7.4 and figure 35 shows an overall view of the intensity (Kc/R) vs q plot at three pH values and 25 °C.

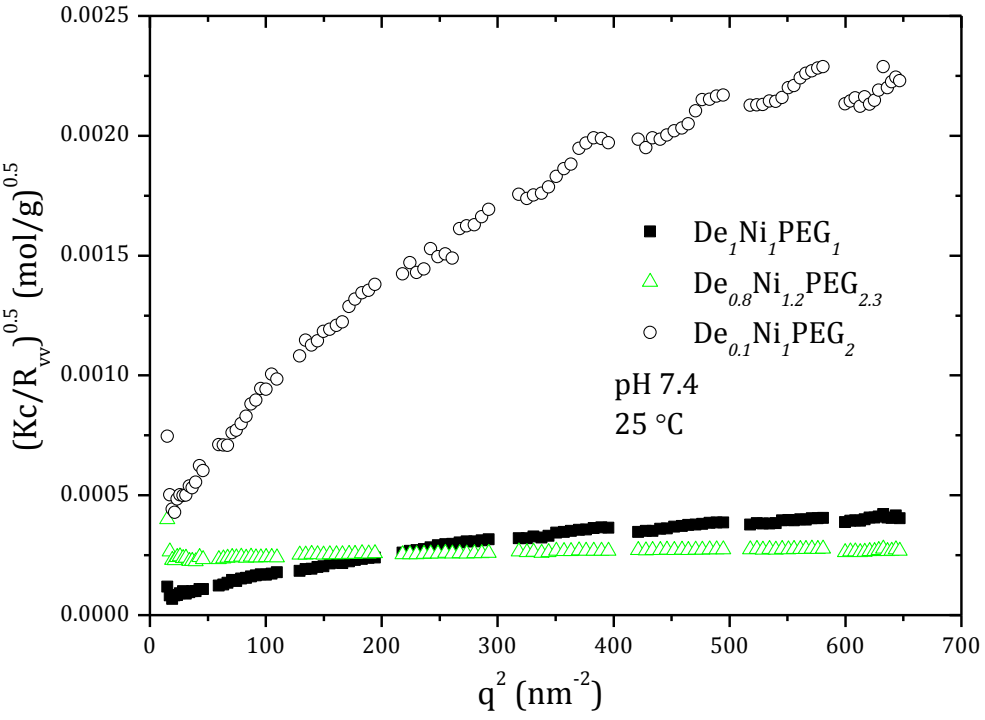

Figure 34 –Reduced scattering intensity as a function of q^2 at the concentration of 0.5% w/w in D_2O

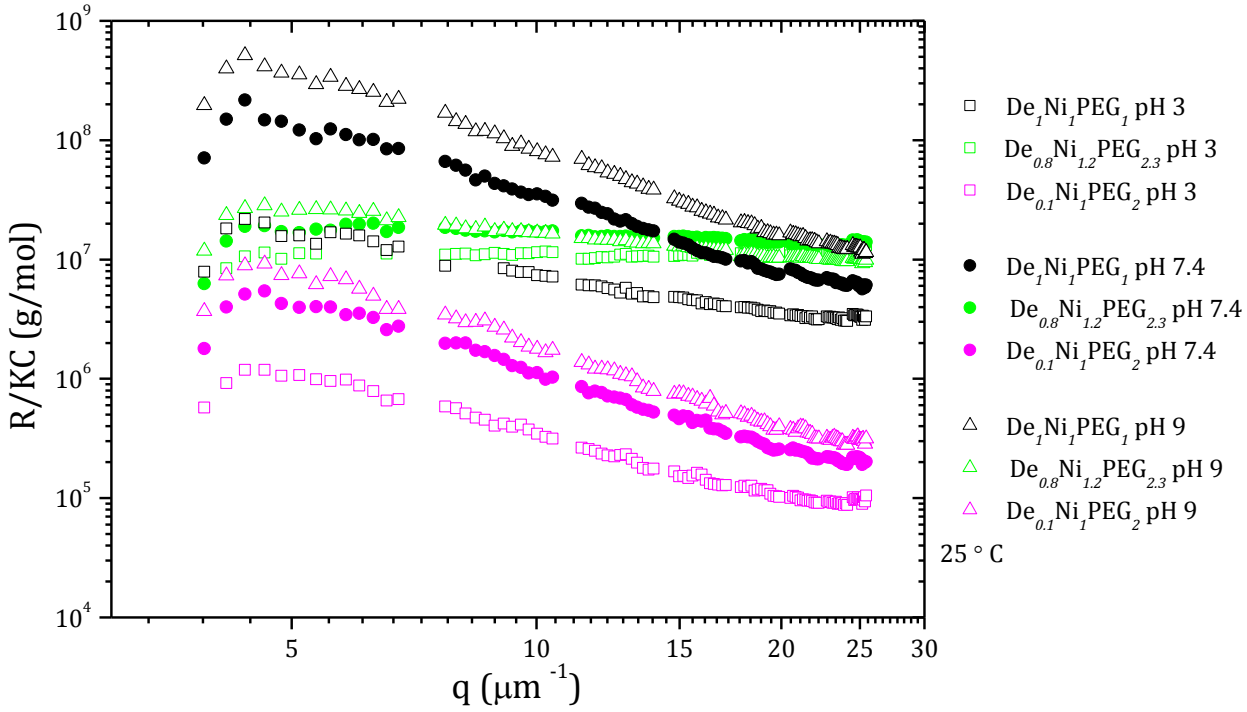

Figure 35 – Scattering intensity versus wavevector for PDEAEMA$_x$-*b*-PNIPAAM$_y$-*b*-PEG$_z$-*b*-PNIPAAM$_y$-*b*-PDEAEMA$_x$, in D_2O, 0.5% w/w at 25 °C

According to figure 34 or 35, $De_{0.8}Ni_{1.2}PEG_{2.3}$ exhibits a very weak angular dependency. This could possibly be due to the repulsion interactions among the micelles. The curvature for $De_{0.1}Ni_1PEG_2$ in figure 34 and the lowered scattering intensity in figure 35 could be explained by the appearance of an excluded volume effect or a strong repulsion among polymer chains in the clusters which produce the interference of scattered light from different chains [78].

In order to see temperature and pH effect on the reduced scattering intensity, scattering pattern of $De_{0.1}Ni_1PEG_2$ at the selected temperature and pH was showed in figure 36. For a short range of low-q values, a good linearity was observed for all the solutions. The curvature decreasing of the plot at higher q at 35 °C indicates the stronger hydrophobic interactions due to the weakened hydrogen bonds among PNIPAAM chains as it reaches to the LCST of the $De_{0.1}Ni_1PEG_2$. This led to the interference of scattered light and linearity at higher q.

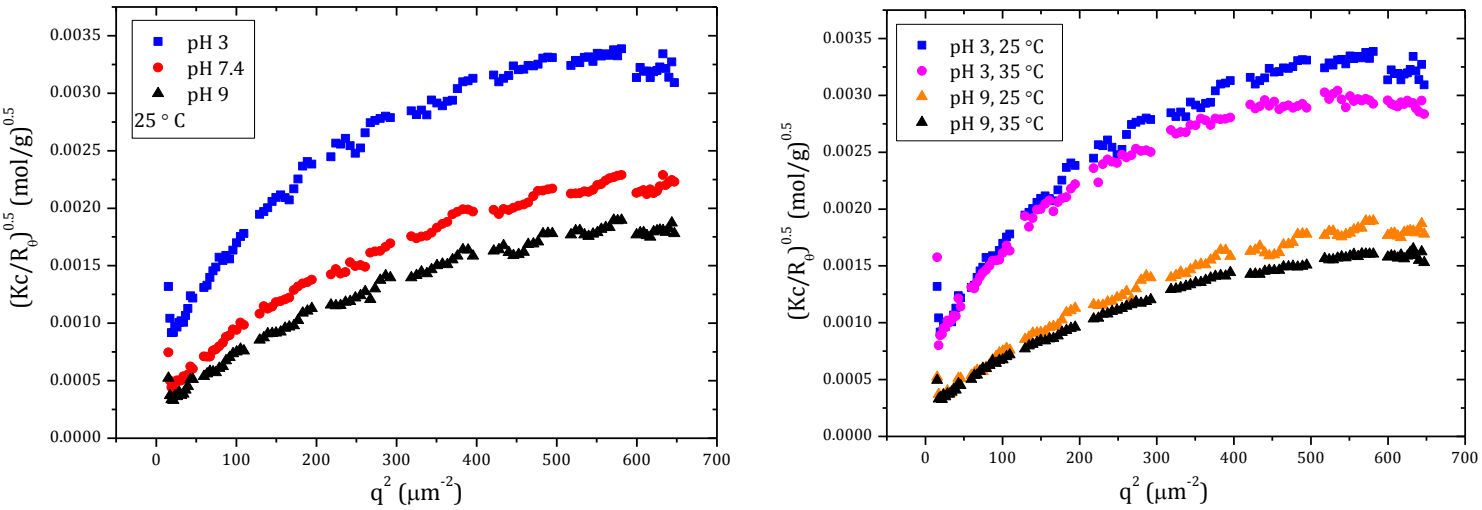

Figure 36 – pH- and temperature dependency of the reduced scattering intensity for $De_{0.1}Ni_1PEG_2$ in D_2O

M_w and R_g/R_h of micelles for all polymer solutions were summarized in table 13. For bimodal systems, the hydrodynamic radius which was comparable with R_g was selected to calculate R_g/R_h ratio. As a general trend, M_w in all systems, if not changed, was increased by increasing pH and temperature. This indicates that the hydrophobic portion in the penta-block terpolymer chain grows as temperature and pH rise, therefore the micelle structure becomes well-developed and bulky.

ABCBA polymer	Temperature (°C)	pH 3 D_2O 0.5% w/w		pH 7.4 D_2O 0.5% w/w		pH 9 D_2O 0.5% w/w	
$De_1Ni_1PEG_1$[16] 34/58/34/58/34		R_g/R_h	M_w (g.mol^{-1})	R_g/R_h	M_w (g.mol^{-1})	R_g/R_h	M_w (g.mol^{-1})
	25	1.3	2.01E7	2.1	3.0E8	1.0	8.5E8
	30	2.1	3.2E7	2.1	4.0E8	1.3	1.1E9
	32	2.3	3.7E7	1.5	2.6E8	1.3	1.1E9
	35	2.2	3.7E7	2.0	3.8E8	1.5	1.9E9
	37	2.1	4.0E7	1.5	3.2E8	1.5	1.3E9

[16] slower mode was considered in R_g/R_h ratio at pH 9

	40	2.3	4.5E7				
	43	2.8	6.8E7				
$De_{0.8}Ni_{1.2}PEG_{2.3}$ 27/68/77/68/27 c^*_{pH3}= 0.07 g.ml^{-1} c^*_{pH7}= 0.018 g.ml^{-1} c^*_{pH9}= 0.009 g.ml^{-1}	25	0.3	1.1E7	0.4	1.6E7	1.3	2.3E7
	30	0.4	1.2E7	0.6	1.7E7	1.4	2.4E7
	32	0.5	1.2E7	0.5	1.7E7	1.7	2.8E7
	35	0.6	1.3E7	0.6	1.8E7	1.6	2.7E7
	37	0.7	1.4E7	0.7	1.9E7	1.5	2.7E7
	40	0.7	1.5E7	0.9	6.2E7	1.6	3.0E7
	43	0.4	2.4E7			0.9	3.5E7
$De_{0.1}Ni_1PEG_2$[17] 2/57/68/57/2	25	1.4	1.6E6	1.7	9.7E6	1.5	1.6E7
	30	2.2	3.1E6	1.6	8.5E6	1.3	1.3E7
	32	2.0	2.1E6	1.9	9.9E6	1.1	1.6E7
	35	1.8	2.0E6	3.3	1.3E7	1.5	1.5E7
	37	1.5	1.6E6	2.0	9.9E6		

Table 13 – Temperature and pH dependence of characteristic parameters for PDEAEMA$_x$-*b*-PNIPAAM$_y$-*b*-PEG$_z$-*b*-PNIPAAM$_y$-*b*-PDEAEMA$_x$, 0.5% w/w in D_2O, obtained by SLS and DLS

In addition, the micellar aggregation number (N_{agg}) which is calculated by equation 28, provides further information on the micellar structure.

$$N_{agg} = \frac{M_{w(micelle)}}{M_{w(unimer)}} \qquad \text{Eq.28}$$

where $M_{w(unimer)}$ was estimated from ^{1}H NMR measurements as shown in table 1 N_{agg} for selected systems were summarized in table 14.

[17] slower mode was considered in R_g/R_h ratio at pH 3, 7.4 and 9

ABCBA polymer	Temperature (°C)	N_{agg} pH 3 D_2O 0.5% w/w	N_{agg} pH 7.4 D_2O 0.5% w/w	N_{agg} pH 9 D_2O 0.5% w/w
$De_1Ni_1PEG_1$ 34/58/34/58/34	25	7.4E2	1.1E4	3.2E4
	37	1.5E3	1.2E4	4.8E4
	43	2.5E3		
$De_{0.8}Ni_{1.2}PEG_{2.3}$ 27/68/77/68/27	25	3.8E2	5.5E2	7.9E2
	37	4.8E2	6.6E2	9.3E2
	40	5.2E2	2.1E3	1.0E3
	43	8.3E2		1.2E3
$De_{0.1}Ni_1PEG_2$ 2/57/68/57/2	25	9.4E1	5.7E2	9.4E2
	35	1.2E2	7.7E2	8.8E2
	37	9.4E1	5.8E2	

Table 14 – Temperature and pH dependence of aggregation number N_{agg} for $PDEAEMA_x$-*b*-$PNIPAAM_y$-*b*-PEG_z-*b*-$PNIPAAM_y$-*b*-$PDEAEMA_x$, 0.5% wt in D_2O

Number of chains aggregated into the micelles followed the same trend as the M_w obtained from SLS. $De_1Ni_1PEG_1$ and $De_{0.1}Ni_1PEG_2$ at a constant temperature and pH represented the highest N_{agg} and lowest N_{agg}, respectively. It suggests that the total hydrophobicity of $De_1Ni_1PEG_1$ is the highest in comparison to the other penta-block terpolymers, while $De_{0.1}Ni_1PEG_2$ shows the highest hydrophilicity [79]. This observation is consistent with the assumption made in 3.4 ^1H NMR.

In order to elucidate chain conformation in the micelles, the dimensionless ratio of the average radius of gyration to the hydrodynamic radius (R_g/R_h) was calculated. On average, R_g/R_h for $De_{0.8}Ni_{1.2}PEG_{2.3}$ at pH 3 and 7.4 was lower than 0.78 which is a characteristic R_g/R_h for hard sphere, suggesting spherical micelles with a dense core covered by a corona possessing low mass distribution [79-80].

By increasing pH and consequently hydrophobicity of the polymer which manifested as an increase in N_{agg}, the ratio of R_g/R_h rises could be possibly indicating the larger micelle with a relatively loose corona, as the ratio of 1.5-1.7 is proposed for coil like structures [81]. R_g/R_h of 2 and higher is proposed for rigid cylindrical structures [81]. This could be the case for $De_1Ni_1PEG_1$ at pH 3 and 7.4, with the cluster-like structure explained before, however at pH 9 micelles turn to the spherical loose structures. The latter structure could be applied to $De_{0.1}Ni_1PEG_2$. The coil-like structure for $De_{0.1}Ni_1PEG_2$ is consistent with the hypothesis made earlier. It is worth pointing out that R_g/R_h is not the only and the most powerful asset to determine the micelle architecture and it has to be regarded along with other methods, particularly SANS experiments for which the complete form factor can be determined.

3.6.3 Small Angle Neutron Scattering (SANS)

In order to further investigate on the micellar structure, at the smaller wavelength scales (see table 2), SANS measurements on 0.5% w/w and 20.0% w/w systems were performed at selected pH values and temperatures below and above the threshold found in the turbidity measurements, as well as at an intermediate temperature. Figure 37 shows the scattering pattern at 25 °C and pH 3, 7.4 and 9. The low-q scattering increased more than a factor of ten, demonstrates a significant structural organization in the size regime probed by SANS [61], which is the case for $De_1Ni_1PEG_1$ and $De_{0.8}Ni_{1.2}PEG_{2.3}$. For $De_{0.1}Ni_1PEG_2$, there was only weak small angle scattering, suggesting a loose assembly of polymer chains, which in comparison to $De_1Ni_1PEG_1$ and $De_{0.8}Ni_{1.2}PEG_{2.3}$ is barely considered as a well-shaped classic micelle. This is consistent with a low N_{agg} of $De_{0.1}Ni_1PEG_2$. This suggests that PDEAEMA block length has a profound effect on scattering intensity (comparing $De_{0.8}Ni_{1.2}PEG_{2.3}$ and $De_{0.1}Ni_1PEG_2$). Moreover, it is of crucial importance to consider that, within the SANS q-range, large cluster-like structures obtained by DLS measurement, particularly in case of bimodal systems, are not characterized and does not refute existence of these structures either. In general, the scattering intensity at pH 9 is relatively stronger than it is at lower pH.

This affirmed the effect of PDEAEMA block, which at higher pH, becomes more hydrophobic and results in stronger scattering.

The data were fit with a spherical core-shell model for $De_1Ni_1PEG_1$ and $De_{0.8}Ni_{1.2}PEG_{2.3}$, with a form factor as followed in equation [68]29:

$$P_{\text{core-shell}}(q) = \left[\frac{3j_1(qR_c)(k_c - k_s)V_c}{qR_c} + \frac{3j_1(qR_c)(k_s - k_{solv})V_c}{qR_c}\right]^2 \qquad \text{Eq.29}$$

where $J_1(x)$ is denotes as:

$$j_1(x) = (\sin x - x\cos x)/x^2$$

and R_c, R_s are the radius of the core and shell, respectively, V_c and V_s are the volume of the core and shell, respectively, and k_c, k_s and k_{solv} are the scattering length density (SLD) values of the core, shell and solvent, respectively. SLD for each block of PDEAEMA$_x$-*b*-PNIPAAM$_y$-*b*-PEG$_z$-*b*-PNIPAAM$_y$-*b*-PDEAEMA$_x$ was indicated in 3.2 Densitometry. Form factor for $De_{0.1}Ni_1PEG_2$ is definitely different than equation 29. Since it is not conclusive that $De_{0.1}Ni_1PEG_2$ is assembled either as a well-shaped micelle or unimers (individual chains) form factor for unimers were not used either; proposing a decisive structure for this polymer requires further evidence.

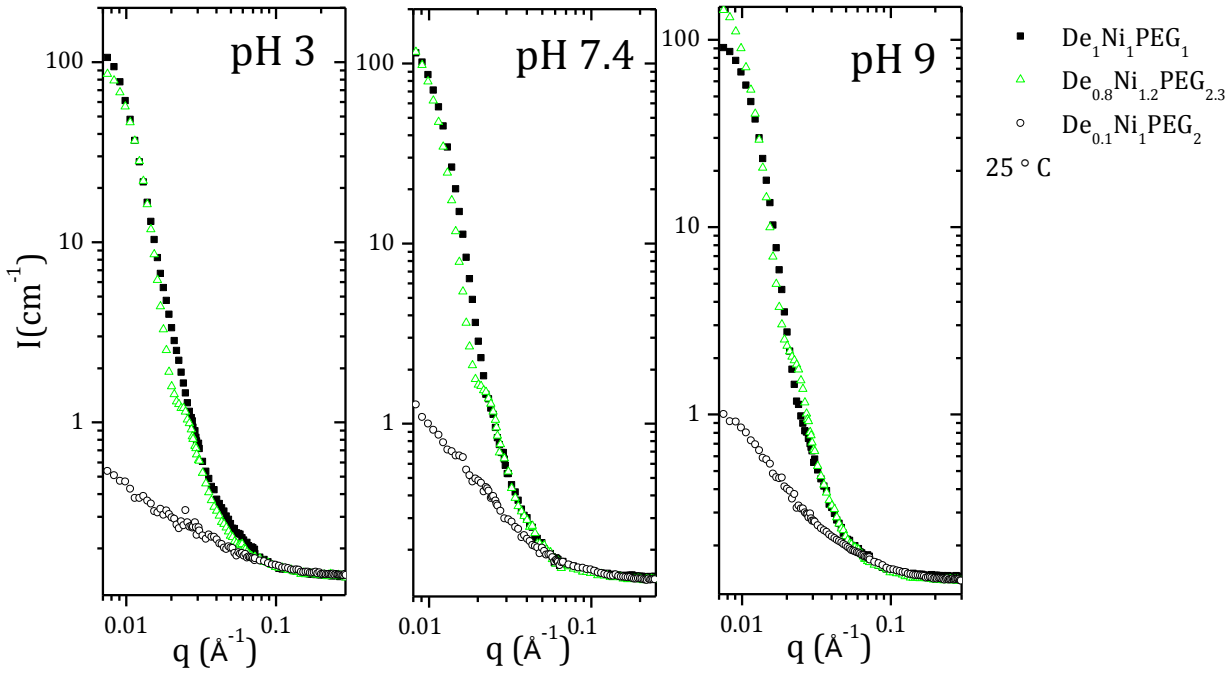

Figure 37 – SANS scattering profile for D_2O PDEAEMA$_x$-*b*-PNIPAAM$_y$-*b*-PEG$_z$-*b*-PNIPAAM$_y$-*b*-PDEAEMA$_x$, 0.5% w/w in D_2O

A typical spherical core-shell fitting curve was displayed in figure 38. An approximate diameter of 43 nm at 25 °C was obtained from the model, which is the size of the core. In comparison to the size obtained from DLS (94 nm), this could be explained by the nature of DLS which measures the hydrodynamic size, including the corona and water moving together with the micelle. $De_{0.8}Ni_{1.2}PEG_{2.3}$ exhibited a bump around 0.25 $Å^{-1}$ suggesting well-developed micelles which is explained by the longer PEG length in comparison to $De_1Ni_1PEG_1$.

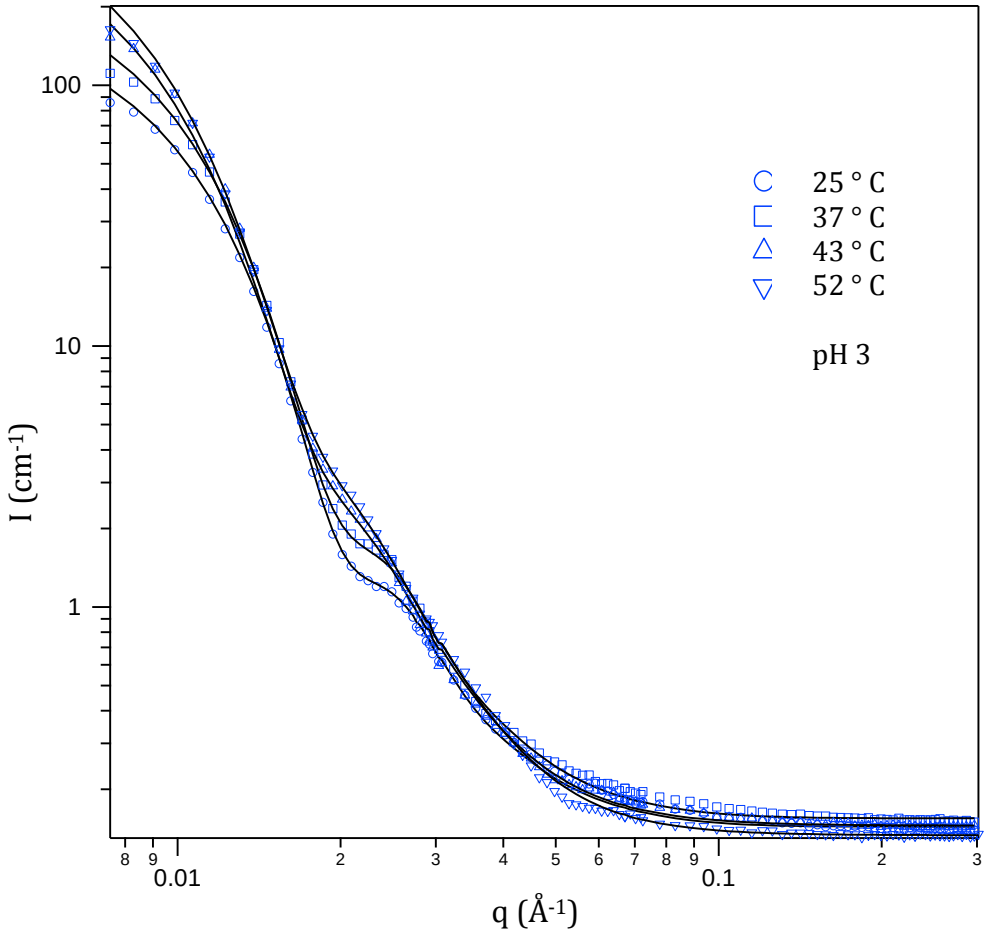

Figure 38 – SANS scattering profile for $De_{0.8}Ni_{1.2}PEG_{2.3}$, at pH 3, 0.5% wt in D_2O

According to figure 38, there was a systematic trend of increased low-q intensity with temperature, indicating an increase in micelle size. Moreover, the bump almost disappeared at a higher temperature, implying a transition, possibly PNIPAAM diffusion into the core and changing the scattering pattern of the core as it was at lower temperature; in other words, increasing the temperature made a rough core-shell interface and a fuzzy micellar structure. Core size obtained from SANS data, for $De_1Ni_1PEG_1$ and $De_{0.8}Ni_{1.2}PEG_{2.3}$ with the core-shell model was

summarized in table 15. This should be emphasized that the main contribution to the scattering profiles on PDEAEMA$_x$-*b*-PNIPAAM$_y$-*b*-PEG$_z$-*b*-PNIPAAM$_y$-*b*-PDEAEMA$_x$ was from the core of micelles, since the corona forms a highly solvated structure that results in a less contrast in SANS. That explains the difference of size in DLS and SANS. In addition, since SANS only probes structure below roughly 100 nm, size obtained with SANS does not exclude the existence of larger micelles in the system.

Temperature (°C)	**Diameter (nm) at pH 3**	
	$De_{0.8}Ni_{1.2}PEG_{2.3}$	$De_1Ni_1PEG_1$
25	43.9	36.8
37	45.0	34.2
43	47.8	28.7
52	48.2	27.8

Table 15 – Core diameter obtained from SANS data with core-shell model, 0.5% w/w in D_2O

According to table 15, at pH 3, $De_1Ni_1PEG_1$ formed a relatively smaller core; this could be explained by the shorter length of PEG and PNIPAAM in comparison to $De_{0.8}Ni_{1.2}PEG_{2.3}$. At this pH, PDEAEMA mainly is situated in the corona; therefore it does not seem to have a contribution in the core scattering profile.

Figure 39 shows scattering data for $De_{0.8}Ni_{1.2}PEG_{2.3}$ at pH 9, to investigate the temperature effect at this pH. Since at pH 7.4 the scattering profile was almost the same as pH 9, it was not shown here.

In comparison to pH 3, scattering intensity at a constant temperature was higher in pH 9 and a relatively larger size was obtained for pH 9, e.g., 47.5 nm at 25 °C. The same pattern was observed by increasing temperature, i.e., a stronger scattering intensity and a faded bump at higher temperature, suggesting the diffusion of both PDEAEMA and PNIPAAM into the core of micelle at a higher temperature. The size became slightly smaller upon heating, as it did in DLS measurements. The difference does not seem to be substantial for drawing a conclusion here, but there is a possibility that both PDEAEMA and PNIPAAM were squeezed through the core while PEG was still solvated, but not as freely as it was at lower temperature.

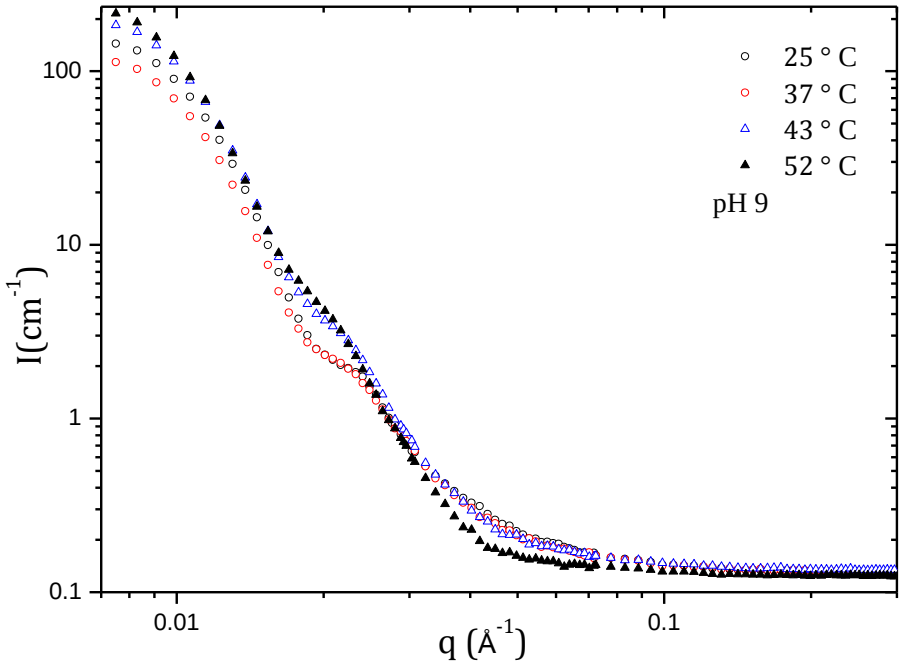

Figure 39 – SANS scattering profile for $De_{0.8}Ni_{1.2}PEG_{2.3}$, at pH 9, 0.5% wt in D_2O

Figure 40 shows scattering profile for $De_{0.1}Ni_1PEG_2$ at pH 3 and 9. The general trend was that with increasing temperature, especially above 37 °C, scattering intensity became stronger, indicating formation of relatively well-shaped micelles. This could not be compared with DLS measurements since above 37 °C due to the multiple scattering effect, no data were reported. Although at very high temperatures, e.g., above 50 °C, the three penta-block terpolymers showed a macroscopic phase separation, even in D_2O, there were still micellar structures dispersed in the solvent that could be analyzed in SANS. For $De_{0.1}Ni_1PEG_2$ at pH 9 and 52 °C, a proper fitting was obtained with the core-shell model with a core diameter of 15 nm (Figure. 41).

An interesting observation with $De_{0.1}Ni_1PEG_2$ at pH 3 and 43 °C was the appearance of a correlation peak around 0.03$Å^{-1}$. This is indicative of some highly ordered structures existing around this temperature, with an approximate packing distance of $d=2\pi /0.03$ $Å^{-1}$ = 209 Å and a core size of 21 nm. This peak does not exist at lower or higher temperatures, suggesting an intermediate regular ordering of small entities.

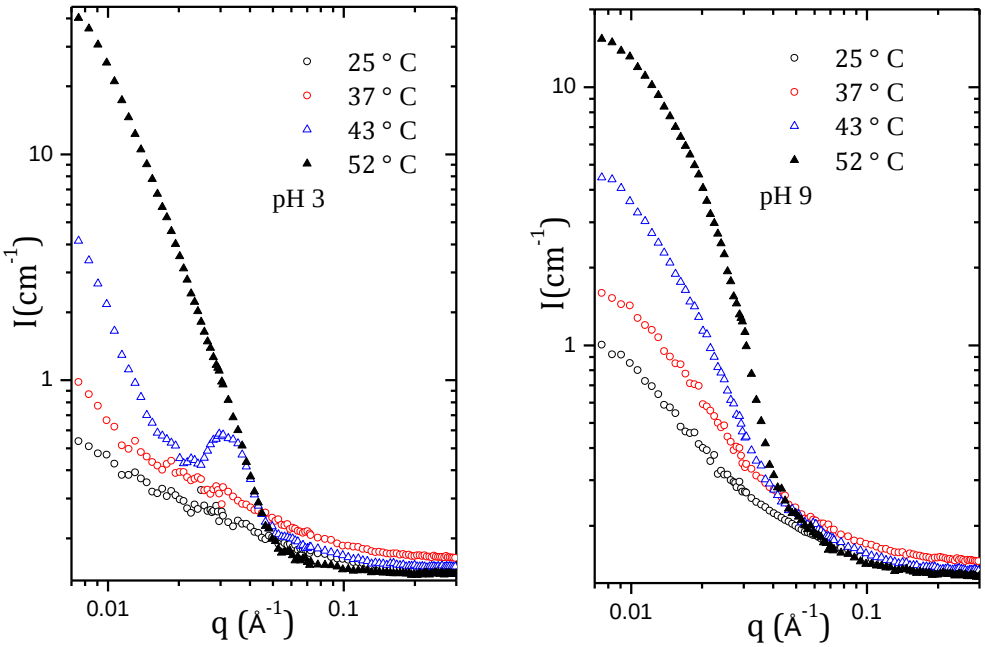

Figure 40– SANS scattering profile for $De_{0.1}Ni_1$ PEG_2, 0.5% wt in D_2O

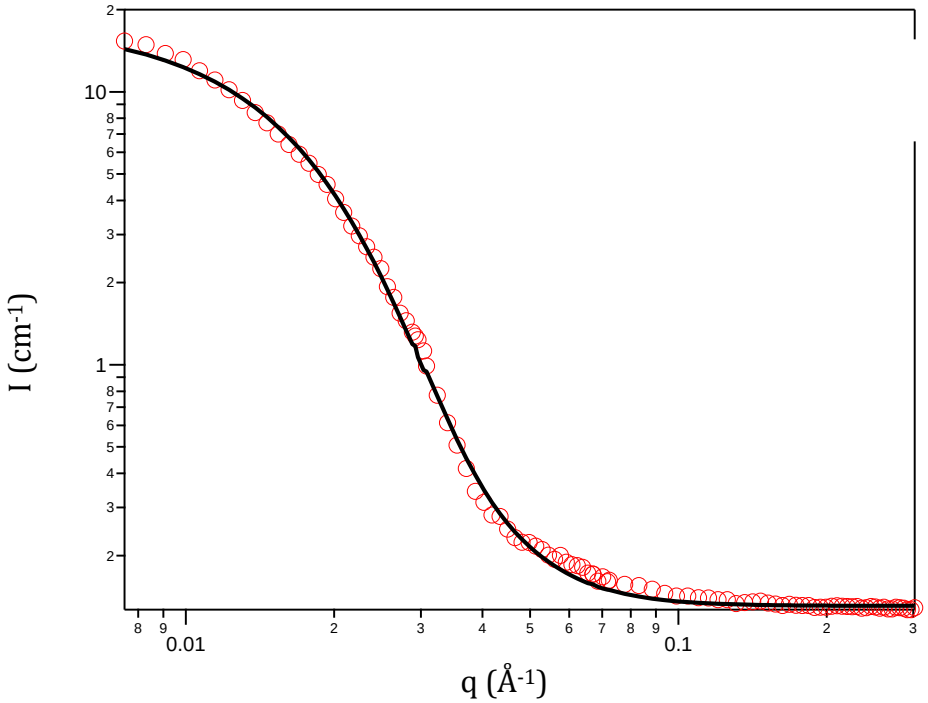

Figure 41 – SANS scattering profile for $De_{0.1}Ni_1PEG_2$, at pH 9, 52 °C, 0.5% wt in D_2O

The mild slope (almost plateau region) in the low-q range for $De_{0.1}Ni_1PEG_2$ at 25 °C pH 3 and 9, provided the possibility to calculate R_g and M_w from SANS data with Zimm formula in Guinier regime [82] (Equation 30).

$$\frac{\Delta k^2 \Phi}{I(q)} \sim \frac{\rho_m}{M_w}\left(1+\frac{R_{g,z}^2 q^2}{3}\right) \qquad \text{Eq.30}$$

where Δk^2, Φ, ρ_m are the squared scattering length density excess of polymer with respect to solvent (in this case D_2O with SLD= 6.36×10^{10} cm^{-2} [72]), volume fraction of the polymer and mass density of the solvent (D2O), respectively.

I^{-1} vs q^2 was plotted; by a linear fitting over a range in the low-q values to keep $qR_g < 1$ (Guinier regime), R_g and M_w were derived (Figure 42)

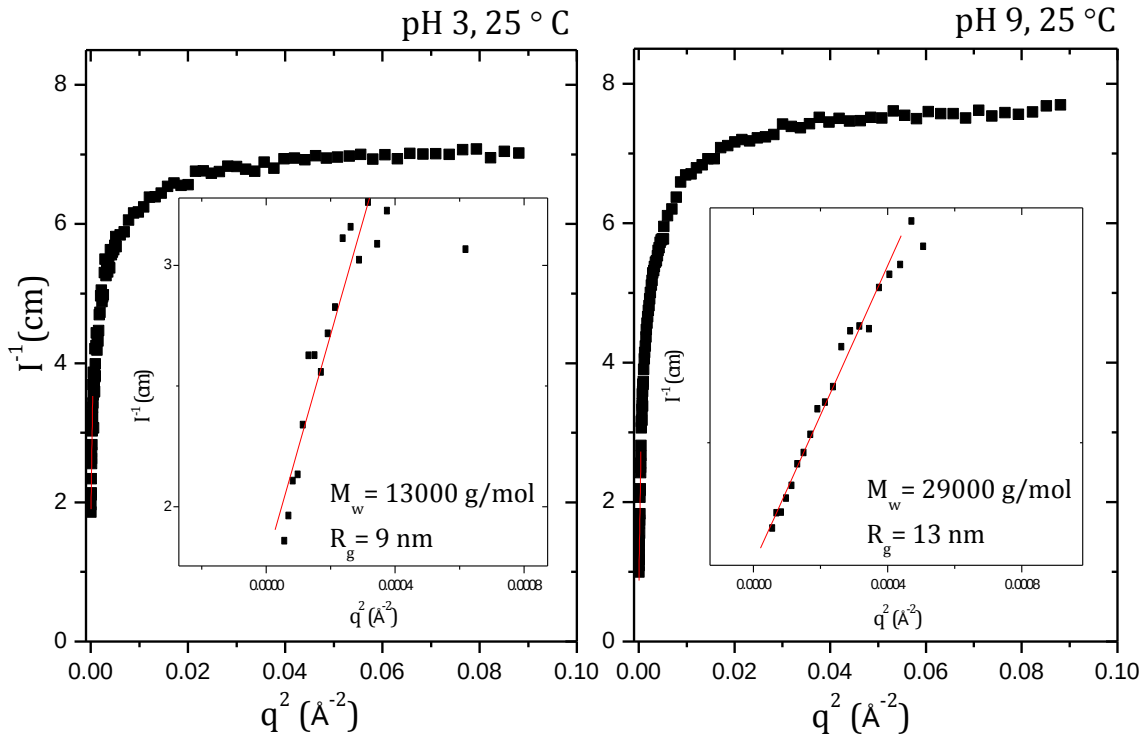

Figure 42 – SANS scattering profile for $De_{0.1}Ni_1PEG_2$, , 0.5% w/w in D_2O

R_g and M_w obtained by SANS seemed more reasonable than the values derived from SLS. As it was expected, at pH 3 and 25 °C, $De_{0.1}Ni_1PEG_2$ with the concentration of 0.5% w/w in D_2O was found more in the form of unimers than proper micelles. M_w of the unimers (13000 g/mol) is comparable with the molecular weight obtained from ^1H NMR (fig. X). At pH 9, higher molecular weight and R_g were obtained but still the values are too small to be able to be self-assembled into a classic micelle.

Figures 43-a, -b show the scattering profile for $De_1Ni_1PEG_1$ at pH 3 and 9. The fitting curve by core-shell model was displayed for pH 3. $De_1Ni_1PEG_1$ represented a strong pH-dependency. At pH 3, this polymer seemed to be stable upon temperature change; there was only a small size reduction at 52 °C, however at pH 9, upon heating above 37 °C a drastic decrease of the size, was observed. This could be explained with the same hypothesis mentioned for figure 39.

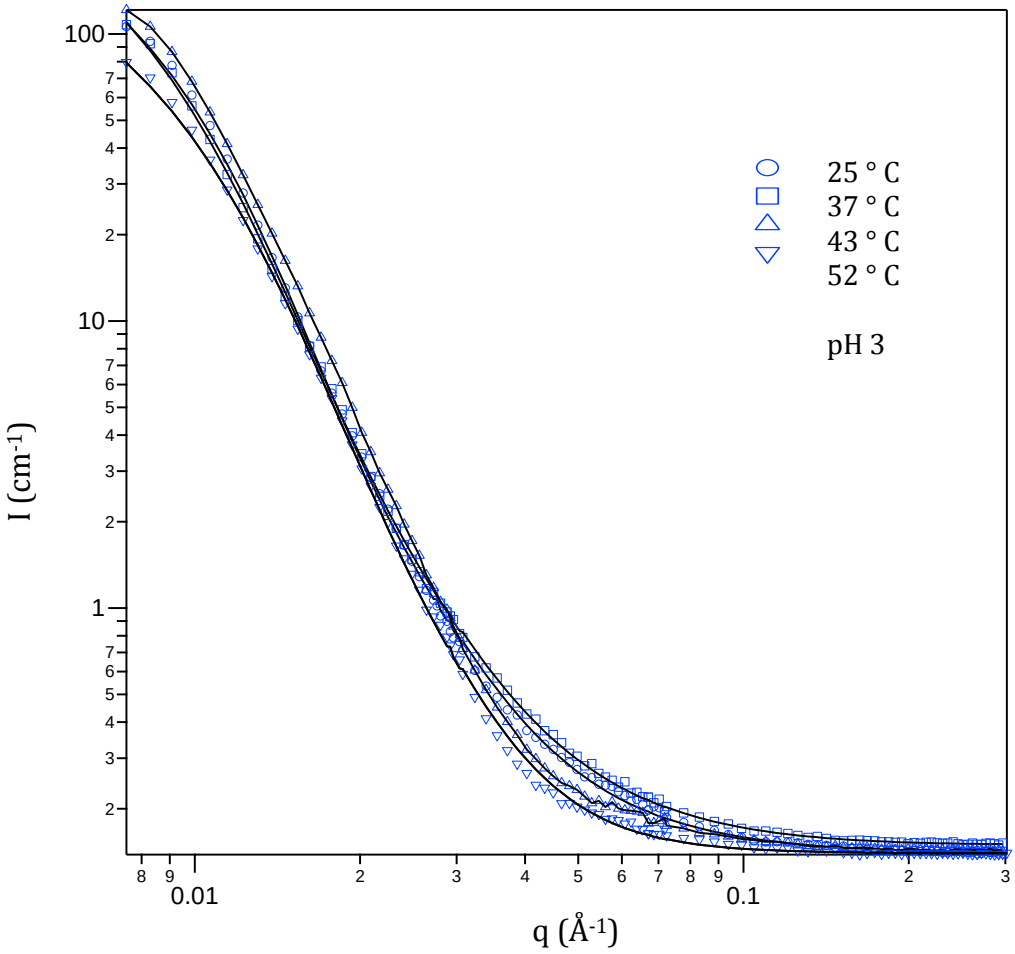

Figure 43-a – SANS scattering profile for $De_1Ni_1PEG_1$, pH 3, 0.5% w/w in D_2O

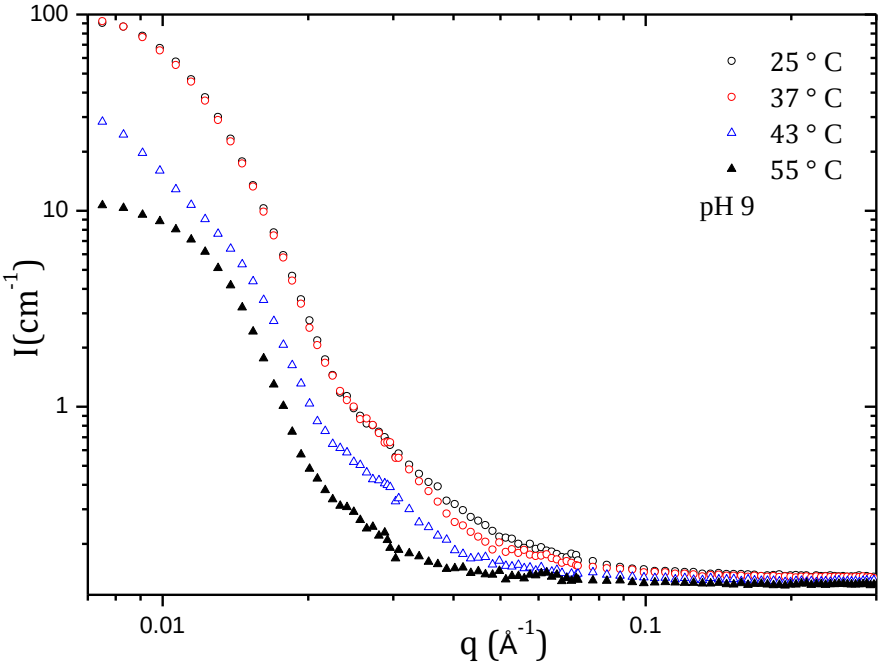

Figure 43-b – SANS scattering profile for $De_1Ni_1PEG_1$, pH 9, 0.5% w/w in D_2O

To expand the window of scattering range, it is possible to combine SLS and SANS; as light probes low q-values, where large scale fluctuations dominate, and SANS probes high q-values, where short-wavelength fluctuations dominate. The combined data can be used to evaluated models that have been proposed [35]. Figure 44-a, -b, -c show the scattering profile of combined SLS and SANS at selected temperatures and pH values. To plot these data, contrast factor for light and neutron were considered for y-axis. For SLS, it is R_θ/KC (g/mol) and for SANS it is defined as $\frac{I \times N_A}{v_p \Phi \Delta k^2}$ (g/mol), where Φ, N_A, Δk^2 and v_p are the polymer volume fraction, Avogadro's number, the squared scattering length density excess of polymer with respect to solvent (in this case D_2O with SLD= 6.36×10^{10} cm^{-2} [72]) and the specific volume of the polymer. For the sake of simplicity, the y-axis was denoted only by I(q). Clearly there was a small missing region between the q-range in SLS and SANS, although both sets of data seemed to be smoothly connected to each other. The strong upturn in the low-q region for $De_1Ni_1PEG_1$ and $De_{0.1}Ni_1PEG_2$, particularly at pH 9, suggests large association complex, as it was observed in DLS results, these two systems tend to develop a bimodal systems, therefore R_g obtained from SLS and R_g obtained from SANS will not be close to each other.

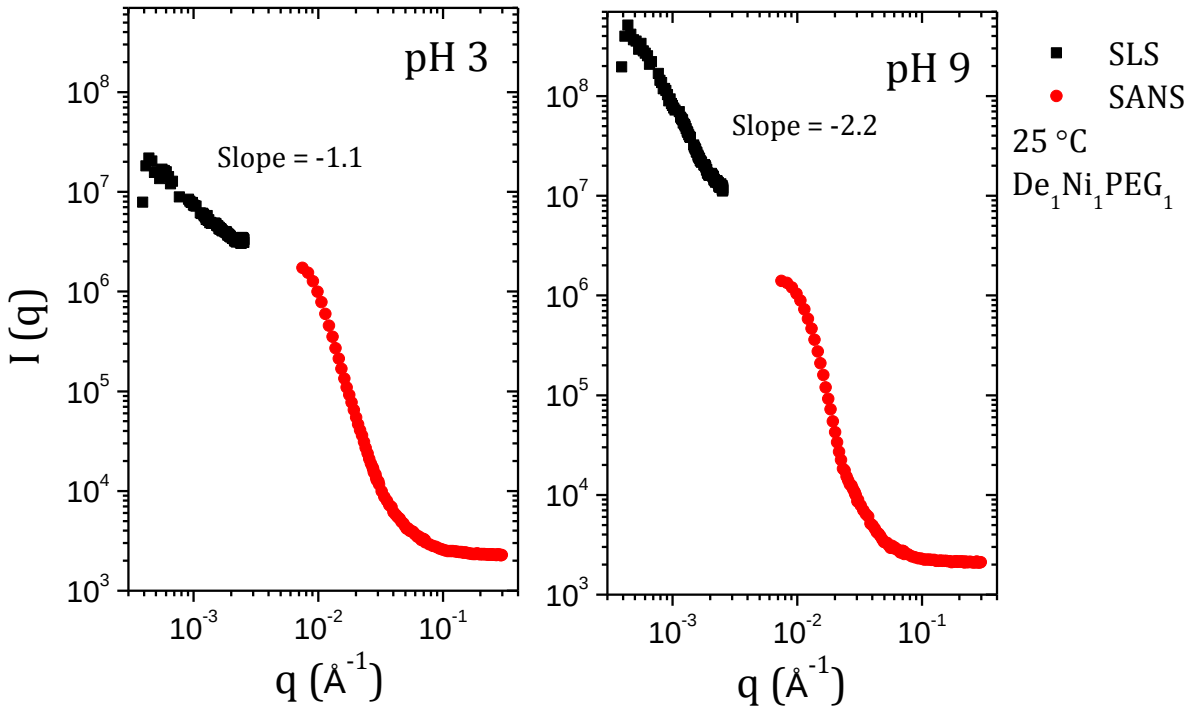

Figure 44-a – Log-log plot of combined SLS and SANS scattering profile for $De_1Ni_1PEG_1$, 25 °C, 0.5% w/w in D_2O

The cluster-like structures could be formed by PEG block situating toward the shell of micelles [83]; however, for $De_{0.8}Ni_{1.2}PEG_{2.3}$ particularly at pH 3, the slope close to zero suggests a monodisperse and relatively smaller micelles (no clusters). In general the slope close to -2 indicates a theta- solvent for the polymers (pH 9), and the slope close to -1.6, indicates a good solvent for the polymer (pH 3). It is possible to use the modified Ornstein-Zernike equation for bimodal system as equation 31:

$$I(q) = \frac{A_{SLS}}{1+ q^2 R^2} + \frac{A_{SANS}}{1+ q^2 \xi^2} \qquad \text{Eq. 31}$$

where A denotes the scattering constants and R (>> ξ) and ξ are the correlation lengths in SLS and SANS respectively. With this conjecture these systems can be considered as one-phase systems that have bimodal concentration fluctuations in submicrometers (low-q region) and a few tens of angstroms (high-q region) [83].

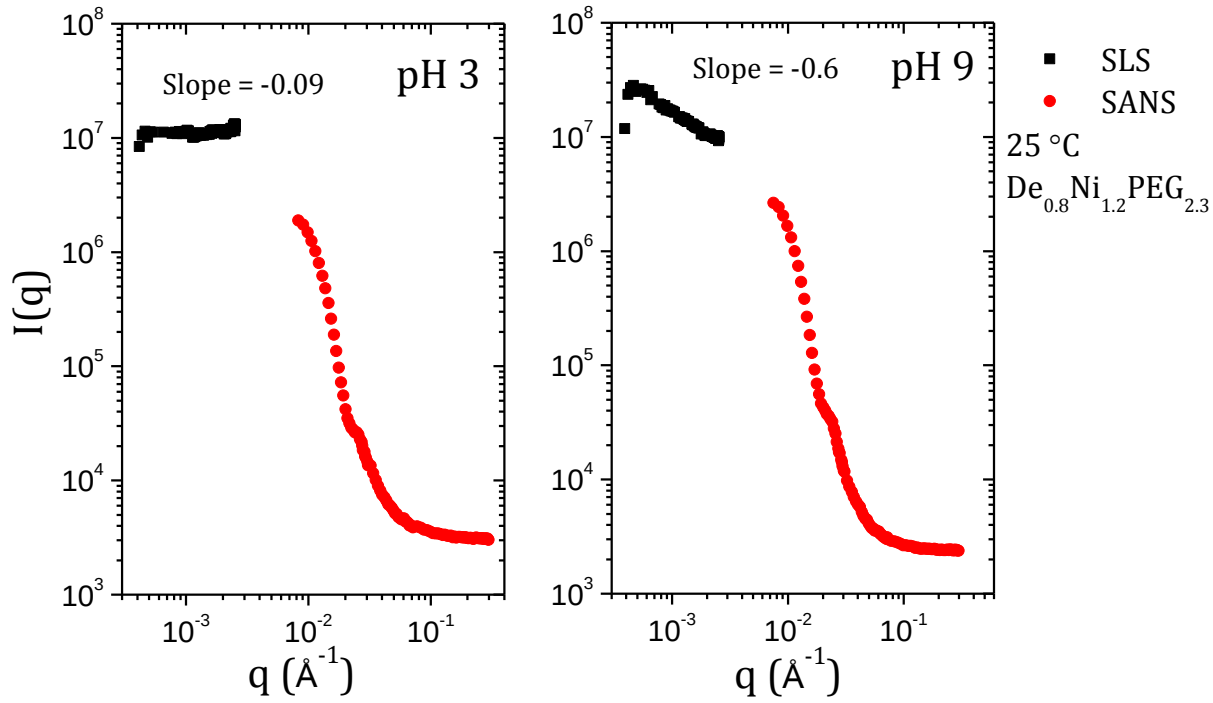

Figure 44-b – Log-log plot of combined SLS and SANS scattering profile for $De_{0.8}Ni_{1.2}PEG_{2.3}$, 25 °C, 0.5% w/w in D_2O

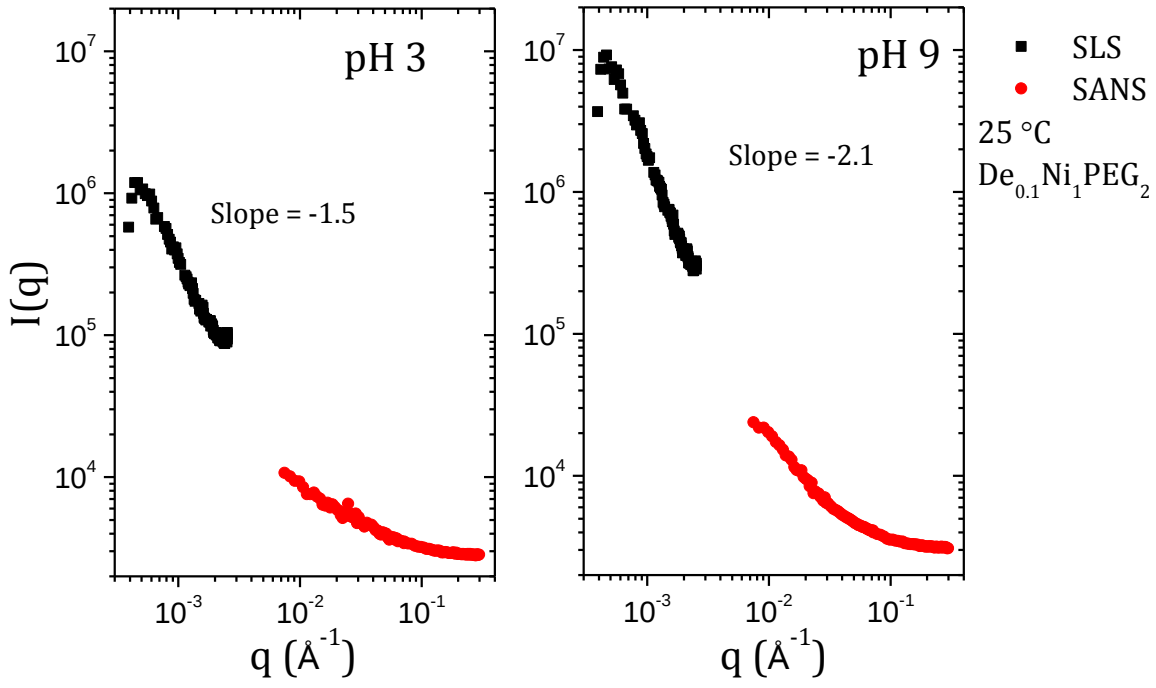

Figure 44-c – Log-log plot of combined SLS and SANS scattering profile for $De_{0.1}Ni_1PEG_2$, 25 °C, 0.5% w/w in D_2O

SANS experiments were also performed at high concentration, 20% w/w at pH 3 and 7.4. Figures 45-a, -b, -c show the scattering profile of the penta-block terpolymers at temperatures 25 °C, 37 °C and 43 °C.

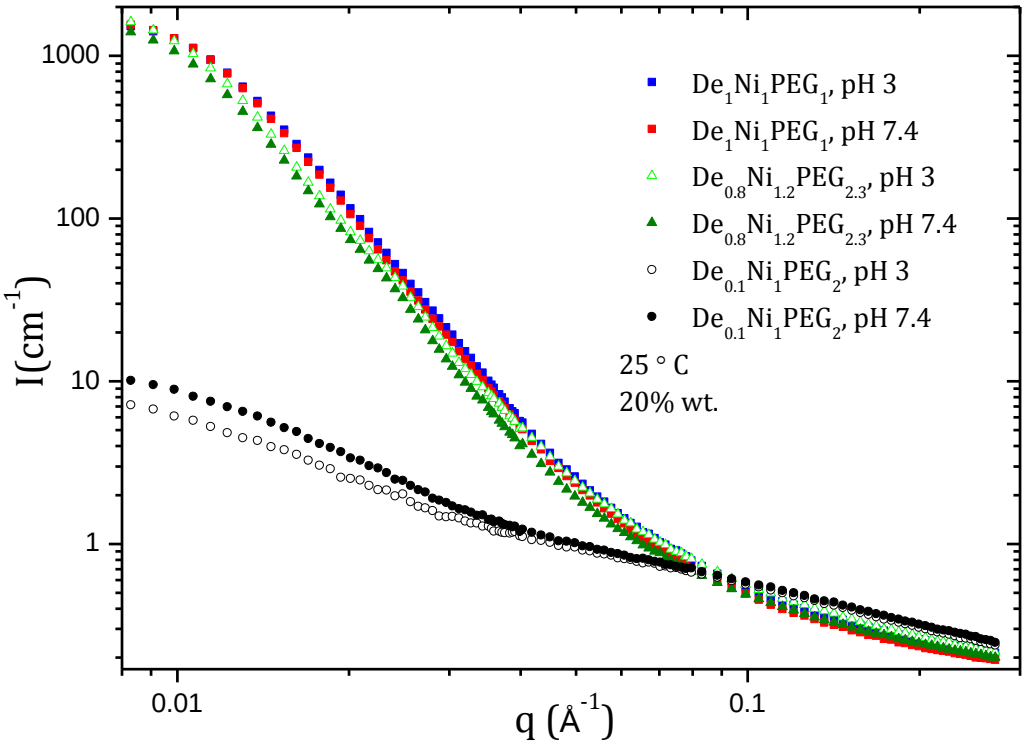

Figure 45-a – SANS scattering profile for PDEAEMA$_x$-*b*-PNIPAAM$_y$-*b*-PEG$_z$-*b*-PNIPAAM$_y$-*b*-PDEAEMA$_x$, 25 °C, 20% w/w in D_2O

According to figure 45-a, at 25 °C profiles are qualitatively similar to those obtained earlier on the low-concentration solutions (0.5 % w/w) at this temperature.

The absolute intensity at low-q values was approximately 10 times higher than it was at 0.5% w/w concentrations, suggesting some additional effects present in the system, since a pure linear increase with concentration would mean a factor of 20/0.5 = 40 times higher intensity at low-q values. One hypothesis is that at this concentration also large aggregates grow which do not contribute to the SANS signals. Patterns at 25 °C and 37 °C seemed relatively similar, while at 43 °C some changes were disclosed.

The characteristic bump around 0.02 Å^{-1} for $De_{0.8}Ni_{1.2}PEG_{2.3}$ at low concentrations disappeared. This is sensible, since at high concentrations interaction between the entities might mask the specific features of the individual micelles.

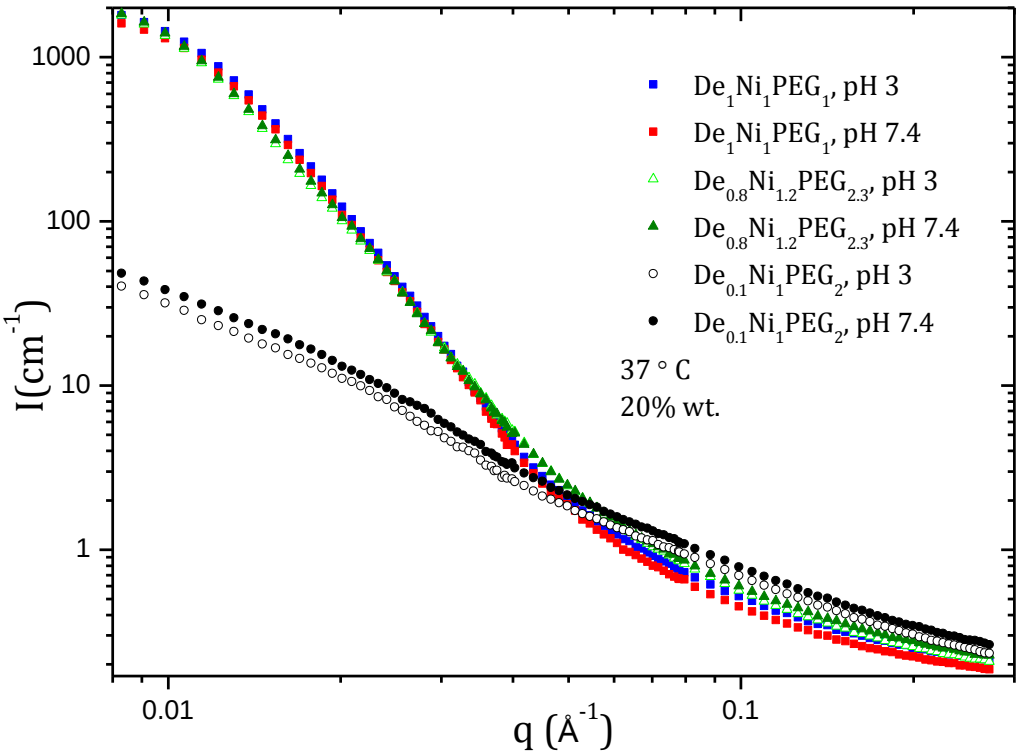

Figure 45-b – SANS scattering profile for PDEAEMA$_x$-*b*-PNIPAAM$_y$-*b*-PEG$_z$-*b*-PNIPAAM$_y$-*b*-PDEAEMA$_x$, 37 °C, 20% w/w in D_2O

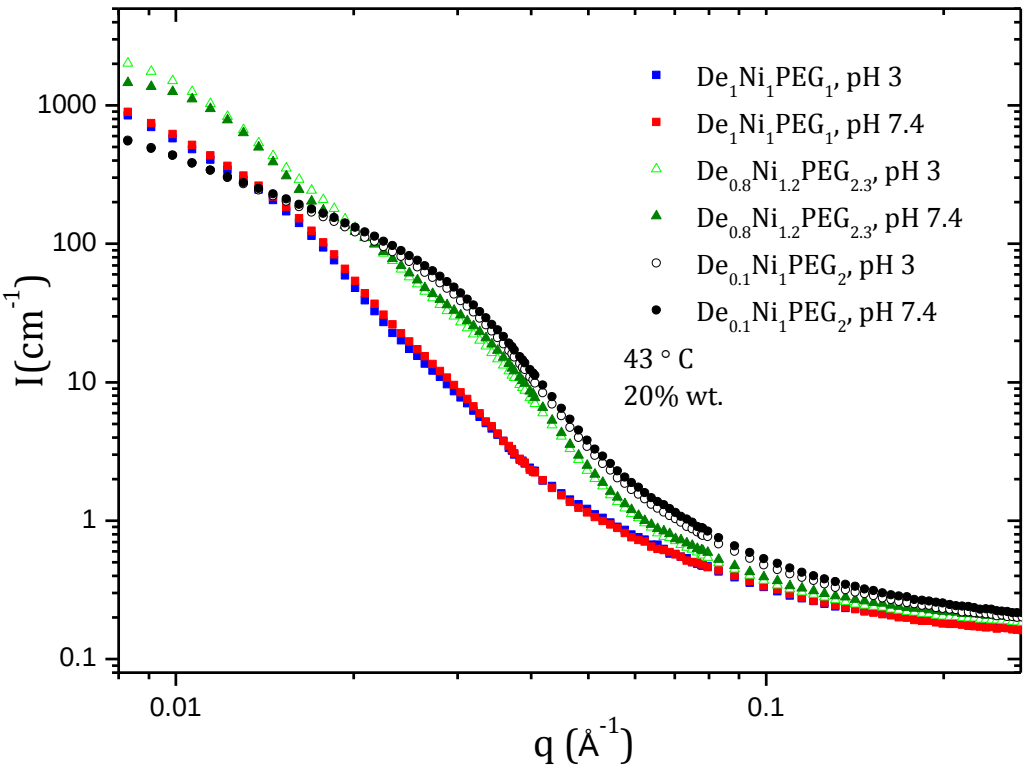

Figure 45-c – SANS scattering profile for PDEAEMA$_x$-*b*-PNIPAAM$_y$-*b*-PEG$_z$-*b*-PNIPAAM$_y$-*b*-PDEAEMA$_x$, 43 °C, 20% w/w in D_2O

Figure 45-c, reveals the difference among the three penta-block terpolymers. $De_{0.8}Ni_{1.2}PEG_{2.3}$ showed a similar scattering profile at both concentrations, apart from the higher intensity at high concentration. However $De_1Ni_1PEG_1$ and particularly $De_{0.1}Ni_1PEG_2$ changed the scattering pattern; for these two polymers elongated structures (slope close to -2 at the lowest q-range) is proposed. Nonetheless, a conclusive fitting model requires further investigation on the systems. At 43 °C, interestingly pH effect on the pattern was negligible, indicating that some hydrophobic interactions dominate any pH effects, at least within the nano-size range probed in SANS.

3.7 Rheometry and Rheo-SALS

In this section, association and disintegration of micellar structure were investigated by shear viscosity measurements.

Figures 46-a, -b, -c, show shear steady viscosity, η (Pa.s) of the penta-block terpolymers under a low shear rate (1 s^{-1}) in PBS of different pH values, with the concentration of 0.5% w/w as a function of temperature.

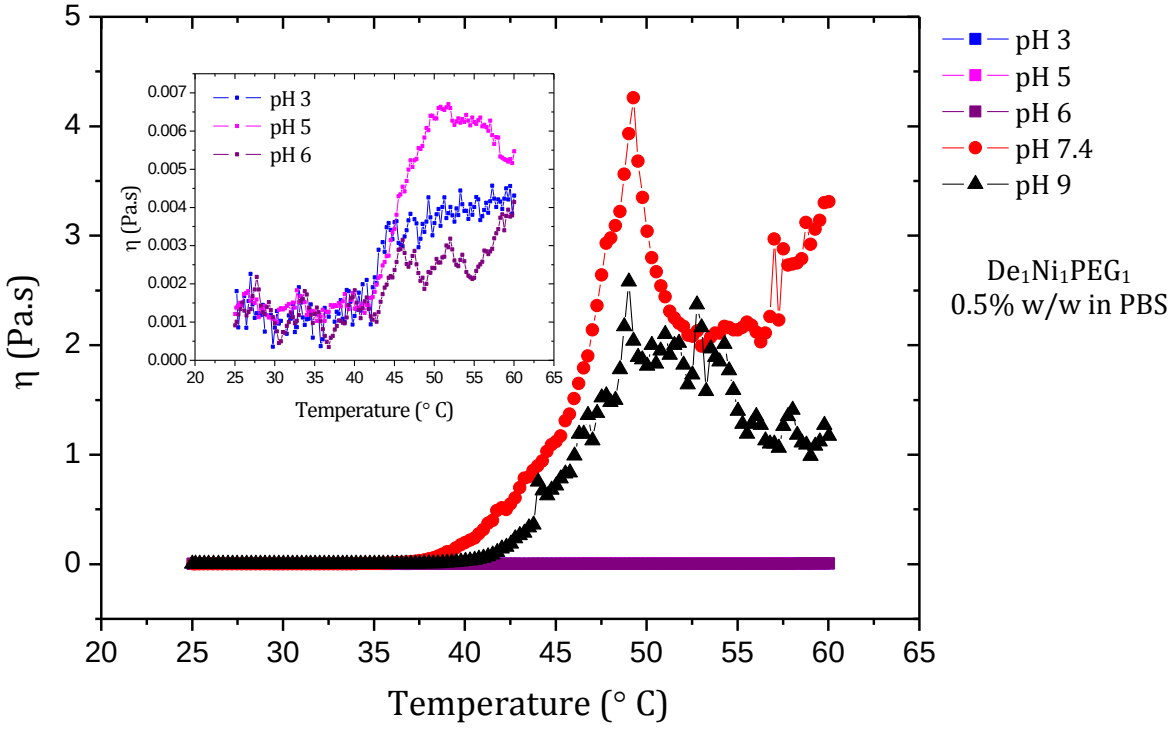

Figure 46-a – Temperature dependence of shear steady viscosity at 1 s^{-1} for $De_1Ni_1PEG_1$, 0.5%w/w in PBS

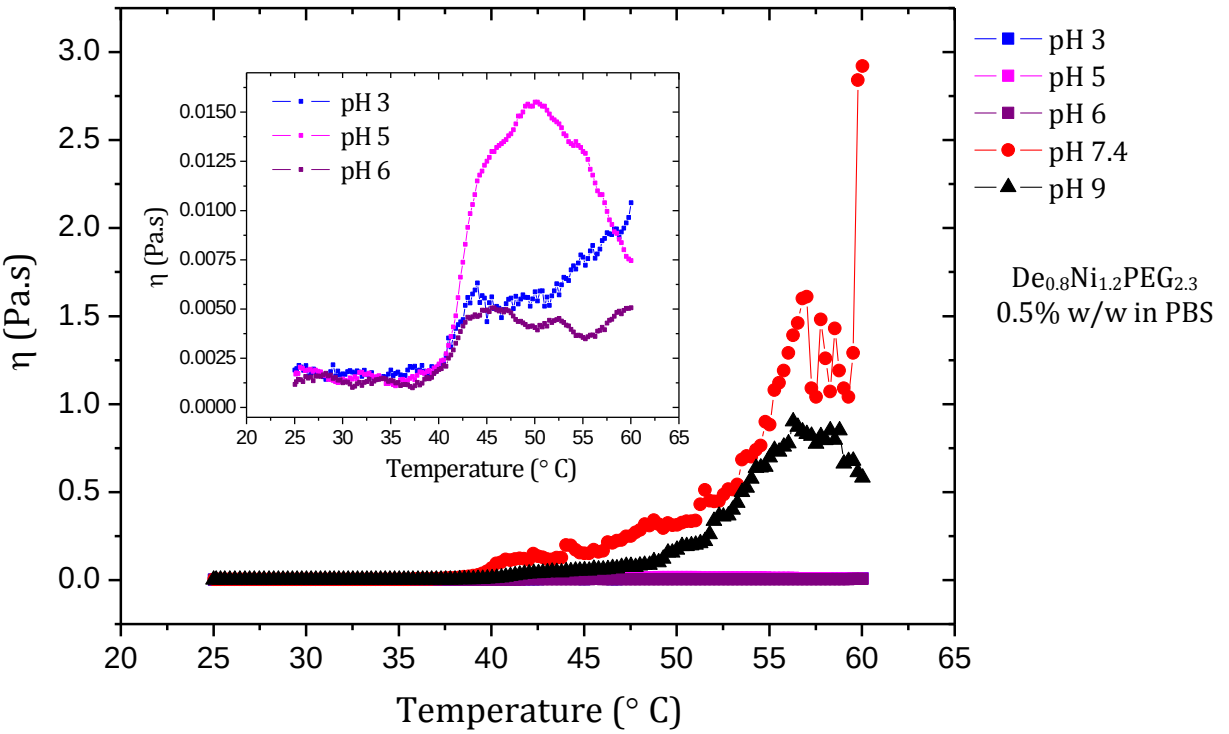

Figure 46-b – Temperature dependence of shear steady viscosity at 1 s^{-1} for $De_{0.8}Ni_{1.2}PEG_{2.3}$, 0.5% w/w in PBS

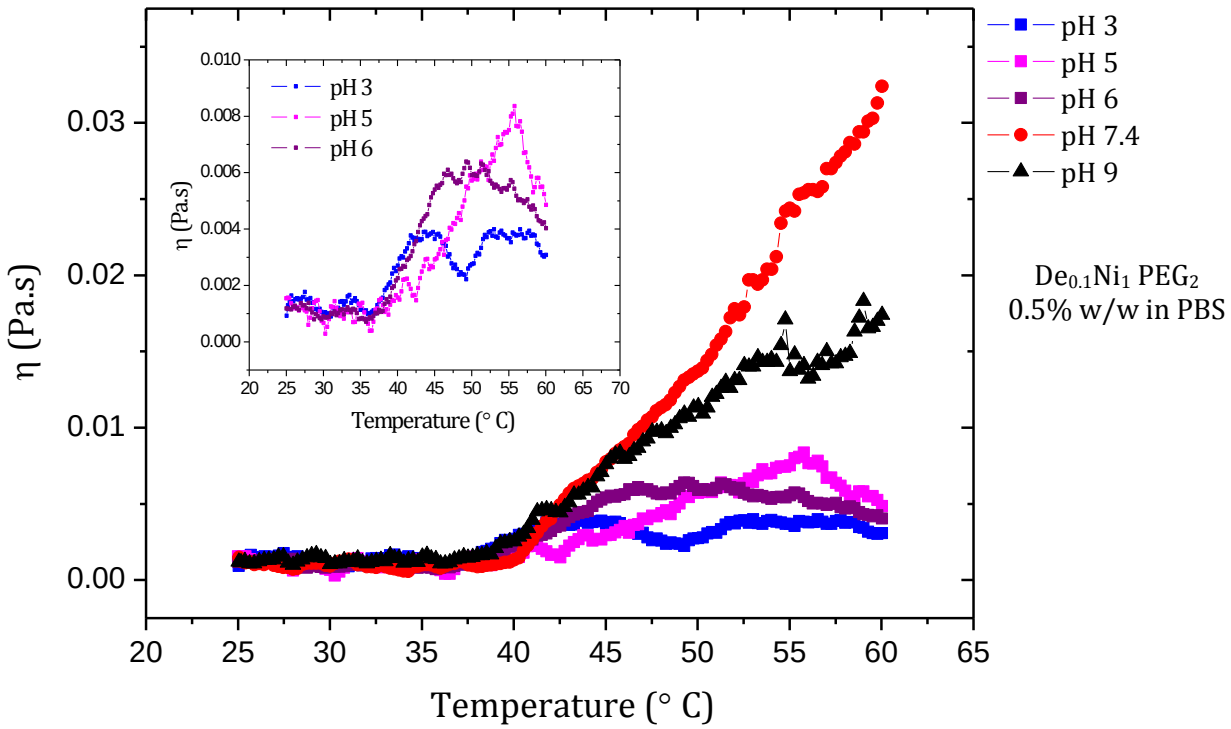

Figure 46-c – Temperature dependence of shear steady viscosity at 1 s^{-1} for $De_{0.1}Ni_1PEG_2$, 0.5% w/w in PBS

The general trend in figure 46 was that before heating all the solutions showed the same viscosity at about 0.002 Pa.s which is comparable with water viscosity (0.001 Pa.s); upon heating the solutions, hydrophobicity within the micelles increased and the stickiness developed among the micelles, resulted in an upturn of viscosity; although the upturn at pH 7.4 and 9 was more intensified in comparison to lower the pH values, 3, 5 and 6, which is sensible since pK_a of the polymer (PDEAEMA) is about 7.3; therefore both high pH and high temperature favor the formation of hydrophobic aggregates. Surprisingly pH 7.4 displayed the highest temperature dependency in the three systems and $De_1Ni_1PEG_1$ showed the highest viscosity values at its peaks. The critical temperature for viscosity upturn at pH 3, 5 and 6, was more or less the same temperature that the solutions became cloudy (see table 9); at pH 7.4 and 9 however not a dramatic decrease was observed in the critical temperature. In most of the cases, a peak of viscosity was observed which could be the temperature that either phase separation happened at or the applied shear dominated the hydrophobic aggregates, therefore above this temperature, the steady shear viscosity dropped. The peak temperature for pH 3, 5 and 6 was almost the same temperature that turbidity reached to its highest value (Figure 20).

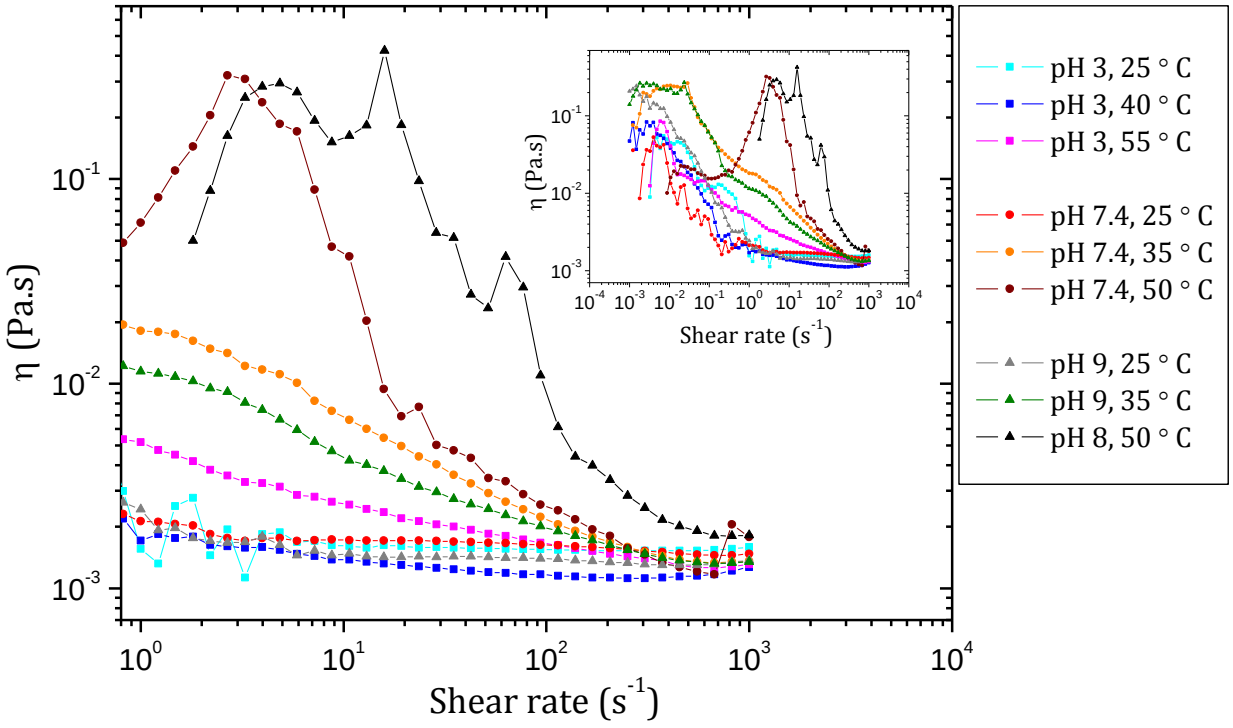

Figure 47-a– Shear rate dependence of shear steady viscosity for $De_1Ni_1PEG_1$, 0.5% w/w in PBS

In the next step, shear rate dependency of the viscosity over a range from 0.001 to 1000 s^{-1} at selected pH values and temperatures is displayed in figures 47-a,-b,-c.

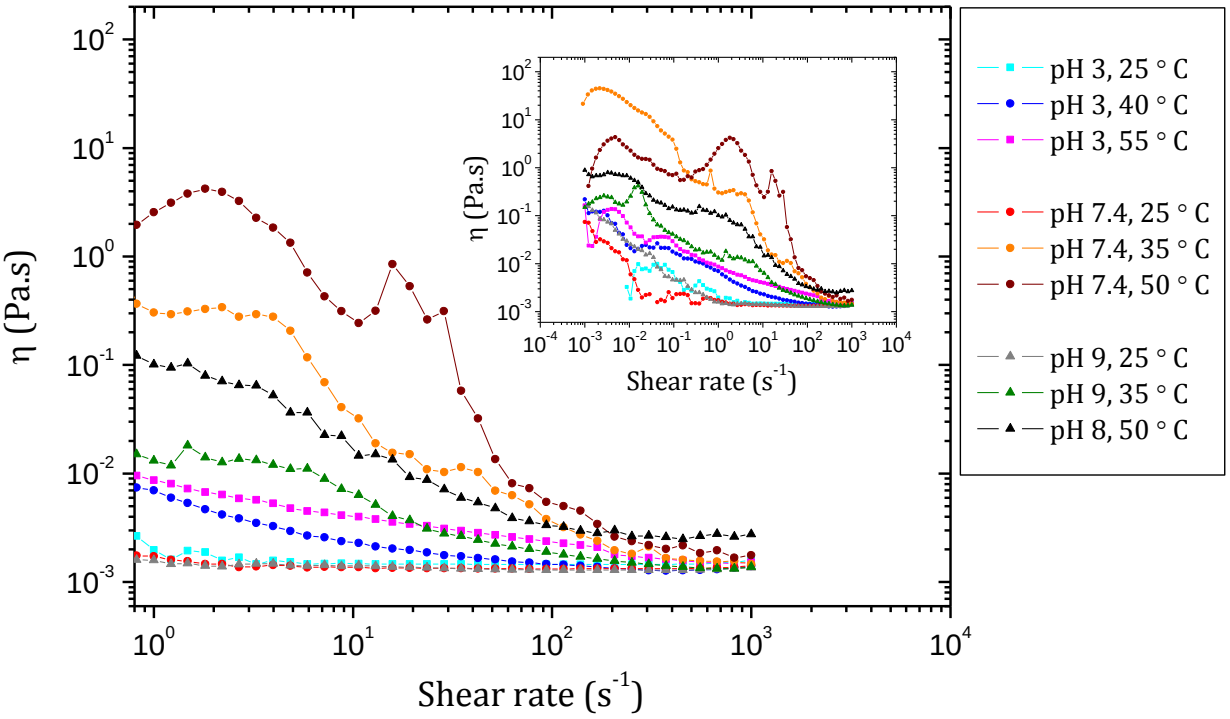

Figure 47-b– Shear rate dependence of shear steady viscosity for $De_{0.8}Ni_{1.2}PEG_{2.3}$, 0.5% w/w in PBS

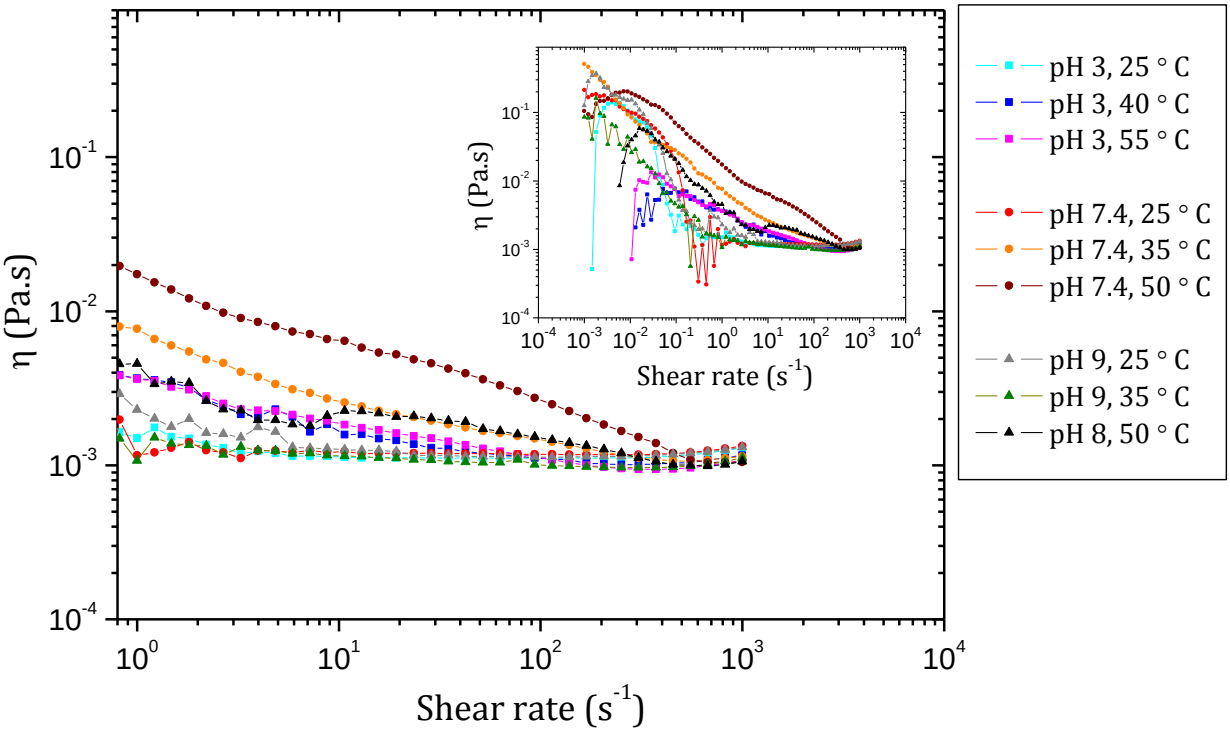

Figure 47-c – Shear rate dependence of shear steady viscosity for $De_{0.1}Ni_{1}PEG_{2}$, 0.5% w/w in PBS

For all the three penta-block terpolymers at shear rates below 1 s^{-1} a strong shear rate dependency was recognized, however at shear rates above 1 s^{-1} at pH 3 Newtonian behavior or nearly Newtonian behavior was observed. It emerges that at pH 7.4 and 9, above 35 °C, the micellar structures show a shear-thinning behavior. The relatively higher viscosity in this condition could be originated from the interaction among the sticky hydrophobic micelles; this shear-induced intermicellar aggregation, known as "ortho-kinetic" aggregation[84] that brings polymer molecules and clusters close to each other faster than Brownian motion does , has been frequently observed in solutions or suspension of sticky moieties at low shear rates [61]. By applying a higher shear rates the connectivity was impaired and the viscosity fell off as a result of this shear-induced disintegration; while the relatively lower viscosity at pH implies that there was no inter-connected structure in the solution.

According to figures 47-a, -b, and –c, over a range of shear rate from 1 to 1000 s^{-1}, $De_{0.8}Ni_{1.2}PEG_{2.3}$ showed the strongest shear-rate dependency, while $De_{0.1}Ni_1PEG_2$ mostly exhibited a nearly Newtonian behavior. This could be ascribed to the larger micelles $De_{0.8}Ni_{1.2}PEG_{2.3}$ formed at pH 7.4 and 9 in PBS (see table 11 for PBS) in comparison to the other two polymers; in addition, the loner PEG and PDEAEMA blocks in $De_{0.8}Ni_{1.2}PEG_{2.3}$ favor interconnection and stickiness, respectively among the micelles. $De_{0.1}Ni_1PEG_2$ as it was explained before did not form rigid micelles at low temperatures and pH values, therefore associated aggregates at lower shear rates, easily was integrated and the weakest shear rate dependency was observed for this polymer.

At a higher concentration (20% w/w) the three polymer solutions showed an interesting behavior, by forming a gel association from the micelles. For ABA-type triblock copolymers, two types of association have been perceived (Figure. 48) [85].

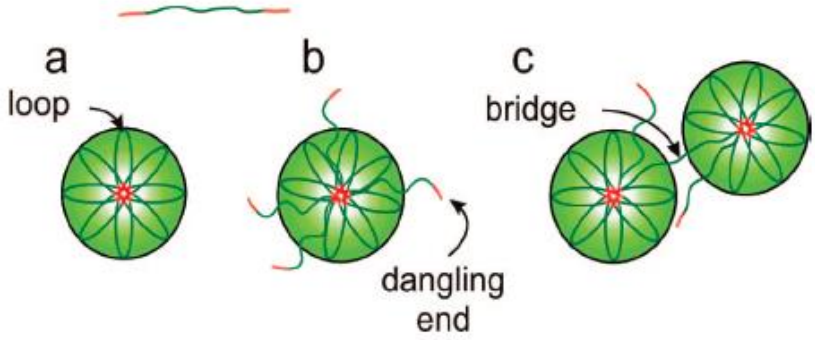

Figure 48 – Most probable types of organization of ABA-type triblock copolymers in B-selective solvents [85]

At "a" state, flowerlike micelles form by the middle block loops with the same micellar core, at "c" state, a branched structure form by bridging the outer block to a different micellar core, and state "b" form when the insoluble block is dangling in the shell. The gel network at a high concentration, in this study could mainly be formed by penetrating the loops or bridging the micelles or even by both. PEG block in this regard, has a significant role to develop intermicellar connection. As temperature increases, micelle aggregations form and due to the partial dehydration of PEG block [86-87] (along with the dehydration of PNIPAAM) molecular motion of PEG blocks is restricted and the gel network is formed. At a higher pH, PDEAEMA block also contributes to create the connections.

Viscoelastic properties of the penta-block terpolymers at the concentration of 20 %w/w were investigated by frequency sweep measurements at 10% strain and pH values 3 and 7.4, over a range of angular frequency and temperature from 0.1 to 100 rad. s^{-1} and 15 to 60 °C, respectively; for all the three systems, a sol-gel transition was observed. Loss tangent, tan δ, complex viscosity η* and storage modulus, G' profiles were summarized in figure 49-a, -b and –c. η* is a frequency-dependent viscosity function, determined during oscillatory shear measurements and it is defined as equation 32:

$$\eta^*(\omega) = \eta'(\omega) - i\eta'' = G''/\omega - iG'/\omega \qquad \text{Eq. 32}$$

where η' and η'' are dynamic viscosity and in-phase component of dynamic complex viscosity, respectively. η* contains information on both the viscose part

and the elastics part of the system [88]. Plots were represented only for pH 3, to avoid repetition. In all the three systems, G' showed an increasing trend; at lower temperature (compared to gel point) G' had a lower order of magnitude; reaching to the gel point, it significantly increased with a milder slope. η* at lower temperatures rose by increasing the angular frequency, while at temperatures close to the gel point, it declined. Tan δ values at different angular frequency converged by approaching the gel point, and diverged at higher temperatures. The same pattern was observed for the exponents n' and n''. All events indicated a sol-gel transition by increasing temperature; as at the lower temperatures the viscose part of the system had a dominant contribution in the viscoelastic properties of the system; reaching the gel point and above that, the elastic contribution dominated, implying a transition from a liquid-like to a solid-like system. Trends in tan δ, n', n'', η* and G' at pH 7.4 followed in a similar but more distinguishable way and the sol-gel transition temperatures took place at a lower temperatures. The results from these experiments were tabulated in table 16.

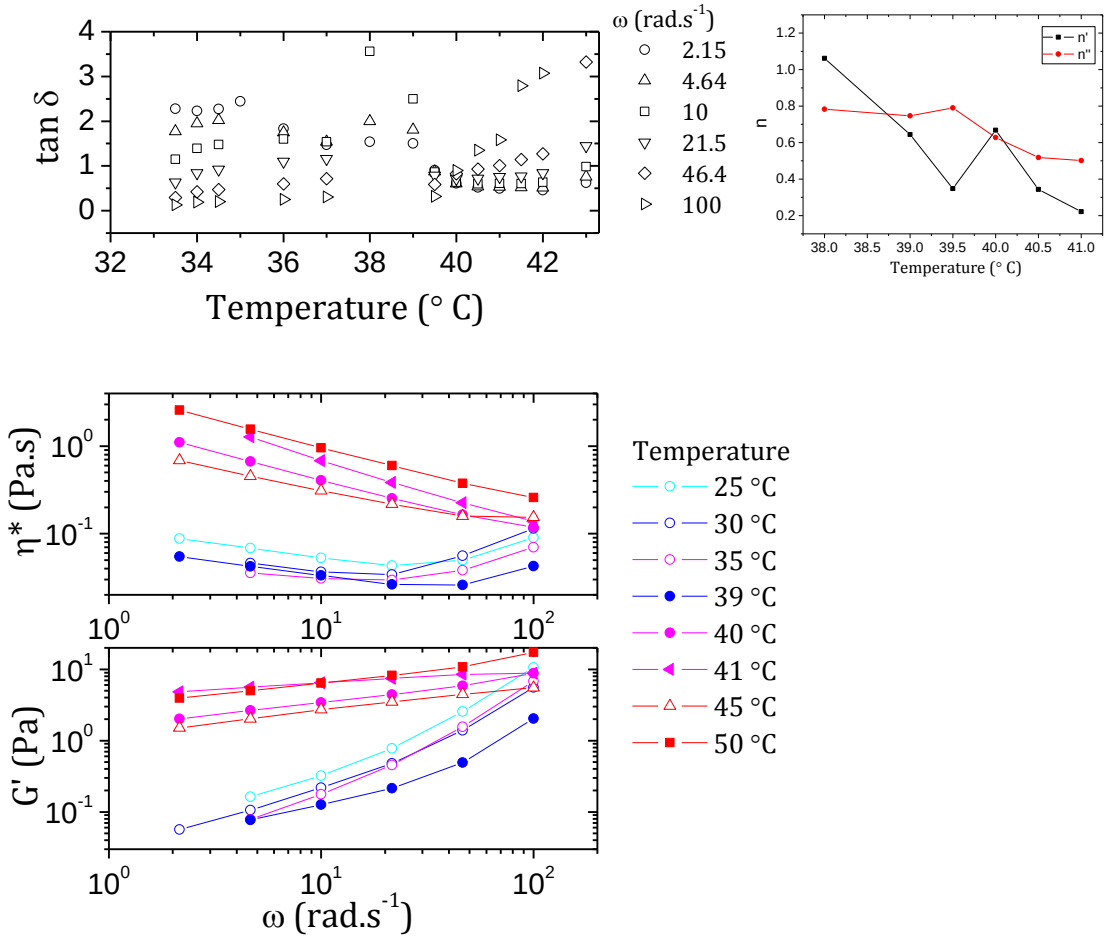

Figure 49-a – Viscoelastic properties for $De_1Ni_1PEG_1$, 20 % w/w in PBS, pH 3

Sol-gel transition temperature was also investigated by tube-tilting method [89-90]. A test tube containing the polymer solution with the same concentration as the previous experiments (20% w/w) was sealed, totally immersed in a water bath equipped with a temperature unit, and heated up with a rate of 0.5 °/min. Every 2 degrees the test tube was tilted to examine whether or not the polymer solution was still fluid. The incipient gel was formed at the first temperature at which no palpable flow was observed for 30 seconds by inverting the test tube. Gel point temperatures were summarized in table 16.

The linear viscoelastic properties of the incipient gel could be characterized by the gel strength parameter S (Eq. 19) and the fractal dimension d_f (Eq. 23- fully screened excluded volume). The parameters were listed in the table 16.

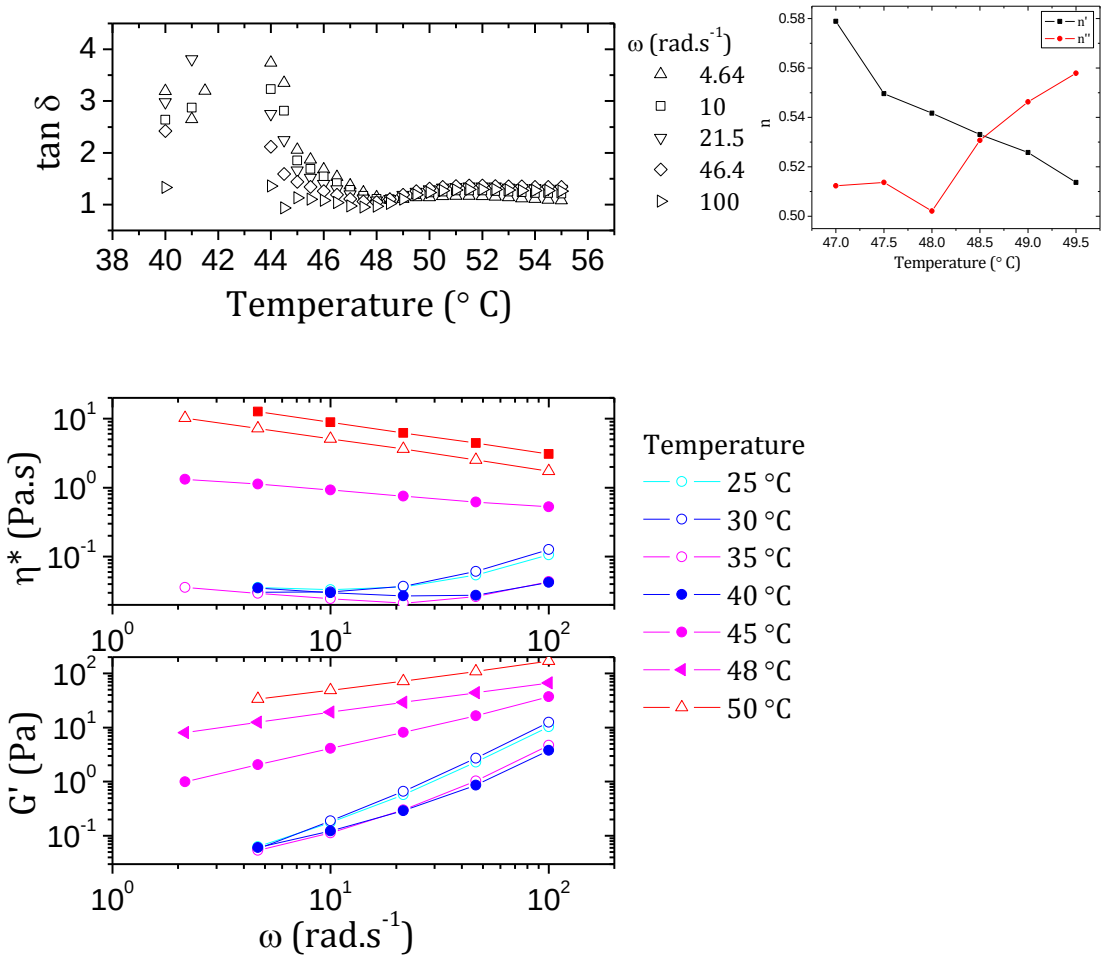

Figure 49-b – Viscoelastic properties for $De_{0.8}Ni_{1.2}PEG_{2.3}$, 20 % w/w in PBS, pH 3

Based on the data in table 16, sol-gel transition in $De_1Ni_1PEG_1$ appeared at lower temperatures in comparison to the other two polymers; this is consistent with the cloud point of theses polymers (table 9). However the gel points obtained by tube-tilting method were not equal to the gel points derived from rheometry; practically tube-tilting temperatures were more close to the clout points, but obviously higher. The difference between the gel points from tube-tilting method and rheometry, is not unreasonable since the measurement conditions and instrumentation in the two methods are not identical. Nonetheless, the trend of the gel point temperatures was the same. At pH 3, considering S, and d_f, $De_{0.8}Ni_{1.2}PEG_{2.3}$ suggested the strongest incipient gel; having the highest S and d_f values, and the lowest n values[91] could be an indicative of a tight network [40, 55]. With the same rationale $De_1Ni_1PEG_1$ formed the softest incipient gel with an open network. At pH 7.4 the same argument applied for $De_1Ni_1PEG_1$ as the strongest incipient gel. However the data represented in table 16, at this pH were inconclusive to determine the weakest network.

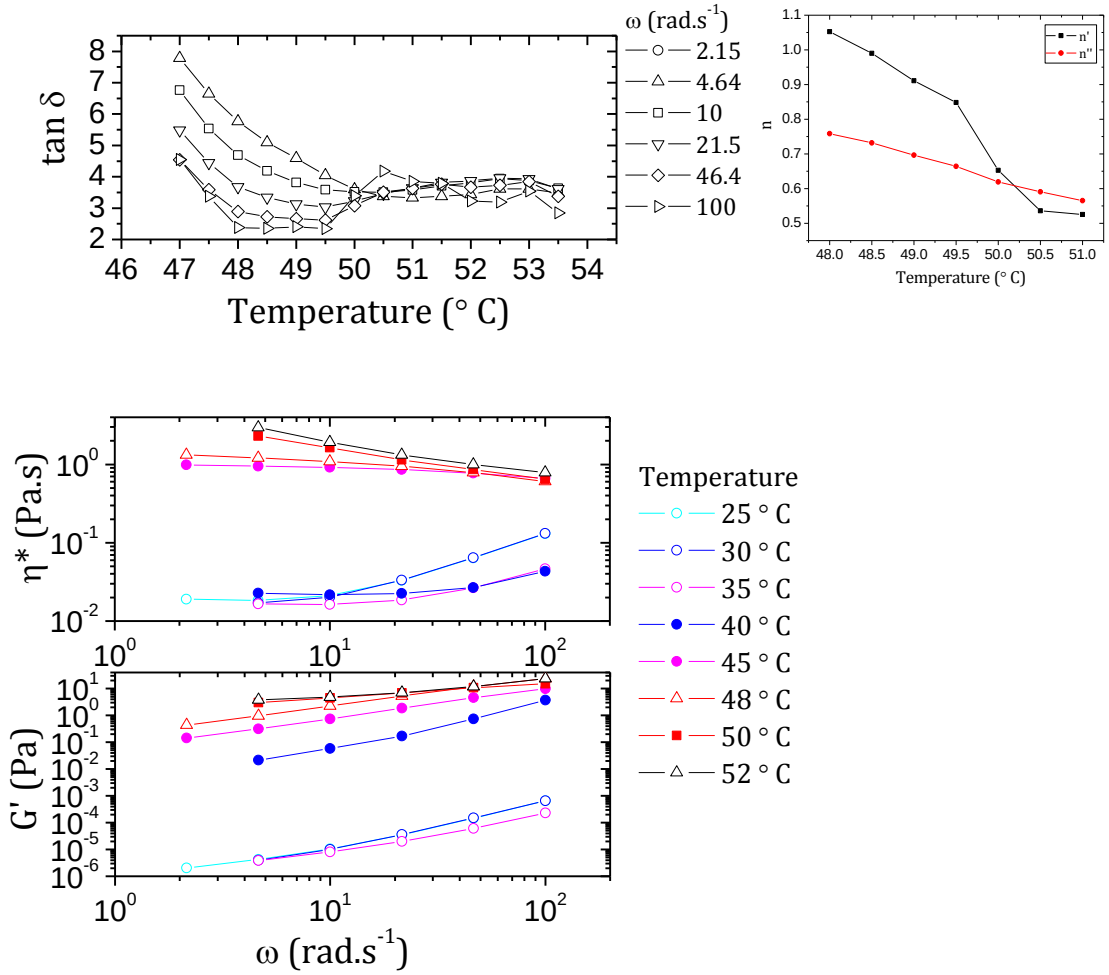

Figure 49-c – Viscoelastic properties for $De_{0.1}Ni_1PEG_2$, 20 % w/w in PBS, pH 3

ABCBA polymer	Gel-point Temperature (°C) **Rheometry**		Gel-point Temperature (°C) **Tube-tilting**		**S (Pas ^{n})**		**n**		**d_f**	
	pH 3	pH 7.4	pH 3	pH 7.4	pH 3	pH 7.4	pH 3	pH 7.4	pH 3	pH 7.4
$De_1Ni_1PEG_1$ 34/58/34/58/34	40	34	38	33	0.15	3.17	0.65	0.29	1.81	2.23
$De_{0.8}Ni_{1.2}PEG_{2.3}$ 27/68/77/68/27	48.5	42	44	38	5.8	0.3	0.53	0.53	1.96	1.96
$De_{0.1}Ni_1PEG_2$ 2/57/68/57/2	50	49.5	46	43	1.34	0.65	0.64	0.65	1.83	1.63

Table 16 – Viscoelastic properties of $PDEAEMA_x$-*b*-$PNIPAAM_y$-*b*-PEG_z-*b*-$PNIPAAM_y$-*b*-$PDEAEMA_x$, 20% w/w in PBS

In order to have a visual understanding of the sol-gel transition by change of association complexes, selected images of Rheo-SALS were collected in figures 50-a-f. Scattering pattern at all the studied systems were isotropic. The circle at the center of each pattern is the beam stop. In the sol-state, the solution scattering pattern seemed relatively weak, with a smaller scattering region, as the temperature reached to the gel point, the scattering region noticeably increased and high intensity regions at lower q values, appeared (in red). At pH 7.4, by comparing the image from figure 50-d at the gel temperature, i.e., 42 °C with the image from figure 50 -f at 49 42 °C, it could be inferred that $De_{0.8}Ni_{1.2}PEG_{2.3}$ formed the softest incipient gel at this pH.

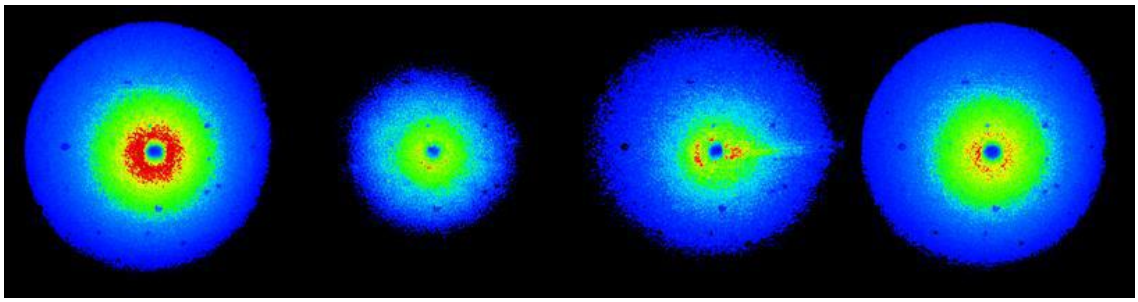

25 °C 30 °C 32 °C 35 °C

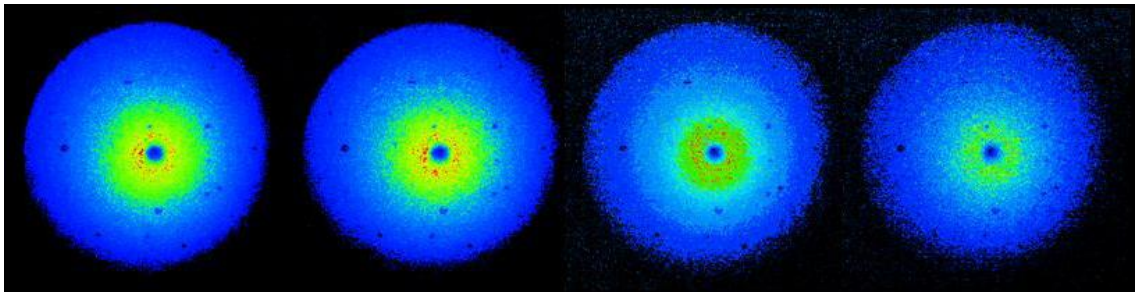

38 °C 40 °C 45 °C 50 °C

Figure 50-a – Rheo-SALS images for $De_1Ni_1PEG_1$, 20 % w/w in PBS, pH 3

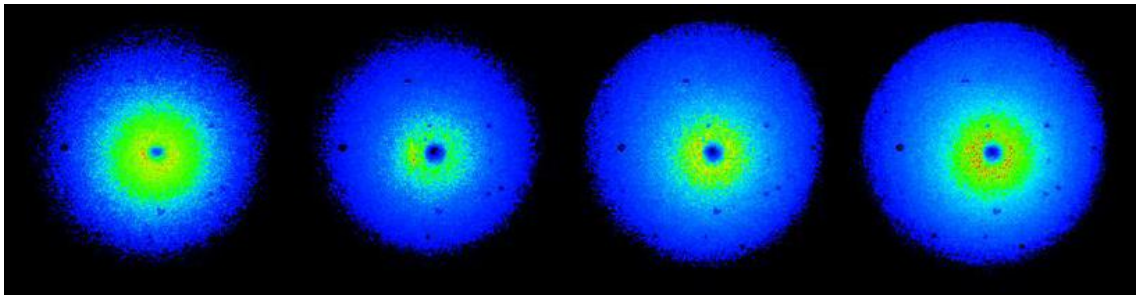

25 °C 30 °C 34 °C 37 °C

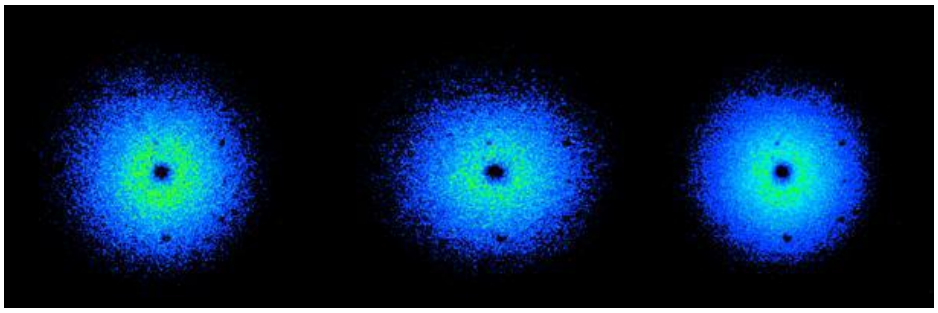

40 °C 45 °C 50 °C

Figure 50-b – Rheo-SALS images for $De_1Ni_1PEG_1$, 20 % w/w in PBS, pH 7.4

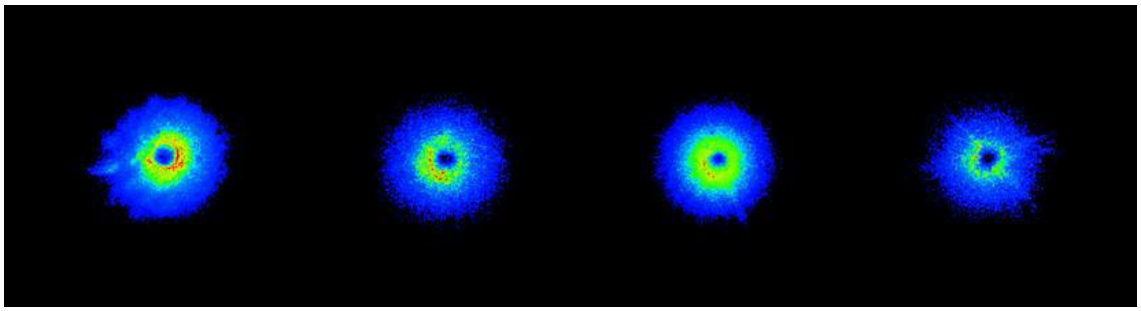

25 °C 30 °C 35 °C 37 °C

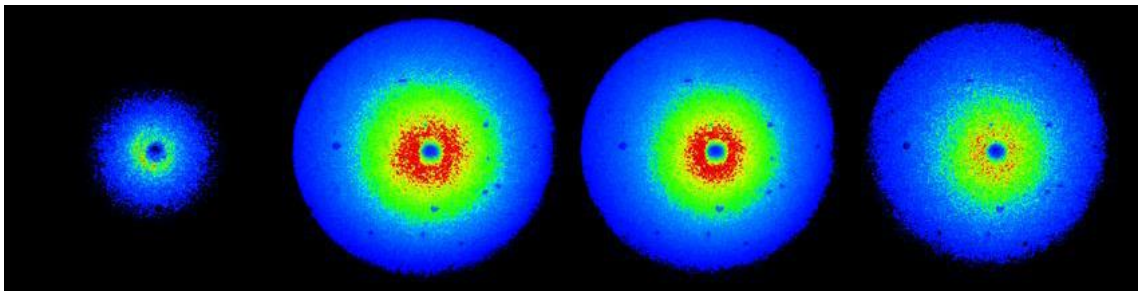

40 °C 45 °C 48 °C 50 °C

Figure 50-c – Rheo-SALS images for $De_{0.8}Ni_{1.2}PEG_{2.3}$, 20 % w/w in PBS, pH 3

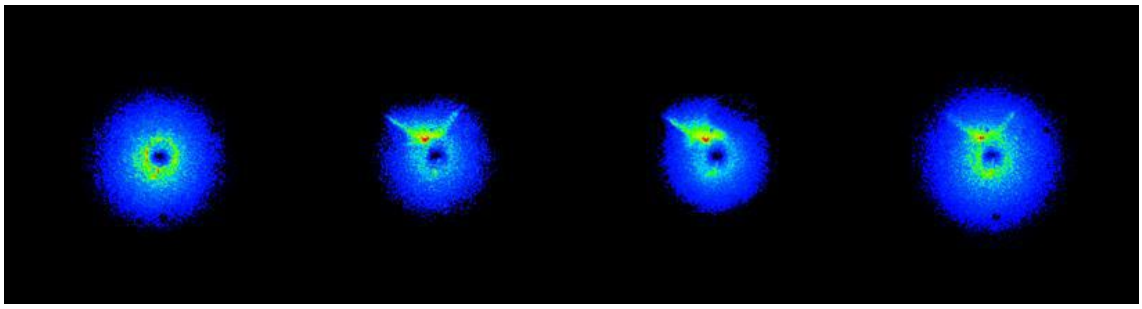

25 °C 30 °C 35 °C 40 °C

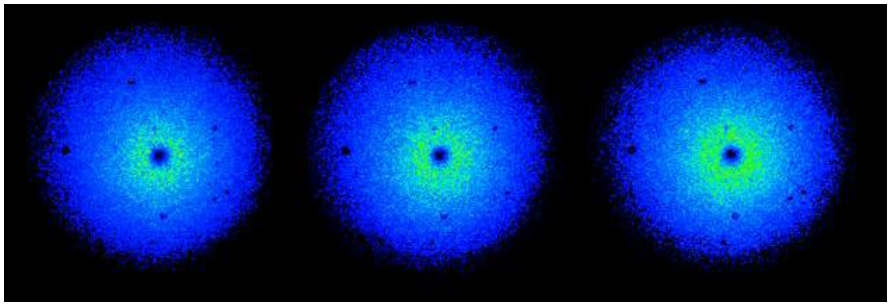

42 °C 45 °C 50 °C

Figure 50-d – Rheo-SALS images for $De_{0.8}Ni_{1.2}PEG_{2.3}$, 20 % w/w in PBS, pH 7.4

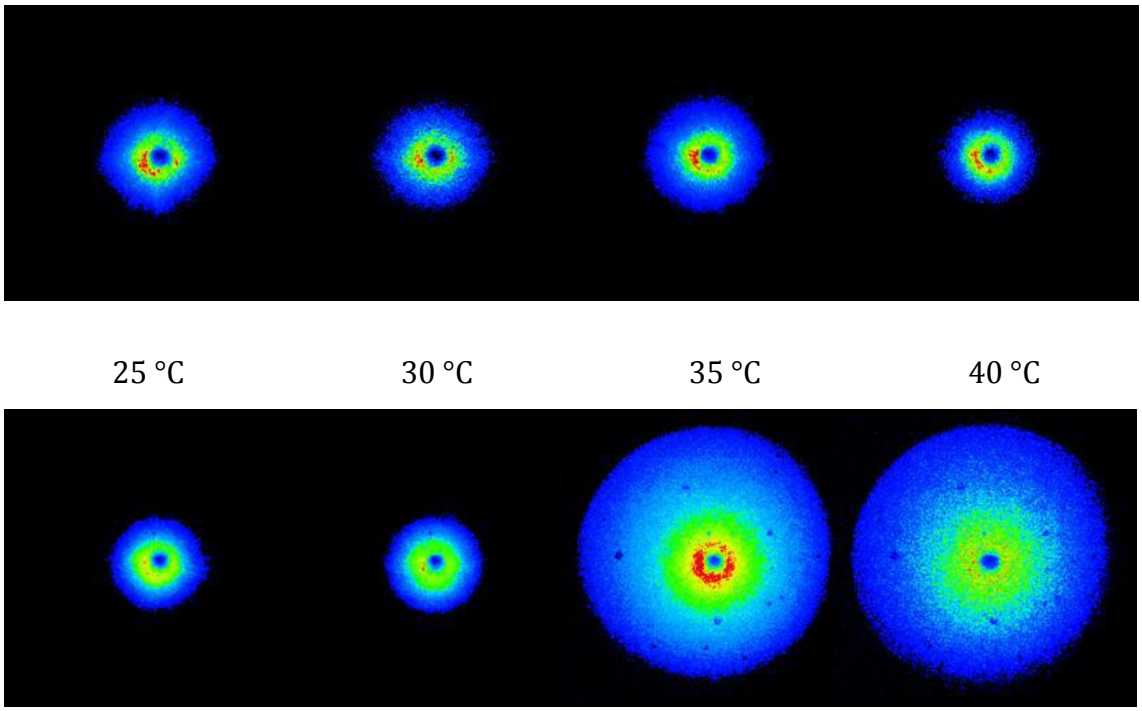

25 °C 30 °C 35 °C 40 °C

45 °C 47 °C 50 °C 53 °C

Figure 50-e – Rheo-SALS images for $De_{0.1}Ni_1PEG_2$, 20 % w/w in PBS, pH 3

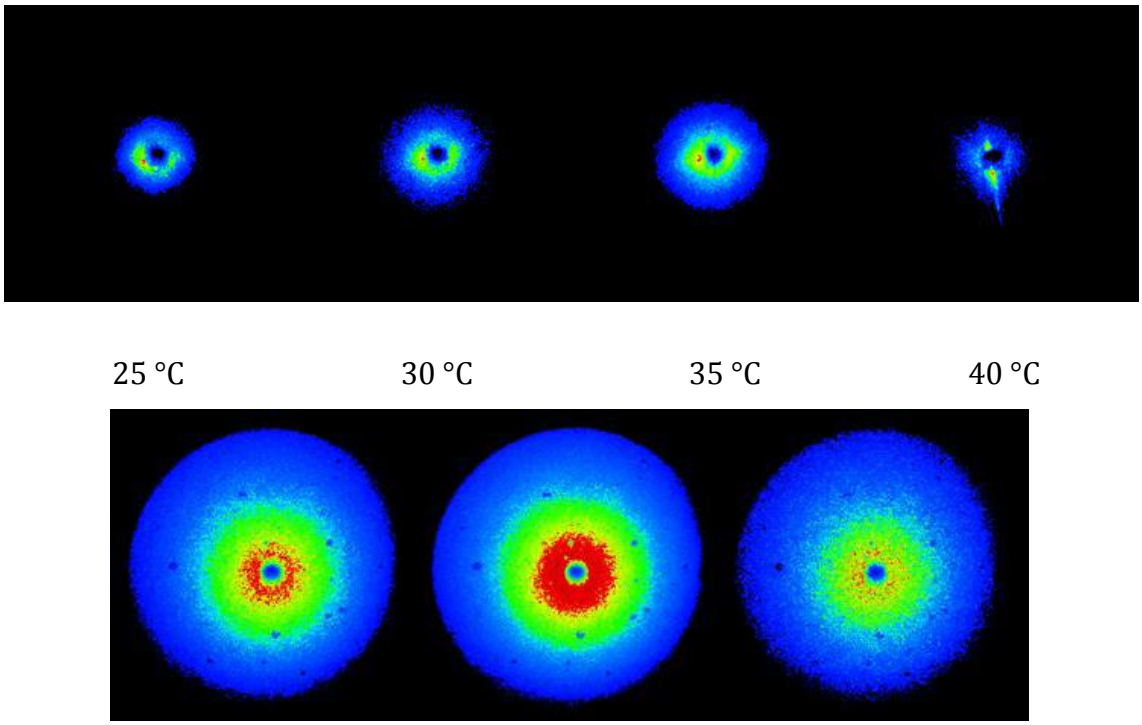

25 °C 30 °C 35 °C 40 °C

45 °C 49 °C 53 °C

Figure 50-f – Rheo-SALS images for $De_{0.1}Ni_1PEG_2$, 20 % w/w in PBS, pH 7.4

A conclusive explanation for the origin of the gel strength in $De_1Ni_1PEG_1$ and $De_{0.8}Ni_{1.2}PEG_{2.3}$ could not be given. The only difference between these two systems is the length of PEG block. As PEG is believed to form the corona of the micelles, at higher concentrations, it possibly develops a gel of bridged micelles or densely packed micelles [42]. This does not seem to be the origin of the gel strength in these systems, as $De_{0.8}Ni_{1.2}PEG_{2.3}$ formed the strongest network at pH 3 and the softest network at pH 7.4. pH effect is equal on both polymers since PDEAEMA block length is unchanged and in addition pH effect according to SANS profiles was negligible. One hypothesis could be based on DLS results (table 12) for micelles of these two systems at dilute regime; micelles at pH 3 were larger and monodisperse in size with $De_{0.8}Ni_{1.2}PEG_{2.3}$, in comparison to smaller and polydisperse micelles in $De_1Ni_1PEG_1$. At pH 7.4 on the other hand, micelles in $De_{0.8}Ni_{1.2}PEG_{2.3}$ solution were still larger but formed a polydisperse system and $De_1Ni_1PEG_1$ was assembled with smaller and monodisperse micelles. By assuming that at higher concentration micelles possibly keep this pattern, it seems that order in the network plays an important role in the network strength. As the strength parameter depends on the crosslinking density and the molecular chain flexibility [40], in the system with monodisperse micelles, the gel network is more compact (less flexible), ordered and stronger than a gel network formed by monodisperse micelles. The effect of polydispersity on the crosslinking system has been pointed out by Muthukumar [55].

4 Conclusion

Micellization behavior at low concentration (0.5% w/w) and sol-gel transition at high concentration (20% w/w) of temperature and pH responsive penta-block terpolymers, $PDEAEMA_{34}$-*b*-$PNIPAAM_{58}$-*b*-PEG_{34}-*b*-$PNIPAAM_{58}$-*b*-$PDEAEMA_{34}$ ($De_1Ni_1PEG_1$), $PDEAEMA_{27}$-*b*-$PNIPAAM_{68}$-*b*-PEG_{77}-*b*-$PNIPAAM_{68}$-*b*-$PDEAEMA_{27}$ ($De_{0.8}Ni_{1.2}PEG_{2.3}$), and $PDEAEMA_{27}$-*b*-$PNIPAAM_{57}$-*b*-PEG_{68}-*b*-$PNIPAAM_{57}$-*b*-$PDEAEMA_2$ ($De_{0.1}Ni_1\ PEG_2$) in aqueous solutions were investigated. $De_{0.8}Ni_{1.2}PEG_{2.3}$ showed the lowest CMC (1.12×10^{-7} gmL^{-1} in PBS pH 7.4); at a higher pH a lower CMC was detected. This polymer at dilute regime showed relatively the highest specific density as well and as pH rose, specific density fell

off. Transition temperature in Densitometry and Turbidimetry were almost the same for the three polymers; density values and turbidity amplitudes were relatively higher in PBS in comparison to the solutions in D_2O. ζ-potential measurements showed the highest surface charge for $De_{0.8}Ni_{1.2}PEG_{2.3}$ (+18 mV at 25 °C, pH 3, D_2O) implying the position of PDEAEMA block near the surface of the micelles. At a higher pH, ζ-potential values decreased and in some cases charge inversion was observed. On the contrary, at a higher temperature, micelles showed higher ζ-potential values. Both events suggest that diffusion of PDEAEMA block into the core causes a lower ζ-potential, while exposure of PDEAEMA block to the aqueous solution results in a higher ζ-potential. DLS results indicated the highest monodispersity for $De_{0.8}Ni_{1.2}PEG_{2.3}$. In D_2O solutions at pH 3, by increasing temperature, this polymer showed a decrease of R_h from 94 nm to 68 nm up to 43 °C, above this temperature an abrupt increase of R_h was observed (140 nm) followed by the multiple scattering. At a higher pH the same trend was recognized, hydrodynamic radii were relatively larger and the turn up point was observed at lower temperatures. In PBS on the other hand, a lower diffusivity and a higher polydispersity was noticed. For $De_{0.8}Ni_{1.2}PEG_{2.3}$ at pH 3, size of the micelles was relatively larger than in D_2O and the trend by increasing the temperature was a continuous rise in R_h from 107 nm to 241 nm up to 40 °C followed by the multiple scattering. At a higher pH in the bimodal systems, by heating up the sample, R_{hf} was almost constant and R_{hs} decreased. On average, $De_{0.8}Ni_{1.2}PEG_{2.3}$ in comparison to $De_1Ni_1PEG_1$ and $De_{0.1}Ni_1\ PEG_2$ offered the smallest micelles in D_2O (R_h= 60-90 nm) and the largest micelles in PBS (60-100 nm for R_{hf} and 100-800 nm for R_{hs}). From SANS, a core-shell model was properly fitted for $De_{0.8}Ni_{1.2}PEG_{2.3}$ and R_g/R_h less than 0.78 suggested spherical micelles for this polymer. From the rheological point of view the steady shear viscosity in dilute solutions of $De_{0.8}Ni_{1.2}PEG_{2.3}$ displayed the strongest shear rate dependency; at the high concentration at pH3 $De_{0.8}Ni_{1.2}PEG_{2.3}$ developed the strongest gel network, while at pH 7.4 it showed the be the softest gel network.

A schematic of $De_{0.8}Ni_{1.2}PEG_{2.3}$ micellar structure at selected temperatures and pH values was represented in figure 51.

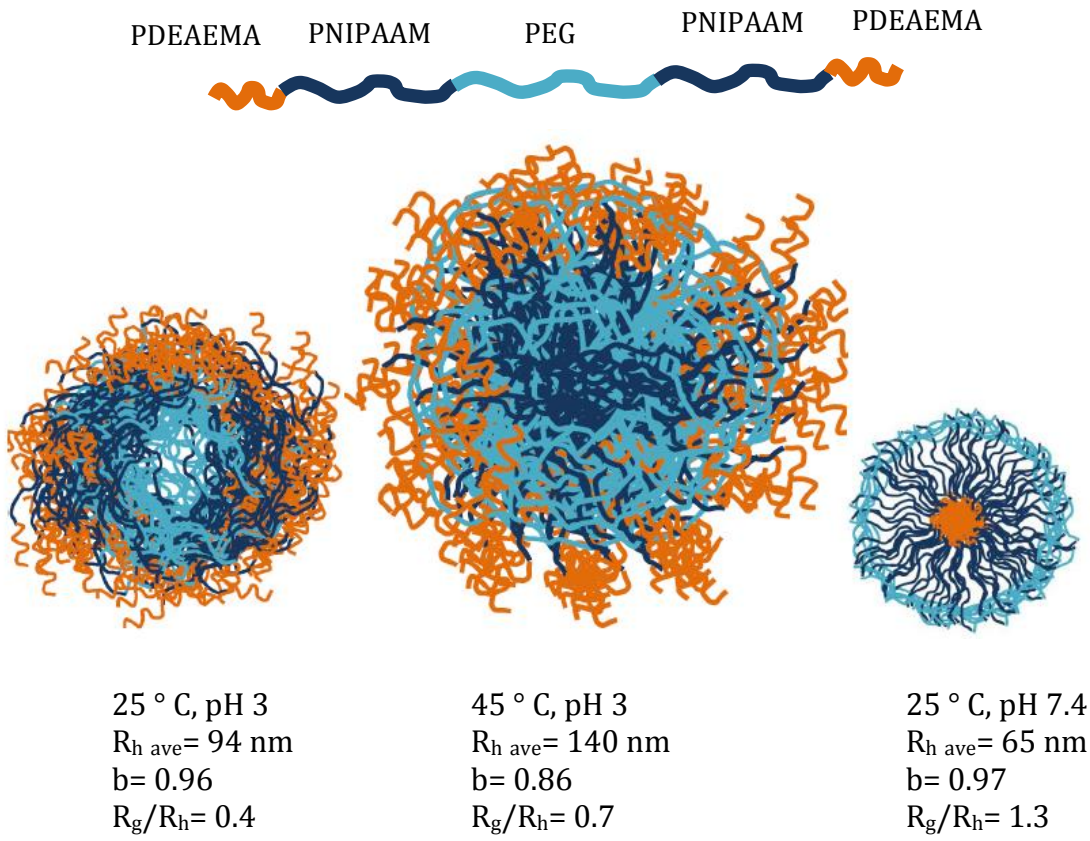

Figure 51 – Proposed schematic of the self-assembly of $De_{0.8}Ni_{1.2}PEG_{2.3}$, in D_2O

$De_1Ni_1PEG_1$, formed the most turbid solutions in comparison to $De_{0.8}Ni_{1.2}PEG_{2.3}$ and $De_{0.1}Ni_1$ PEG_2; it emerged that micelles of this polymer have the highest M_w and N_{agg} ; η-temperature plots of the dilute solutions showed the highest viscosity values at the peaks and at the high concentration the gel network formed at relatively lower temperatures (34 °C in PBS pH 7.4), all implying a higher level of hydrophobicity of $De_1Ni_1PEG_1$ in comparison to $De_{0.8}Ni_{1.2}PEG_{2.3}$ and $De_{0.1}Ni_1$ PEG_2. Interestingly at pH 7.4 this polymer showed to have the strongest network while at pH 3 it grew the softest network. This was ascribed to the polydispersity of the micelles in this polymer solution in PBS pH 3. In D_2O at dilute regime and pH 3, R_h was almost constant (118 nm) up to 40 °C and then decreased to 84 nm followed by multiple scattering. At a higher pH, hydrodynamic radii were larger and the same trend was observed. In PBS, on the other hand, smaller micelles were self-

assembled and a continuous increase in R_h was followed by heating up the solution.

$De_{0.1}Ni_1$ PEG_2 showed the highest polydispersity in comparison to $De_1Ni_1PEG_1$ and $De_{0.8}Ni_{1.2}PEG_{2.3}$. Based on DLS results, it displayed a bimodal system in both D_2O and PBS and reached the multiple scattering state at relatively lower temperatures (37 °). In D_2O solutions at pH 3, by increasing the temperature R_{hf} increased from 9 nm to 18 nm while R_{hs} decreased from 168 nm to 108 nm. At a higher pH, larger hydrodynamic radii were observed. In PBS solutions on the other hand, a continuous increase in R_{hf} and R_{hs} was observed; R_{hf} was larger in comparison to the D_2O solutions, while R_{hs} was smaller. pH effect on R_h was not significant in PBS solutions. The polydispersity issue resulted in misleading information in some cases. In dilute regime, based on DLS, SLS and SANS the hypothesis is that at low temperatures $De_{0.1}Ni_1$ PEG_2 does not form a classic micelle structure and is mainly found as unimers (R_g= 9 nm at 25 °C, pH 3 and R_g= 18 nm at 25 °C, pH 9) while $De_{0.1}Ni_1$ PEG_2 chains, most likely with different sizes have a tendency to aggregate in coil-like structures and not well-shaped micelles. This could be attributed to the very short PDEAEMA block in this polymer which did not provide sufficient stickiness to form micelles (CMC was not determined on the concentration range from 2.5×10^{-11} to 2×10^{-4} g/mL); the long hydrophilic PEG and PNIPAAM blocks favored interconnection of the chains in the associations. At higher temperatures however, along with dehydration of PNIPAAM chains, $De_{0.1}Ni_1$ PEG_2 showed to form well-defined micelles. Overall, $De_{0.1}Ni_1$ PEG_2 offered the highest level of hydrophilicity in comparison to $De_1Ni_1PEG_1$ and $De_{0.8}Ni_{1.2}PEG_{2.3}$. This feature was also manifested in steady shear viscosity measurements as it acted like a Newtonian liquid in most cases, and a the high concentration it formed the gel network at relatively higher temperatures in comparison to $De_1Ni_1PEG_1$ and $De_{0.8}Ni_{1.2}PEG_{2.3}$ (~ 50 °C at pH 3 and 7.4).

Multifunctional amphiphilic block copolymers can greatly enhance the efficacy of drug delivery [14]. $PDEAEMA_x$-*b*-$PNIPAAM_y$-*b*-PEG_z-*b*-$PNIPAAM_y$-*b*-$PDEAEMA_x$ could be promising for pH- and/or temperature controlled drug release. Having the PEG block in this polymer offers a thermodynamic stabilization and increased circulation time in the blood stream as a nanocarrier [13]. It can be

also capable of simultaneous delivery of hydrophilic and hydrophobic agents encapsulated in the core or corona, depending on the self-assembly conditions and the formed structure, e.g. micelles or vesicles [92]. At high concentrations this polymer seems to be an auspicious candidate as a thermosensitive *in-situ* forming gel for localized delivery of therapeutic drugs. By tailoring the block lengths, desired physical or biological properties can be achieved.

References

[1] C. Giacomelli, *Chapter 3.Disordered Phase and Self-Organization of Block Copolymer Systems.* Soft-Matter Characterization, Editors: R.Borsali, R.Pecora, *Springer*, 1 (2008).

[2] J. E. Chung, M. Yokoyama, M. Yamato, T. Aoyagi, Y. Sakurai, T. Okano, *Thermo-responsive drug delivery from polymeric micelles constructed using block copolymers of poly(N-isopropylacrylamide) and poly(butylmethacrylate).* Journal of Controlled Release, 62 (1999) 115.

[3] G. Gaucher, M. -H. Dufresne, V. P. Sant, N. Kang, D. Maysinger, J. -C. Leroux, *Block copolymer micelles: preparation, characterization and application in drug delivery.* Journal of Controlled Release, 109 (2005) 169.

[4] E. S. Lee, K. Na, Y. H. Bae, *Polymeric micelle for tumor pH and folate-mediated targeting.* Journal of Controlled Release, 91 (2003) 1003.

[5] Y. Tang, S.Y. Liu, S. P. Armes,N. C. Billingham, *Solubilization and Controlled Release of a Hydrophobic Drug Using Novel Micelle-Forming ABC Triblock Copolymers.* Biomacromolecules, 4 (2003) 1636.

[6] N. Rapoport, *Physical stimuli-responsive polymeric micelles for anti-cancer drug delivery.* Progress in Polymer Science, 32 (2007) 962.

[7] J. Chen, M. Liu, C. Gao,S. Lu, X. Zhang, Z. Liub, *Self-assembly behavior of pH- and thermo-responsive hydrophilic ABCBA-type pentablock copolymers synthesized by consecutive RAFT polymerization.* Royal Society of Chemistry, 3 (2013) 15085.

[8] F. Xu, S. -Z. Zheng, Y. -L. Luo,, *Thermosensitive t-PLA-b-PNIPAAm Tri-armed Star Block Copolymer Nanoscale Micelles for Camptothecin Drug Release.* Journal of Polymer Science, Part A: Polymer Chemistry, 51 (2013) 4429.

[9] V. Butun, N. C. Billingham, S. P. Armes, *Unusual Aggregation Behavior of a Novel Tertiary Amine Methacrylate-Based Diblock Copolymer: Formation of Micelles and Reverse Micelles in Aqueous Solution.* Journal of American Chemical Society, 120 (1998) 11818.

[10] Q. Zhang, J.-D. Hong, R. Hoogenboom, *A triple thermoresponsive schizophrenic diblock copolymer.* Polymer Chemistry, 4 (2013) 4322.

[11] S. Liu, S. P. Armes, *Polymeric Surfactants for the New Millennium: A pH-Responsive, Zwitterionic, Schizophrenic Diblock Copolymer.* Angewandte Chemie International Edition, Communication, 41 (2002) No.8.

[12] M. Arotcuarena, B. Heise, S. Ishaya, A. Laschewsky, *Switching the Inside and the Outside of Aggregates of Water-Soluble Block Copolymers with Double Thermoresponsivity.* Journal of American Chemical Society, 124 (2002) 3787.

[13] H. Hillaireau, P. Couvreur, *Nanocarriers' entry into the cell: relevance to drug delivery.* Cellular and Molecular Life Sciences, 66 (2009) 2873.

[14] X. Yang, J. J. Grailer, I. J. Rowland, A. Javadi, S. A. Hurley,V. Z. Matson, D. A. Steeber, S. Gong, *Multifunctional Stable and pHResponsive Polymer Vesicles Formed by Heterofunctional Triblock Copolymer for Targeted Anticancer Drug Delivery and Ultrasensitive MR Imaging.* ACS Nano, 4 (2010) 6805.

[15] H. G. Schild, D. A. Tirrell, *Microheterogeneous Solutions of Amphiphilic Copolymers of N-Isopropylacrylamide. An Investigation via Fluorescence Methods.* Langmuir, 7 (1991) 1319.

[16] R. Pamies, K. Zhu, A.-L. Kjøniksen, B. Nyström,, *Thermal response of low molecular weight poly-(N-isopropylacrylamide) polymers in aqueous solution.* Polymer Bulletin, 62 (2009) 487.

[17] K. Chang, N. C. Rubright, P. D. Lowery, L. J. Taite, *Structural Optimization of Highly Branched Thermally Responsive Polymers as a Means of Controlling Transition Temperature.* Journal of Polymer Science, Part A: Polymer Chemistry, 51 (2013) 2068.

[18] N. Tanaka, S. Matsukawa, H. Kurosu, I. Ando, *A study on dynamics of water in crosslinked poly (N-isopropylacrylamide) gel by n.m.r. spectroscopy.* Polymer, 39 (1998) 4703.

[19] E. Costa, M. Coelho, L. M. Ilharco,A. Aguiar-Ricardo, P. T. Hammond, *Tannic Acid Mediated Suppression of PNIPAAm Microgels Thermoresponsive Behavior.* Macromolecules, 44 (2011) 612.

[20] V. V. A. Fernandez, N. Tepale, J. C. Sanchez-Dıaz, E. Mendizabal, J. E. Puig, J. F. A. Soltero, *Thermoresponsive nanostructured poly (N-isopropylacrylamide) hydrogels made via inverse microemulsion polymerization.* Colloid and Polymer Science, 284 (2006) 387.

[21] X. Jiang, Z. Ge, J. Xu, H. Liu, S. Liu, *Fabrication of Multiresponsive Shell Cross-Linked Micelles Possessing pH-Controllable Core Swellability and Thermo-Tunable Corona Permeability.* Biomacromolecules, 8 (2007) 3184.

[22] R. H. Pelton, P. Chibante, *Preparation of aqueous latices with N-isopropylacrylamide.* Colloids and Surfaces, 20 (1986) 247.

[23] Y. Özcan, S. Ide, U. Jeng, V. Bütün, YH. Lai, CH. Su, *Micellization behavior of tertiary amine-methacrylate-based block opolymers characterized by small-angle X-ray scattering and dynamic light scattering.* Materials Chemistry and Physics, 138 (2013) 559.

[24] A. Schmalz, M. Hanisch, H. Schmalz, A. H. E. Muller, *Double stimuli-responsive behavior of linear and star-shaped poly(N,N-diethylaminoethyl methacrylate) in aqueous solution.* Polymer, 51 (2010) 1213.

[25] R. Pecora, *Chapter 1.Basic Concepts – Scattering and Time Correlation Functions.* Soft-Matter Characterization, Editors: R.Borsali, R.Pecora, *Springer*, 1 (2008).

[26] B. Chu, *Chapter 7. Dynamic Light Scattering.* Soft-Matter Characterization, Editors: R.Borsali, R.Pecora, *Springer*, 1 (2008).

[27] C. M. Sorensen, N. Lu, J. Cai, *Fractal Cluster Size Distribution Measurement Using Static Light Scattering.* Journal of Colloid and Interface Science 174 (1995) 456.

[28] M. B. Thomas , J. L. Roger, R. Pecora, *Absolute Rayleigh Ratios of Four Solvents at 488 nm.* Macromolecules, 19 (1986) 244.

[29] U. Olsson, P. Schurtenberged, *Structure, Interactions, and Diffusion in a Ternary Nonionic Microemulsion Near Emulsification Failure.* Langmuir, 9 (1993) 3389.

[30] W. Burchard, *Light Scattering from Polymers.* Advances in Polymer Science, Springer-Verlag, 48 (1983).

[31] G. C. Berry, *Chapter 2.Total Intensity Light Scattering from Solutions of Macromolecules.* Soft-Matter Characterization, Editors: R.Borsali, R.Pecora, *Springer*, 1 (2008).

[32] R. P. Rambo, J. A. Tainer, *Characterizing Flexible and Instrinsically Unstructured Biological Macromolecules by SAS using the Porod-Debye Law.* Biopolymers, 95 (2011) 559.

[33] A. J. F. Siegert, *Radiation Laboratory Report no. 465.* Massachusetts Institute of Technology, (1943).

[34] S. Bayati, R. Pamies, S. Volden, K. Zhu, A. -L. Kjøniksen, W. R. Glomm, B. Nystrom, *Influence of poly(ethylene glycol) block length on the adsorption of thermoresponsive copolymers onto gold surfaces.* Journal of Materials Science, 48 (2013) 7055.

[35] D. B. Ermi, E. J. Amis, *Domain Structures in Low Ionic Strength Polyelectrolyte Solutions.* Macromolecules, 31 (1998) 7378.

[36] H. Sadeghi Abandansari, E. Aghaghafari, M.R. Nabid, H. Niknejad, *Preparation of injectable and thermoresponsive hydrogel based on penta-block copolymer with improved sol stability and mechanical properties.* Polymer, 54 (2013) 1329.

[37] C. He, S. W. Kim, D. S. Lee, *In situ gelling stimuli-sensitive block copolymer hydrogels for drug delivery.* Journal of Controlled Release, 127 (2008) 189.

[38] M. K. Nguyen, D. K. Park, D. S. Lee, *Injectable Poly(amidoamine)-poly(ethylene glycol)-poly(amidoamine) Triblock Copolymer Hydrogel with Dual Sensitivities: pH and Temperature.* Biomacromolecules, 10 (2009) 728.

[39] R. G. Larson, *Chapter 1. Introduction to complex Fluids.* The structure and Rheology of Complex Fluids, *Oxford University Press, New York*, 1 (1999).

[40] B. Nystrom, A. -L. Kjøniksen, C. Iversen, *Characterization of association phenomena in aqueous systems of chitosan of different hydrophobicity.* Advances in Colloid and Interface Science, 79 (1999) 81.

[41] X. Zhu, H. Saba, Y. Zhang, H. Wang, *The Viscoelastic Behavior of Concentrated Polyacrylonitrile/1-Butyl-3-Methylimidazolium Chloride from Solution to Gel.* Polymer Engineering and Science (2013) DOI 10.1002/pen.23593.

[42] A. Miasnikova, A. Laschewsky, G. De Paoli, C. M. Papadakis, P. Müller-Buschbaum, S. S. Funari, *Thermoresponsive Hydrogels from Symmetrical Triblock Copolymers Poly(styrene-block-(methoxy diethylene glycol acrylate)- block-styrene).* Langmuir, 28 (2012) 4479.

[43] M. Sahimi, *Chapter 11. In Application of Percolation Theory.* Taylor and Francis, London, (1994) 176.

[44] J. Zhao, B, Majumdar, M. F. Schulz, F. S. Bates, *Phase Behavior of Pure Diblocks and Binary Diblock Blends of Poly(ethylene)-Poly(ethylethylene).* Macromolecules, 29 (1996) 1204.

[45] F. T. Tadros, *Rheology of Dispersions: Principles and Applications.* Wiley-VCH: Weinheim, Germany, (2010).

[46] H. -H. Lin, Y. -L. Cheng, *In-Situ Thermoreversible Gelation of Block and Star Copolymers of Poly(ethylene glycol) and Poly(N-isopropylacrylamide) of Varying Architectures.* Macromolecules, 34 (2001) 3710.

[47] F. Chambon, H. H. Winter, *Linear Viscoelasticity at the Gel Point of a Crosslinking PDMS with Imbalanced Stoichiometry.* Journal of Rheology, 31 (1987) 683.

[48] F. Tanaka, *Chapter 3. Classical theory of gelation.* Polymer Physics, Applications to Molecular Association and Thermoreversible Gelation, *Cambridge University Press*, 1 (2011).

[49] H. H. Winter, M. Mours, *Rheology of Polymers Near Liquid-Solid Transitions.* Advances in Polymer Science, *Springer*, 134 (1997).

[50] P. J. Flory, *Molecular size distribution in three dimensional polymers. ii. trifunctional branching units.* Journal of the American Chemical Society, 63 (1941) 3083.

[51] W. H. Stockmayer, *Theory of Molecular Size Distribution and Gel Formation in Branched-Chain Polymers.* Journal of Chemical Physics, 11 (1943) 45.

[52] S. R. Broadbent, J. M. Hammersley, *Percolation processes I. Crystals and mazes.* Proceedings of the Cambridge Philosophical Society, 53 (1957) 629.

[53] D. Stauffer, A. Coniglio, M. Adam, *Gelation and critical phenomena.* Advances in Polymer Science, 44 (1982) 103.

[54] M. Muthukumar, H. H. Winter, *Fractal dimension of a crosslinking polymer at the gel point.* Macromolecules, 19 (1986) 1284.

[55] M. Muthukumar, *Screening effect on viscoelasticity near the gel point.* Macromolecules, 22 (1989) 4656.

[56] T. Hashimoto, *Chapter 8. Light Scattering from Multicomponent Polymer Systems in Shear Fields: Real-time, In Situ Studies of Dissipative Structures in Open Nonequilibrium Systems.* Soft-Matter Characterization, Editors: R.Borsali, R.Pecora, *Springer*, 1 (2008).

[57] K. Zhu, H. Jin, A. -L. Kjøniksen, B. Nystrom, *Anomalous Transition in Aqueous Solutions of a Thermoresponsive Amphiphilic Diblock Copolymer.* Journal of Physical Chemistry B, 111 (2007) 10862.

[58] D. Wang, J. Tan, H. Kang, L. Ma, Xin Jin, R. Liu, Yong Huang, *Synthesis, self-assembly and drug release behaviors of pH-responsive copolymers ethyl cellulose-graft-PDEAEMA through ATRP.* Carbohydrate Polymers, 84 (2011) 195.

[59] C. Sommer, J. S. Pedersen, *Apparent Specific Volume Measurements of Poly(ethylene oxide), Poly(butylene oxide), Poly(propylene oxide), and Octadecyl Chains in the Micellar State as a Function of Temperature.* Journal of Physical Chemistry B, 108 (2004) 6242.

[60] A. -L. Kjøniksen, A. Laukkanen, C. Galant, K. D. Knudsen, H. Tenhu, B. Nystrom, *Association in Aqueous Solutions of a Thermoresponsive PVCL-g-C11EO42 Copolymer.* Macromolecules, 38 (2005) 948.

[61] N. Beheshti, K. Zhu, A.-L. Kjøniksen, K. D. Knudsenc, B. Nystrom, *Characterization of temperature-induced association in aqueous solutions of charged ABCBA-type pentablock tercopolymers.* Soft Matter, 7 (2011) 1168.

[62] H. Jonassen, A.-L. Kjøniksen, M. Hiorth, *Effects of ionic strength on the size and compactness of chitosan nanoparticles.* Colloid and Polymer Science, 290 (2012) 919.

[63] A. Ghoorchian, K. Vandemark, K. Freeman, S. Kambow, N. B. Holland, K. A. Streletzky, *Size and Shape Characterization of Thermoreversible Micelles of Three-Armed Star Elastin-Like Polypeptides.* Journal of Physical Chemistry B, 117 (2013) 8865.

[64] L. Gu, C. Feng, D. Yang, Y. Li, J. Hu, G. Lu, X. Huang, *PPEGMEA-g-PDEAEMA: Double Hydrophilic Double-Grafted Copolymer Stimuli-Responsive to Both pH and Salinity.* Journal of Polymer Science: Part A: Polymer Chemistry, 47 (2009) 3142.

[65] M. Wilhelm, C. -L. Zhao, Y. Wang, R. Xu, M. A. Winnik, *Poly(styrene-ethylene oxide) Block Copolymer Micelle Formation in Water: A Fluorescence Probe Study.* Macromolecules, 24 (1991) 1033.

[66] D. S. Karpovich, G. J. Blanchard, *Relating the Polarity-Dependent Fluorescence Response of Qrene to Vibronic Coupling. Achieving a Fundamental Understanding of the py Polarity Scale.* Journal of Physical Chemistry, 99 (1995) 3951.

[67] D. W. Ball, *Chapter 8, Electrochemistry and Ionic Solutions.* Physical Chemistry, Brooks/Cole- Thomson Learning, (2003).

[68] I. Grillo, *Chapter 13. Small-Angle Neutron Scattering and Applications in Soft Condensed Matter.* Soft-Matter Characterization, Editors: R.Borsali, R.Pecora, *Springer*, 2 (2008).

[69] V. F. Sears, *Neutron scattering lengths and cross sections.* Neutron News, 3 (1992) 26.

[70] N. Dingenouts, S. Seelenmeyer, I. Deike, S. Rosenfeldt, M. Ballau, P. Lindnerb, T. Narayananc, *Analysis of thermosensitive coreshell colloids by small-angle neutron scattering including contrast variation.* Physical Chemistry Chemical Physics, 3 (2001) 1169.

[71] W. Wang, E. Metwalli, J. Perlich, C. M. Papadakis, R. Cubitt, P. Muller-Buschbaum, *Cyclic Switching of Water Storage in Thin Block Copolymer Films Containing Poly(N-isopropylacrylamide).* Macromolecules, 42 (2009) 9041.

[72] T. Riley, C. R. Heald, S. Stolnik, M. C. Garnett, L. Illum, and S. S. Davis, *Core-Shell Structure of PLA-PEG Nanoparticles Used for Drug Delivery.* Langmuir, 19 (2003) 8428.

[73] P. D. Topham, A. Glidle, D. T. W. Toolan, M. P. Weir, M. W. A. Skoda, R. Barker, J. R. Howse, *The Relationship between Charge Density and Polyelectrolyte Brush Profile Using Simultaneous Neutron Reflectivity and In Situ Attenuated Total Internal Reflection FTIR.* Langmuir, 29 (2013) 6068.

[74] E. Karjalainen, N. Chenna, P. Laurinmaki, S. J. Butcherb, H. Tenhu, *Diblock copolymers consisting of a polymerized ionic liquid and poly(N-isopropylacrylamide). Effects of PNIPAM block length and counter ion on selfassembling and thermal properties.* Physical Chemistry, 4 (2013) 1014.

[75] Y. Hu, J. Xie, Y. W. Tong, C. -H. Wang, *Effect of PEG conformation and particle size on the cellular uptake efficiency of nanoparticles with the HepG2 cells.* Journal of Controlled Release, 118 (2007) 7.

[76] M. Karg, I. Pastoriza-Santos, B. Rodriguez-Gonzalez, R. von Klitzing, S. Wellert, T. Hellweg, *Temperature, pH, and Ionic Strength Induced Changes of the Swelling Behavior of PNIPAM-Poly(allylacetic acid) Copolymer Microgels.* Langmuir, 24 (2008) 6300.

[77] S. Saha, K. Fischer, M. Muthukumar, M. Schmidt, *Apparent Molar Mass of a Polyelectrolyte in an Organic Solvent in the Low Ionic Strength Limit As Revealed by Light Scattering.* Macromolecules, 46 (2013) 8296.

[78] R. Kita, G. Kircher, S. Wiegand, *Thermally induced sign change of Soret coefficient for dilute and semidilute solutions of poly N-isopropylacrylamide in ethanol.* Journal of Chemical Physics, 121 (2004) 9140.

[79] J. Zhang, M. Zou, J. Dong, X. Li, *Synthesis and self-assembly behaviors of well-defined poly(lauryl methacrylate)-block-poly [N-(2-methacryloylxyethyl)pyrrolidone] copolymers.* Colloid and Polymer Science, 291 (2013) 2653.

[80] Y. Tu, X. Wan, D. Zhang, Q. Zhou, C. Wu, *Self-Assembled Nanostructure of a Novel Coil-Rod Diblock Copolymer in Dilute Solution.* Journal of American Chemical Society, 122 (2000) 10201.

[81] W. Burchard, *Chapter 1, Static and Dynamic Light Scattering Approaches to Structure Determination of Biopolymers.* Laser Light Scattering in Biochemistry, Editor: S. E. Harling, D. B. Sattelle, V. A. Bloomfield, *The Royal Society of Chemistry*, 1, (1991).

[82] J. -N. Roux, D. Broseta, B. Deme, *SANS Study of Asphaltene Aggregation: Concentration and Solvent Quality Effects.* Langmuir, 17 (2001) 5085.

[83] T. Matsunaga, T. Sakai, Y. Akagi, U.-I. Chung, M. Shibayama, *SANS and SLS Studies on Tetra-Arm PEG Gels in As-Prepared and Swollen States.* Macromolecules, 42 (2009) 6245.

[84] H. Paine, Kolloid-Z., 11 (1912) 2115.

[85] F. C. Giacomelli, I. C. Riegel, C. L. Petzhold, N. P. da Silveira, P. Stepanek, *Aggregation Behavior of a New Series of ABA Triblock Copolymers Bearing Short Outer A Blocks in B-Selective Solvent: From Free Chains to Bridged Micelles.* Langmuir, 25 (2009) 731.

[86] U. P. Shinde, M. K. Joo, H. J. Moon, B. Jeong, *Sol–gel transition of PEG–PAF aqueous solution and its application for hGH sustained release.* Journal of Materials Chemistry, 22 (2012) 6072.

[87] Y. Cheng, C. He , J. Ding, C. Xiao, X. Zhuang, X. Chen, *Thermosensitive hydrogels based on polypeptides for localized and sustained delivery of anticancer drugs.* Biomaterials, 34 (2013) 10338.

[88] S. Li, P. K. Jarvela, Pirkko A. Jarvela, *A Comparison Between Apparent Viscosity and Dynamic Complex Viscosity for Polypropylene/Maleated Polypropylene Blends.* Polymer Engineering and Science, 37 (1997).

[89] H. Tsuji, F. Horii, S. -H. Hyon, Y. Ikada, *Stereocomplex Formation between Enantiomeric Poly(1actic acid)s. 2. Stereocomplex Formation in Concentrated Solutions.* Macromolecules, 24 (1991) 2719.

[90] A. Petit, B. Müller, R. Meijboom, P. Bruin, F. van de Manakker, M. Versluijs-Helder, L. G. J. de Leede, A. Doornbos, M. Landin, W. E. Hennink, T. Vermonden, *Effect of Polymer*

Composition on Rheological and Degradation Properties of Temperature-Responsive Gelling Systems Composed of Acyl-Capped PCLA-PEG-PCLA. Biomacromolecules, 14 (2013) 3172.

[91] A. Koike, N. Nemoto, M. Takahashi, K. Osaki, *Dynamic viscoelasticity of end-linking α,ω-dimethyl silyl poly(propylene oxide) solutions near the gel point.* Polymer, 35 (1994) 3005.

[92] A. E. Smith, X. Xu, S. E. Kirkland-York, D. A. Savin, C. L. McCormick, *"Schizophrenic" Self-Assembly of Block Copolymers Synthesized via Aqueous RAFT Polymerization: From Micelles to Vesicles.* Macromolecules, 43 (2010) 1210.